

AD-A066 150

LOCKHEED MISSILES AND SPACE CO INC PALO ALTO CALIF PA--ETC F/G 4/1
LOW-ENERGY PARTICLE EXPERIMENT. (U)

FEB 79 R D SHARP

N00014-72-C-0234

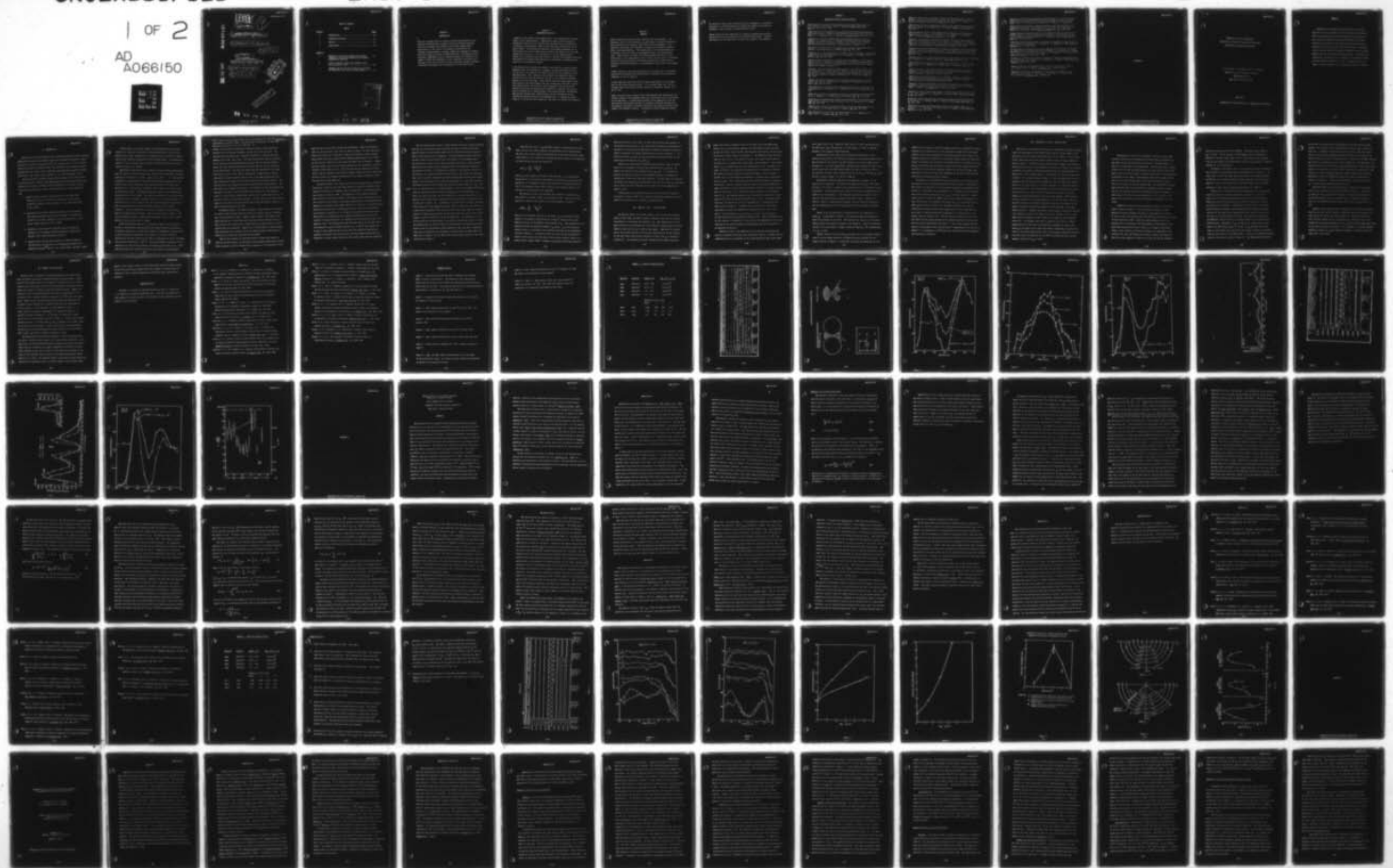
UNCLASSIFIED

LMSC/D673078

NL

1 OF 2

AD
A066150



28 February 1979

LEVEL

⑨ FINAL REPORT

⑥ Contract N00014-72-C-0234
LOW-ENERGY PARTICLE EXPERIMENT
A053920

⑮ N00014-72-C-0234

⑫ 124 p.

⑩ Prepared by
R. D. Sharp
Space Sciences Laboratory
Lockheed Palo Alto Research Laboratory
Lockheed Missiles & Space Company, Inc.

⑭ LMSC/D673078

⑪ 28 Feb 79

DDC
REFINED
MAR 21 1979
ALULU C

This document has been approved
for public release and sale; its
distribution is unlimited.

ADA066150

DDC FILE COPY

79 03 05 075

240 118

slf

TABLE OF CONTENTS

<u>Section</u>	<u>Title</u>	<u>Page</u>
1	INTRODUCTION.....	1-1
2	BACKGROUND/RELEVANCE.....	2-1
3	RESULTS.....	3-1
4	BIBLIOGRAPHY.....	4-1
 <u>Appendix</u>		
A	ENERGETIC PARTICLE MEASUREMENTS FROM WITHIN IONOSPHERIC STRUCTURES RESPONSIBLE FOR AURORAL ACCELERATION PROCESSES.	A-1
B	SCALE OF ELECTRIC FIELD ALONG MAGNETIC FIELD IN AN INVERTED-V EVENT.....	B-1
C	DOWNWARD FLOWING IONS AND EVIDENCE FOR INJECTION OF IONOSPHERIC IONS INTO THE PLASMA SHEET.....	C-1

ACCESSION for	
NTIS	White Section <input checked="" type="checkbox"/>
DOC	Buff Section <input type="checkbox"/>
UNANNOUNCED	<input type="checkbox"/>
JUSTIFICATION	
BY	
DISTRIBUTION AT LIBRARY LOSES	
DATE	SPECIAL
A	

SECTION 1

INTRODUCTION

This was a program directed toward an improved understanding of the sources and energization, transport and loss processes associated with the low-energy (keV) plasmas in the earth's magnetosphere, particularly as they relate to ionospheric perturbations and ionospheric-magnetospheric coupling. Under this program the Lockheed Palo Alto Research Laboratory (LPARL) conducted a low-energy particle experiment (ONR-118) on the S3-3 spacecraft, which was launched in the summer of 1976. The experiment is still operating successfully and has made several major discoveries about previously unknown ionospheric acceleration mechanisms and the composition of the ring current.

Section 2

BACKGROUND/RELEVANCE

A number of Navy systems either depend upon, or are affected by, the ionosphere and the magnetosphere. Communication links utilize ionospheric propagation paths which are significantly disturbed by the precipitation of energetic magnetospheric plasma in the keV range, particularly in the polar regions. The heating and expansion of the upper atmosphere due to this precipitation can increase drag and affect the orbits of low altitude navigational satellites. The interaction of the hot magnetospheric plasma with synchronous satellites leads to a variety of phenomena associated with spacecraft charging which degrades the performance of communications satellites in operational systems.

A new dimension has recently been added to our ability to study the above phenomena with the development of energetic ion mass spectrometers which for the first time allow for the identification of the ion species in the measured plasma. This capability has produced some remarkable results, principal of which was the discovery that O^+ is on occasion the dominant species in the few keV range. Since the O^+ ions have a much smaller range than protons of the same energy, they have dramatically different interaction characteristics with both the upper atmosphere and with sensitive spacecraft surfaces and therefore the capability to identify the ion species is required for an understanding of the plasma effects. The ONR-118 spectrometer provides this identification via the utilization of both velocity and energy analysis on the measured ions. It covers the energy range 0.6 to 16 keV per unit charge for ions and 0.1 to 20 keV for electrons.

Section 3

RESULTS

Several important discoveries have resulted from the experiment. The principal result is the discovery of large fluxes of energized ionospheric ions streaming up the magnetic field lines from the ionosphere. This discovery establishes the existence of a major new ionospheric-magnetospheric coupling phenomenon. The characteristics of the phenomenon point to parallel electric fields as the immediate cause of the accelerated ions. These results and those of the ONR companion experiment on S3-3, which makes in situ measurements of the electric fields, put on a firm basis the many recent speculations and inferences relating to large electric potential differences parallel to the geomagnetic field lines in the magnetosphere.

Another important result was the discovery of a second type of ionospheric acceleration mechanism which preferentially accelerates the perpendicular component of the ion velocity.

A third important result was the first direct measurement of the composition of the storm-time ring current. In the energy range from 1-16 keV the main phase ring current has been found to be primarily composed of H^+ and O^+ ions.

Some of our more recent results derive from detailed case studies and statistical studies of the phenomena which were discovered in the initial phases of the experiment. A quantitative analyses of the signatures in the ion and electron distribution functions is leading to detailed information on the geometry and physical processes involved in the parallel electric field regions (see Appendix A and B). A statistical study of downward flowing

ion events has led to the conclusion that the ionosphere is a principle contributor to the circulating ion clouds which dominate the plasma environment in the vicinity of the geostationery orbit.

These results have been described in a series of publications and presentations which are included in the following bibliography. Preprints and reprints of the most recent articles are included in the Appendix.

SECTION 4

S3-3 PUBLICATIONS AND PRESENTATIONS

"Satellite Observations of an Ionospheric Acceleration Mechanism," by E. G. Shelley, R. D. Sharp, and R. G. Johnson, Geophys. Res. Lett., Vol. 3, No. 11, 654, 1976.

"Observation of an Ionospheric Acceleration Mechanism Producing Energetic (keV) Ions Primarily Normal to the Geomagnetic Field Direction," by R. D. Sharp, R. G. Johnson, and E. G. Shelley, J. Geophys. Res., 82, 3324, 1977.

"Composition of the Hot Plasma Near Geosynchronous Altitude, by R. G. Johnson, R. D. Sharp, and E. G. Shelley, Proceedings of the Spacecraft Charging Technology Conference, edited by C. P. Pike and R. E. Lovell, Air Force Geophysical Laboratory, AFGL-TR-770051, February 1977.

"Satellite Observations of an Ionospheric Acceleration Mechanism," by E. G. Shelley, R. D. Sharp and R. G. Johnson, EOS, 57, 992, 1976.

"Characteristics of Upward-Flowing, Energetic (keV), Ionospheric Ions During a Magnetically-Disturbed Period," by R. G. Johnson, R. D. Sharp, and E. G. Shelley, EOS, 57, 993, 1976.

"Recent Results of Energetic Ion Composition Measurements in the Magnetosphere," by R. D. Sharp, R. G. Johnson and E. G. Shelley, presented at the International Symposium on the Magnetosphere and Its Environment, Christchurch, New Zealand, January 1977.

"Energetic (keV) Ion Composition Observations on the S3-3 Satellite," by R. G. Johnson, R. D. Sharp, and E. G. Shelley, invited paper presented at the special session on the S3-3 satellite at the Spring 1977 meeting of the American Geophysical Union in Washington, D. C., May 1977, EOS, 58, 991, 1977.

"Angular Distribution Characteristics of Up-Streaming Energetic (keV) O^+ and H^+ Ions," by A. Ghielmetti, R. G. Johnson, E. G. Shelley, and R. D. Sharp, EOS, 58, 473, 1977.

"The Morphology of Upward-Flowing Field-Aligned Energetic Ion Fluxes," by A. Ghielmetti, E. G. Shelley, R. G. Johnson and R. D. Sharp, EOS, 58, 716, 1977.

"Observation of Ions of Ionospheric Origin in the Storm-Time Ring Current," by R. G. Johnson, R. D. Sharp, and E. G. Shelley, EOS, 58, 753, 1977.

"Distribution of Electrostatic Potential Along Magnetic Field Inferred from Observations of Electron and Ion Fluxes," by J. B. Cladis and R. D. Sharp, EOS, 58, 716, 1977.

"Observations of Ions of Solar Wind Origin in the Inner Magnetosphere," by E. G. Shelley, R. D. Sharp, and R. G. Johnson, EOS, 58, 716, 1977.

"Ion Composition of the Quiet Time Magnetosphere," E. G. Shelley, R. D. Sharp, and R. G. Johnson, EOS, 58, 1217, 1977.

"Energetic Heavy Ions of Ionospheric Origin in the Magnetosphere," by E. G. Shelley, invited review paper presented at the IAGA General Assembly in Seattle, Washington, August 1977, EOS, 58, 752, 1977.

"Observations of Ions of Ionospheric Origin in the Storm Time Ring Current," by R. G. Johnson, R. D. Sharp, and E. G. Shelley, Geophys. Res. Letters, 4, 403, 1977.

"The Latitudinal, Diurnal, and Altitudinal Distributions of Up-Streaming Field Aligned Ion Fluxes, A. Ghielmetti, R. G. Johnson, E. G. Shelley and R. D. Sharp, Geophys. Res. Letters, 5, 59, 1978.

"Satellite Measurements from Within Ionospheric Structures Responsible for Auroral Acceleration Processes," R. D. Sharp, E. G. Shelley, R. G. Johnson, Paper 2-12, Proceedings of the Ionospheric Effects Symposium, Naval Research Laboratory, and the Office of Naval Research, January 24-26, 1978.

"A Review of Particle Measurements from Within Ionospheric Structures Responsible for Auroral Acceleration Processes," R. D. Sharp invited review paper presented at the Fall, 1977 meeting of the American Geophysical Union, EOS, 58, 1209, 1977.

"Average Properties of Upstreaming Energetic Field Aligned Ions," A. Ghielmetti, R. G. Johnson, E. G. Shelley, and R. D. Sharp, EOS, 58, 1211, 1977.

"Observations of the Ring Current Composition During the 29 July 1977 Magnetic Storm," R. G. Johnson, R. D. Sharp, and E. G. Shelley, EOS, 58, 1217, 1977.

"Scale of Electric Field Along Magnetic Field in Structures of Inverted V Events," J. B. Cladis and R. D. Sharp, presented at Solar Terrestrial Physics Symposium, Innsbruck, Austria, June 1978.

"Heavy Ions in the Magnetosphere," E. G. Shelley, invited review paper presented at the Solar Terrestrial Physics Symposium, Innsbruck, Austria, June 1978, Space Science Reviews (in press) 1979.

"Energetic Particle Measurements from Within Ionospheric Structures Responsible for Auroral Acceleration Processes," R. D. Sharp, R. G. Johnson, and E. G. Shelley, J. Geophys. Res., (in press) 1978.

"Evidence for Ions of Solar Wind Origin in the Storm Time Ring Current Near $L = 4$," R. G. Johnson, E. G. Shelley, R. D. Sharp, (EOS) Trans. Am. Geophys. U, 59, 348, 1978.

"Energetic Particle Measurements Within an Inverted V Acceleration Region," R. D. Sharp, E. G. Shelley, and R. G. Johnson, (EOS) Trans. Am. Geophys. U, 59, 358, 1978.

"Downward Streaming Field Aligned Ion Fluxes in the Auroral Zone," A. G. Ghielmetti, E. G. Shelley, R. D. Sharp, and R. G. Johnson, (EOS) Trans. Am. Geophys. U, 59, 348, 1978.

"Observation of Electrostatic Hydrogen Cyclotron Waves in the Polar Magnetosphere," presented at the URSI XIX General Assembly, Helsinki, Finland, August 1978, P. M. Kintner, M. C. Kelley, R. D. Sharp, A. G. Ghielmetti.

"Simultaneous Observations of Upgoing Energetic Ions and Electrostatic Hydrogen Cyclotron Waves," P. M. Kintner, M. C. Kelley, R. D. Sharp, A. G. Ghielmetti, M. Temerin, (EOS) Trans. Am. Geophys. U., 59, 1155, 1978.

"Upward Flowing Ion Characteristics in the High Latitude Ionospheric Acceleration Regions," invited review paper presented at the 1978 Fall Meeting of the American Geophysical Union, A. G. Ghielmetti, (EOS) Trans. Am. Geophys. U., 59, 1155, 1978.

"Counterstreaming Electron Beams at Altitudes of $1R_E$ Over the Auroral Zone," R. D. Sharp, E. G. Shelley, R. G. Johnson, A. G. Ghielmetti, (EOS) Trans. Am. Geophys. U., 59, 1158, 1978.

"An Ionospheric Precursor of an Auroral Substorm as Observed by the Chatanika Radar and the S3-3 Satellite," R. R. Vondrak, R. D. Sharp, R. G. Johnson, F. S. Mozer, C. A. Catell, R. B. Torbert, J. F. Fennell, P. F. Mizera, (EOS) Trans. Am. Geophys. U., 59, 1167, 1978.

"Evidence for Injection of Clouds of Ionospheric Ions into the Plasma Sheet," A. G. Ghielmetti, R. D. Sharp, R. G. Johnson, E. G. Shelley, (EOS) Trans. Am. Geophys. U., 59, 1164, 1978.

"Scale of Electric Field Along Magnetic Field in an Inverted V Event," J. B. Cladis and R. D. Sharp, J. Geophys. Res., 1979 (in press).

"Downward Flowing Ions and Evidence for Injection of Ionospheric Ions into the Plasma Sheet," A. Ghielmetti, R. D. Sharp, E. G. Shelley and R. G. Johnson, J. Geophys. Res., (submitted).

APPENDIX A

ENERGETIC PARTICLE MEASUREMENTS
FROM WITHIN IONOSPHERIC STRUCTURES RESPONSIBLE
FOR AURORAL ACCELERATION PROCESSES

R. D. Sharp, R. G. Johnson, and E. G. Shelley

Lockheed Palo Alto Research Laboratory

3251 Hanover Street

Palo Alto, California 94304

MAY 1978

Accepted for Publication J. Geophysical Research

ABSTRACT

Measurements of energetic electrons ($0.07 \leq E \leq 24$ keV) and ions ($0.5 \leq E \leq 16$ keV) on the S3-3 satellite show features which are interpreted in terms of parallel potential drops of up to several kV magnitude existing simultaneously both above and below the satellite. This leads to the inference that the satellite is within an auroral acceleration region. Two events of this type are examined in which the satellite is in the 7000-8000 km altitude range and at auroral latitudes. Both events are interpreted as traversals of an "inverted V" acceleration region of broad latitudinal width ($2^\circ - 4^\circ$). In both cases, one can infer a vertical extent to the acceleration region of $\geq 10^3$ km.

I. INTRODUCTION

Previous results have suggested that at least some types of auroral electron acceleration processes occur within large scale ionospheric structures containing potential drops of the order of 10^4 volts aligned parallel to the magnetic field and situated at altitudes above those which have been repeatedly sampled by experiments on rockets and low altitude, polar-orbiting satellites [Gurnett, 1972; Evans, 1974; Swift, 1975; Kauffman et al., 1976, Falthammer, 1977].

The S3-3 satellite (8,000 km apogee, 240 km perigee, 97.5° inclination) is now sampling this region of the magnetosphere and has discovered that such structures are indeed a commonly occurring phenomena at altitudes of about $1 R_E$ at auroral latitudes. Some of the manifestations of these phenomena are:

1. Upward flowing, narrowly collimated beams of energetic (keV) field aligned ions, indicative of electrostatic acceleration of ambient ionospheric ions. [Shelley et al., 1976, Ghielmetti et al., 1978]
2. Occasional conical pitch angle distributions in the energetic ions indicating additional processes providing a perpendicular as well as a parallel component to the ion acceleration. [Sharp et al., 1977; Ghielmetti et al., 1978].
3. Signatures of keV potential drops both above and below the satellite in the energetic electron populations [Mizera and Fennell, 1977; Cladis and Sharp, 1977a, b].
4. Narrow spatial regions with measured d.c. electric fields $\gtrsim 10^2$ mV/m which are referred to as electrostatic shocks by the Berkeley experiment/ [Mozer et al., 1977; Torbert and Mozer, 1978].

In this paper we show some examples of the plasma observations from within these ionospheric structures, focusing primarily on the use of the electron pitch angle distributions as a diagnostic tool to probe for indicators of their geometry, particularly their vertical extent. A detailed discussion of the use of this type of analysis on another event has been presented by Cladis et al. [1977].

The Lockheed experiment on S3-3 consists of three ion-mass-spectrometers and four magnetic electron spectrometers which have been described in previous publications [Shelley et al., 1976, Sharp et al., 1977]. The satellite is spinning at approximately 3 rpm with its spin axis perpendicular to the orbital plane and the instruments are mounted with their view directions perpendicular to the spin axis, providing almost complete pitch angle scans of the measured fluxes. The angular acceptance range for the spectrometers is approximately 6° full width. The electron spectrometers have broad energy bands and nearly rectangular response functions so as to include almost all electrons with $.07 \leq E \leq 24$ keV in the four measured intervals (See Table I). They are sampled twice per second providing approximately 9° angular resolution. The ion spectrometers each have 4 energy-per-charge settings which are stepped every 16 seconds. These are also listed in Table I. The ion spectrometers provide a complete mass-per-charge sweep at each of three energy-per-charge values every 1 second.

Since the satellite spins at ~ 3 rpm and it requires several spins to be able to differentiate characteristic pitch angle structure from spatial or temporal variations, we focus these studies on ionospheric structures with a broad latitudinal extent which, as we will see, may have relatively weak parallel electric fields (of the order of millivolts per meter) extending over vertical dimensions of $\sim 10^3$ km. These are possibly a different class of phenomena than those being studied by the Berkeley group [Nozer et al., 1977] whose experiment more naturally focuses on high electric field phenomena

• ($\sim 10^4$ mv/m) which are found to occur over narrow (\leq few km) latitudinal dimensions [Torbert and Mozer 1978]. The two classes of phenomena are generally associated spatially but are not identical. An

example of this spatial association is given in Figure 1 which shows data obtained over the northern hemisphere auroral zone on 29 July 1976. The abscissa shows universal time, altitude in kilometers, invariant latitude, magnetic local time, and L value. The four lowest panels show the logarithm of the counts per half-second counting interval for the electron spectrometers. The panel labeled PITCH shows the pitch angle of the look direction of the spectrometer. The next four panels show the logarithm of the counts from ions with $m/q = 1, 2, 4$, and 16, respectively, summed once per second from selected output channels from all three of the mass spectrometers giving an approximate measure of the relative flux of the relevant species. The top panel shows the energy step of each of the three mass spectrometers. The spin numbers are labeled for reference. For example, for the 16-second period associated with spin 12 the three spectrometers were set at E/q values of 1.28, 4.5, and 16.0 keV, respectively, and the $m/q = 1$ plot shows the sum of the proton counts at these three energies. In fact, on this spin the observed counts derived almost entirely from the high energy spectrometer indicating a peak in the spectrum at $E \gtrsim 16$ keV.

In examining Figure 1 one sees two regions, labeled Region I and Region II, each of which contains particle fluxes with common signatures extending over a wide latitudinal range. Region I shows symmetric, 90° peaked pitch angle distributions in the three lowest energy electron channels which, as will be shown, are indicative of a broad region of parallel electric fields located above the spacecraft. Region II is a broad region of upward flowing ions associated with a drop-out in the low energy electron fluxes which is indicative of a potential drop below the spacecraft.

Both of these regions are contained within a larger scale region in which the electron fluxes, as measured by the Aerospace Corporation's electrostatic analyzers, show the characteristic signature of an "inverted V" event

when plotted on a grey scale energy-time spectrogram. [Mizera and Fennell, 1978; the spectrogram for this event is shown in Figure 3 of this reference.] Within this large scale "inverted V" region four discrete, narrow, electrostatic shocks have been reported by the Berkeley group [Mozier et al., 1977] at the locations indicated on the lowest horizontal axis in Figure 1. Upward flowing energetic ions are occasionally observed at the locations of the electrostatic shocks [Mizera et al., 1977] when the plasma analyzers are fortuitously oriented downward at the times of passage through the narrow structures. On this occasion the Lockheed spectrometers saw no upward flowing ions until the satellite reached Region II.

As indicated above, this report will focus on the broad scale structures. Preliminary indications are that these regions are generally spatially associated with enhanced low frequency noise or turbulence in the electric field data [Torbert and Mozer, 1978]. The signatures of the parallel potential drops within the structures consist of the upward flowing ion beams plus certain features of the electron pitch angle distributions to be described below. Signatures of potential drops above and below the satellite are often observed simultaneously indicating a substantial vertical extent to the structures. As discussed by Ghielmetti et al. [1978] the ion beams often show the combined effects of perpendicular and parallel accelerations as well as the transfer of energy between the two components by the mirroring action of the magnetic field. This complication plus the time lags in the ion data due to the substantial times of flight involved (e.g., 1 keV O^+ ions require over 9 secs to travel 1000 km) make the ion data less useful for quantitative analysis in possibly time-varying events than the rapidly moving electrons. Therefore, in these initial studies we will focus on the electron signatures.

For the following discussion we define primary electrons as those electrons entering the acceleration region from above and those electrons which have passed through the acceleration region and are reflected below the spacecraft before interacting with the atmosphere. We define degraded primary electrons as those primary electrons which have lost energy in the atmosphere below the acceleration region, and we define secondary electrons as those electrons which have been produced in the atmosphere below the acceleration region by the primary electrons. As illustrated in Figure 2, the electrons observed in the presence of a parallel upward-directed electric field above the spacecraft fall into two general categories; primaries and degraded primaries with energy greater than the potential drop above the spacecraft, ($E > \phi_A$), and secondaries and degraded primaries with energy less than the potential drop ($E < \phi_A$). The latter class is characterized by an up-down symmetry in their pitch angle distributions since the upcoming electrons from the atmosphere are all reflected by ϕ_A . Since the primary electrons are all accelerated to energies greater than ϕ_A , a detector whose energy band is entirely below ϕ_A will show an up-down symmetry as indicated in Figure 2a. In addition to the short-lived particles topologically connected to the atmosphere (shaded region in Figure 2a), one often sees a quasi-stable component of the fluxes in this energy range which are trapped between the magnetic mirror below the spacecraft and the electric mirror above (angular regions indicated by circles in Figure 2a). This population is fed by scattering and by fluctuations in the electric fields and, because of intensity fluctuations in the flux levels of the primaries, can build up to levels greater than the instantaneous levels observed in the loss cone. Examples of this class of signatures are the Region I electron fluxes in CMEA, CMEB, and CMEC shown in Figure 1 and the CMEA fluxes in the central portion of the event illustrated in Figure 7.

The electrons with $E > \phi_A$, generally exhibit a well-defined loss cone which destroys the up-down symmetry and establishes their identification. The loss cone is both widened and deepened by the potential below the spacecraft [Cladis et al., 1977] with the widening simply related to the magnitude of this potential through the expression:

$$\sin^2 \alpha_L = \frac{B_S}{B_T} \cdot \frac{E_S + \phi_B}{E_S} \quad (1)$$

where α_L is the angular half width of the loss cone. ϕ_B is the kinetic energy gained in the parallel field below the satellite, B_S and B_T are the magnitudes of the magnetic field at the location of the satellite and the top of the atmosphere respectively, and E_S is the measured energy of the electrons at the location of the satellite.

The primary electrons with energies only moderately greater than ϕ_A also exhibit an angular cutoff in the vicinity of 90° . This can be interpreted as a result of the action of the first adiabatic invariant:

$$\sin^2 \alpha_C = \frac{B_S}{B_1} \cdot \frac{E_S - \phi_A}{E_S} \quad (2)$$

where α_C is the angular location of the cutoff, ϕ_A is the kinetic energy gained in the parallel field between the satellite altitude and Z_1 (see Figure 2) and B_1 is the magnetic field strength at Z_1 . This equation has two quantities which are generally unknowns, ϕ_A and B_1 . B_1 is of particular interest since it is related to the vertical scale size of the ionospheric structure (labeled d in Figure 2) which can serve to help differentiate between various models for the cause of the parallel potential drops (e.g., double layers, oblique shocks, anomalous resistivity) which have character-

istically different scale sizes. In this work we will assume isotropy of the incident spectrum (for $Z > Z_1$) and utilize simultaneous measurements of electrons in the different energy ranges to provide information on both unknowns in Equation (2) thereby inferring values for the parameter d , as well as obtaining estimates of ϕ_A and ϕ_B from the measured cutoffs in the pitch angle distributions at α_C and α_L .

Since we are utilizing broad band electron detectors some uncertainty arises in the assignment of E_S in these expressions for α_C and α_L . To improve the accuracy of the estimates of ϕ_A , ϕ_B , and d one can fit an assumed distribution function to the detector response or otherwise use supplementary information from other detectors. We have taken this approach to estimate the energy E_S to be associated with the pitch angle α_C corresponding to 50% of the total reduction in the count rate in the region of the angular cutoff.

A more general and extended discussion of these and other signatures of parallel electric fields in the particle distribution functions has been presented by Kauffman et al. [1976], and Whipple [1977].

II. JULY 29, 1976, 11:28 UT EVENT

As discussed above, the up-down symmetry in the pitch angle distributions in CMEA, CMEB, and CMEC in Region I indicates that they are responding primarily to electrons with energies $< \phi_A$. This implies that the primary electrons are accelerated out of the detector's energy range and establishes a lower limit of $\phi_A \geq 5$ keV in this region. CMED which is responding to the primary portion of the electron spectrum shows the 90° minimums in the pitch angle distributions expected to result from ϕ_A as discussed in Section I. The transition from 90° maximum to 90° minimum type pitch

angle distributions evidently occurs in the lower end of the CMED energy window since the observed 90° minimums are occasionally somewhat obscured by electrons which retain the 90° peaked angular distributions characteristic of the lower energy channels (see Figure 1). The CMED pitch angle distribution for spin 3+ (i.e., the second of the two pitch angle scans on spin 3) is illustrated in expanded form as the upper curve of Figure 3. The average value of α_C as defined above for this distribution is 63° . In order to attempt to determine the uncertainty introduced by the contribution from the 90° peaked low energy electrons, we note from Figure 1 that the shape of the 90° maxima in the angular distributions is generally not a strong function of energy. This is illustrated in more detail for spin 3+ in Figure 4. We therefore subtract a quantity with the shape of the measured CMED pitch angle distribution from the CMED distribution in Figure 3 in order to evaluate the uncertainty such a contribution might introduce to the estimated value of α_C . The maximum magnitude such a contribution could have is that required to reduce the measured CMED 90° flux to zero. The residual CMED flux after the subtraction of such a distribution is illustrated by the lowest curve in Figure 3. A similar curve corrected for a 90° peaked contribution of half this magnitude is illustrated by the center curve. Both of these distributions yield average α_C values of 63° equivalent to that derived from the uncorrected (solid) curve. Thus the measured value of this quantity is insensitive in this case to the magnitude of the correction and can be used to estimate B_1 from Equation (2) and the parameter d as discussed in Section I.

Within the range of the CMED detector the electron flux during this period is generally decreasing with increasing energy [P. F. Mizera, private communication] and the midpoint of the energy band (15.4 keV) can be taken

as an upper limit on E_S . Using the lower limit of 5 keV on ϕ_A derived from the CMEC pitch angle distribution, we obtain $B_S/B_1 \geq 1.2$ and $d \geq 800$ km assuming a $1/r^3$ magnetic field dependence.

An alternative lower limit can be obtained provided there is some residual primary flux at 90° within the bandpass of the detector which has not been excluded by the action of ϕ_A (for example one of the two upper curves in Figure 3). In these circumstances, electrons with energies at least as low as the upper end of the CMED energy window (23.5 keV) can reach $\alpha \geq 90^\circ$ at the satellite altitude. Thus in Equation (2) we can set $\alpha_C = 90^\circ$ and $E_S \leq 23.5$ keV for a limit on $B_S/B_1 \geq 1.3$ and $d \geq 1100$ km.

The parallel potential drop below the spacecraft in region I is of relatively low magnitude. The width of the CMED loss cone ($\alpha_L = 19^\circ$) shown for spin 3+ in Figure 3 is equal to its expected value in the absence of such a potential. No upward-flowing ions (with $E > 0.5$ keV) were observed in the Lockheed mass spectrometers. The Aerospace electrostatic analyzers did in fact see weak upstreaming ion fluxes in the 100 eV range. [Mizera and Fennell, 1978] so a weak potential probably did exist below the spacecraft, but its magnitude was too low to be detected with the techniques utilized here.

Region II on the other hand is characterized by the signatures of a large ϕ_B . As discussed in Section I, one sees continuous upstreaming ion beams with energies up to 16 keV. The electron loss cones are also significantly widened with respect to Region I (see Figure 1). This is illustrated for spin 7+ in more detail in Figure 5 where for CMED $\alpha_L = 28^\circ$ corresponding to a $\phi_B = 13$ keV.

Another indicator of the strong ϕ_B in Region II is the dramatic suppression of the low energy secondary and degraded primary electrons in this region relative to Region I. A potential drop above the spacecraft is also

implied by this signature since the primary spectrum is accelerated to higher energies, but in general this is not sufficient to suppress the low energy electron fluxes since, depending on the primary spectrum, the fluxes of up-coming and reflected secondaries in a given low energy region can exceed the fluxes of primaries that existed in that region prior to the onset of the ϕ_A . The ϕ_B on the other hand acts both to reflect the lowest energy secondaries and reduce the level of the degraded primaries by the factor $E_S/(E_S + \phi_B)$ relating the flux at the top of the atmosphere to the flux at the satellite which enters through Liouville's theorem.

In contrast to the potential below the spacecraft, the potential above the spacecraft has not changed substantially between Region I and Region II. Even though the magnitude of the low energy secondaries and degraded primary electrons is suppressed, when detectable (i.e., in CMEC) they still exhibit the up-down symmetry characteristic of $\phi_A \gtrsim 5$ keV (see Figure 6). (Later, toward the end of Region II [spin 12] one sees in CMEC the transition to a loss cone/antiloss cone asymmetry indicating that ϕ_A is decreasing to the CMEC energy range [see Figure 1].) The CMED distribution for spin 7+ illustrated in Figure 5 shows a 90° minimum with $\alpha_C = 62^\circ$, about the same as in spin 3+, again approximately independent of a correction for a low energy component peaked at 90° . From the Aerospace spectrogram (op. cit.) one finds that the energy spectrum of the primary electrons in this period has not deviated appreciably from Region I. Thus we can conclude that the electric field geometry above the spacecraft is approximately the same as in Region I (d extending to $\gtrsim 10^3$ km) but that the field below the spacecraft has dramatically increased.

III. SEPTEMBER 15, 1976, 1058 UT EVENT

The July 29 event described in Section II was selected primarily to illustrate the relationship of the broad parallel electric field regions to the electrostatic shock regions observed by Mozer et al. [1977]. It was a relatively complicated event with overall potential drops of larger magnitude than are typical. In this section we will describe a simpler, less intense, and isolated event with a quasi-symmetric structure that allows for separation of spatial and temporal variations which generally are indistinguishable in measurements from a single satellite. Survey plots for this event are shown in Figure 7 in a format similar to Figure 1. One sees significant fluxes of upflowing ions and substantially widened loss cones in CMEB in the central portion of the event (spins 2, 3, and 4) indicative of a potential drop below the spacecraft. The maximum energy at which the upstreaming ion fluxes were observed was 1.76 keV on spin 3. In this same region one sees 90° peaked pitch angle distributions with an up-down symmetry in CMEA similar to those found in the low energy channels in the July 29 event. There are also 90° minimums in the CMEB distributions which are most obvious in the wings of the event, outside the region of the 90° maximums in the lower energy electrons. Narrowly collimated, field-aligned, downward-flowing electron "spikes" are seen at the edges of the event in CMEA. This is a commonly observed signature in this channel at the edges of the ionospheric structures. We interpret these data to indicate that there is a field-aligned potential drop above the spacecraft throughout the event, with weak ϕ_A at the edges of the event where CMEA is responding to primary electrons in the field-aligned spikes; and an increasing ϕ_A toward the center of the event where the depression in the CMEA flux levels and their up-down symmetry implies that $\phi_A \gtrsim .24$ keV.

The symmetric nature of the ionospheric structure in this event is best illustrated by intercomparing the pitch angle distributions at the high and low latitude edges of the event by "folding" Figure 7 so that the two CMEA spikes are superimposed. This has been done in Figure 8 where both the CMEA and CMEB responses are shown plotted versus pitch angle rather than time in order to provide a more precise intercomparison. As indicated in the figure, time progresses from left to right for the data from the high latitude edge of the structure and from right to left for the data from the low latitude edge. The remarkable correspondence indicates that we are traversing a temporally stable structure and that the observed variations are primarily spatial and angular. It also suggests that there is some significance to this pattern at the edges of the structure in terms of the mechanism responsible for its origin.

A CMEB pitch angle distribution measured near the center of the event is shown in Figure 9. As in the previous example, the 90° minimum is possibly somewhat obscured by a contribution from fluxes at the low end of the energy window with 90° peaked distributions similar to those observed in CMEA. Again this seems plausible since it is unlikely that the transition from 90° maximums to 90° minimums in the pitch angle distributions occurs exactly at the edge of the energy window. Also, similar to the July 29 example, the uncertainty in α_C introduced by such a 90° peaked contribution is small (see Figure 9). From the up-down symmetry of CMEA we can infer that all the primaries

have been accelerated out of its passband. This sets a lower limit on $\phi_A \geq .24$ keV. The low response in CMEC suggests that the spectrum is falling in the CMEB energy range, so for a lower limit on the parameter d we use the midpoint of the CMEB energy band for E_S and obtain $d \geq 1200$ km through the use of Equation 2.

As before an alternative limit can be obtained for models represented by the family of curves between the two extremes shown in Figure 9. For these cases, and for the upper curve, where there is a residual response at 90° due to the assumed isotropic incident spectrum, one can set E_S in Equation 2 equal to the upper edge of the CMEB energy window (1.13 keV) and obtain a lower limit on B_S/B_1 corresponding to $d \geq 1000$ km.

Burch et al. [1976] have found from measurements on a low altitude satellite beneath the electron acceleration regions in "inverted V" events that the electron distribution functions are well described by Maxwellian primary electron beams which have been accelerated through an electrostatic potential. A Maxwellian distribution has the property that acceleration through an electrostatic potential changes the magnitude but not the shape of the energy spectrum for energies greater than the value of the electrostatic potential. Thus under this assumption, the CMEB/CMEC response ratio R is a unique measure of the temperature of the Maxwellian, independent of ϕ_A , as long as ϕ_A is less than the lower edge of the CMEB energy window or .35 keV. As ϕ_A increases above this level it will depress this ratio since the primary electrons are excluded from the lower portion of the CMEB window. A plot of the CMEB/CMEC response ratio for this event is shown in Figure 10. The CMEB response was taken

at the peak of the pitch angle distribution on each spin while the CMEC response was averaged over the approximately isotropic region outside the loss cone. A plausible interpretation of these data is that the temperature is slowly varying throughout the event (except for the region of obvious hardening near spin 5+ associated with an increase in the CMEC response; see Figure 8) following the dashed curve in Figure 10. The depression in R from the dotted curve is then due to ϕ_A increasing above .35 keV. This interpretation is supported by the fact that we know from the depression in CMEA that ϕ_A is in fact increasing toward the center of the event, and by the approximate constancy in CMEC which would most likely be affected by a change in temperature. Under this interpretation, for spin 3+ we obtain $\phi_A = .54$ keV from the measured depression in R.

The widest CMEB loss cone in this event, indicative of the maximum value of ϕ_B , occurred on spin 3+ and is shown in Figure 9. Using this α_L value and the E_S obtained from fitting the above described Maxwellian to the CMEB response function, we obtain $\phi_B = 1.9$ keV from Equation 1. Thus the total parallel potential drop in this case is approximately 2.4 keV.

Another useful inference about the geometry of this event is obtained from the fact that the 90° minimums in CMEB are wider at the edges of the event (Figure 8) than in the center (Figure 9). We infer from the fact that the CMEA response has not yet fallen to the intensity level of the secondaries and degraded primaries that ϕ_A is less in these edge regions than in the central portion of the event. For a constant d , the 90° minimums should get narrower as ϕ_A gets smaller. Therefore d must be less at the edges than in the center.

4. Narrow spatial regions with measured electric fields of 10^2 mV/m which are referred to as electrostatic shocks by the Berkeley experiment/ [Mozers et al., 1977; Torbert and Mozers, 1978].

A-3

LMSC/D673078

IV. SUMMARY AND CONCLUSIONS

We have shown two examples of plasma measurements from within large scale ionospheric structures containing parallel electric fields. In the July 29, 1976 example there is an "inverted V" electron event of 4° latitudinal width within which there are two broad regions of parallel electric fields and a number of intense, narrow electrostatic shocks. Region I is inferred to have a parallel potential drop above the spacecraft of 5 kV or greater with a vertical dimension extending to $\sim 10^3$ km above the spacecraft. Region II has a similar field geometry above the spacecraft and in addition shows evidence of a potential drop below the spacecraft of 13 kV or greater. In the September 15, 1976 example we infer: 1. A stable spatial structure of approximately 2° latitudinal width; 2. A vertical dimension extending to $> 10^3$ km above the spacecraft, larger in the center of the structure than at the edges; 3. A total field aligned potential drop of 2.4 kV with both ϕ_A and ϕ_B reaching their maximum values in the center of the structure. All of these features are qualitatively consistent with the V-shaped potential models proposed by Gurnett [1972], Swift [1975], and others to explain "inverted V" events.

The simultaneous observation of signatures of ϕ_A and ϕ_B implies that the electric fields involved extend over a large vertical dimension. If we assume that the fields determined from the inferred potentials and vertical scale sizes are continuous and roughly independent of altitude, we obtain field strengths of the order of \sim mV/m in these broad scale regions in contrast to the $\sim 10^2$ mV/m fields reported in the narrow electrostatic shocks [Mozers et al., 1977]. The inferred vertical scale sizes are much larger than characteristic dimensions such as the deBye length or the ion gyro radius;

over vertical dimensions of $\sim 10^3$ km. These are possibly a different class of phenomena than those being studied by the Berkeley group [Mozer et al., 1977] whose experiment more naturally focuses on high electric field phenomena

A-4

LMSC/D673078

however, this analysis cannot in fact differentiate between extended regions of low field and multiple double layers with regions of intense fields extending over short vertical dimensions situated both above and below the satellite.

ACKNOWLEDGMENTS

We thank J. B. Cladis for valuable discussions and P. F. Mizera and J. F. Fennell for providing unpublished data. This work was supported by the Atmospheric Sciences section of the National Science Foundation and the Office of Naval Research.

which the electron fluxes, as measured by the Aerospace Corporation's electrostatic analyzers, show the characteristic signature of an "inverted V" event

A-5

LMSC/D673078

References

- Burch, J. L., S. A. Fields, W. B. Hanson, R. A. Heelis, R. A. Hoffman, R. W. Janetzke, Characteristics of auroral electron acceleration regions observed by atmospheric explorer C, J. Geophys. Res., 81, 2223, 1976.
- Cladis, J. B. and R. D. Sharp, Electrostatic potential differences along magnetic field lines inferred from satellite measurements of electron and ion distributions EOS, 58, 473, 1977a.
- Cladis, J. B. and R. D. Sharp, Distribution of electrostatic potential along magnetic field inferred from observations of ion and electron fluxes, EOS 58, 716, 1977b.
- Cladis, J. B., L. L. Newkirk, M. Walt, G. T. Davison, and W. E. Francis, Investigation of ionospheric disturbances, Report No. DNA-4225F, Defense Nuclear Agency, Washington, D. C. 20305, Jan. 28, 1977.
- Evans, D. S., Precipitating electron fluxes formed by a magnetic field-aligned potential difference, J. Geophys. Res., 79, 2853, 1974.
- Falthammer, C. G., Problems related to macroscopic electric fields in the magnetosphere, Rev. Geophys. and Space Phys., 15, 457, 1977.
- Ghielmetti, A. G., R. G. Johnson, R. D. Sharp, and E. G. Shelley, The latitudinal, diurnal, and altitudinal distributions of upward flowing energetic ions of ionospheric origin, Geophys. Res. Lett., 5, 59, 1978.
- Gurnett, D. A., Electric field and plasma observations in the magnetosphere in Critical problems of magnetospheric physics, edited by E. R. Dyer, IUCSTP Secretariat, National Academy of Sciences, Nov., 1972.
- Kauffman, R. L., D. N. Walker, R. L. Arnoldy, Acceleration of auroral electrons in parallel electric fields, J. Geophys. Res., 81, 1673, 1976.

LMSC/D673078

- Mizera, P. F., J. F. Fennell, and A. L. Vampola, Charged particle distributions in the presence of large d. c. electric fields, EOS, 58, 472, 1977.
- Mizera, P. F. and J. F. Fennell, quoted in Physics of heavy ions in the magnetosphere, by J. M. Cornwall and M. Schulz, in Solar System Plasma Physics, edited by C. F. Kennel, L. Lanzerotti, and E. Parker, North Holland Publ. Co., 1978 (in press).
- Mizera, P. F., and J. F. Fennell, Signatures of electric fields from high and low altitude particle distributions, Geophys. Res. Lett., 4, 311, 1977.
- Mozer, F. S., and C. W. Carlson, M. K. Hudson, R. B. Torbert, B. Parady, T. Yatteau, and M. C. Kelley, Observations of paired electrostatic shocks in the polar magnetosphere, Phys. Rev. Letters, 38, 292, 1977.
- Sharp, R. D., R. G. Johnson, and E. G. Shelley, Observation of an ionospheric acceleration mechanism producing energetic (keV) ions primarily normal to the geomagnetic field direction, J. Geophys. Res., 82, 3324, 1977.
- Shelley, E. G., R. D. Sharp, and R. G. Johnson, Satellite observations of an ionospheric acceleration mechanism, Geophys. Res. Lett., 3, 654, 1976.
- Swift, D. W., On the formation of auroral arcs and the acceleration of auroral electrons, J. Geophys. Res., 80, 2096, 1975.
- Torbert, R. B., and Mozer, F. S., Electrostatic shocks as the source of discrete auroral arcs, Geophys. Res. Lett., 5, 135, 1978.
- Whipple, E. D., Jr., The signature of parallel electric fields in a collisionless plasma, J. Geophys. Res., 82, 1525, 1977.

LMSC/D673078

FIGURE CAPTIONS

Figure 1 - Survey plots for July 29, 1976. Universal time (labeled SYST) is given on the abscissa. The location of four electrostatic shocks reported by Mozer et.al. (1977) are indicated by broad horizontal lines along the abscissa. The energy setting of the ion mass spectrometers (step number) is indicated at the top (see Table I.).

Figure 2 - Expected electron pitch angle distributions in the presence of a parallel electric field.

Figure 3 - CMED angular distribution on spin 3^+ , July 29, 1976. See figure 1 for definition of spin numbers.

Figure 4 - CMEA, CMEB and CMEC angular distribution on spin 3^+ , July 29, 1976.

Figure 5 - CMED angular distribution on spin 7^+ , July 29, 1976.

Figure 6 - CMEC angular distribution on spin 7 and 8, July 29, 1976.

Figure 7 - Survey plots for September 15, 1976. Format is similar to figure 1.

Figure 8 - CMEA and CMEB angular distributions at the two edges of the acceleration region. The vertical arrows indicate the direction of motion of the measured electrons.

between various models for the cause of the parallel potential drops (e.g., double layers, oblique shocks, anomalous resistivity) which have character-

A-8

LMSC/D673078

-2-

Figure 9 - CMEB angular distribution on spin 3^+ , September 15, 1976.

See figure 8 for definition of spin numbers.

Figure 10 - CMEB to CMEC response ratios over the acceleration region on September 15, 1976. The right hand ordinate shows the temperature of a Maxwellian determined by this ratio.

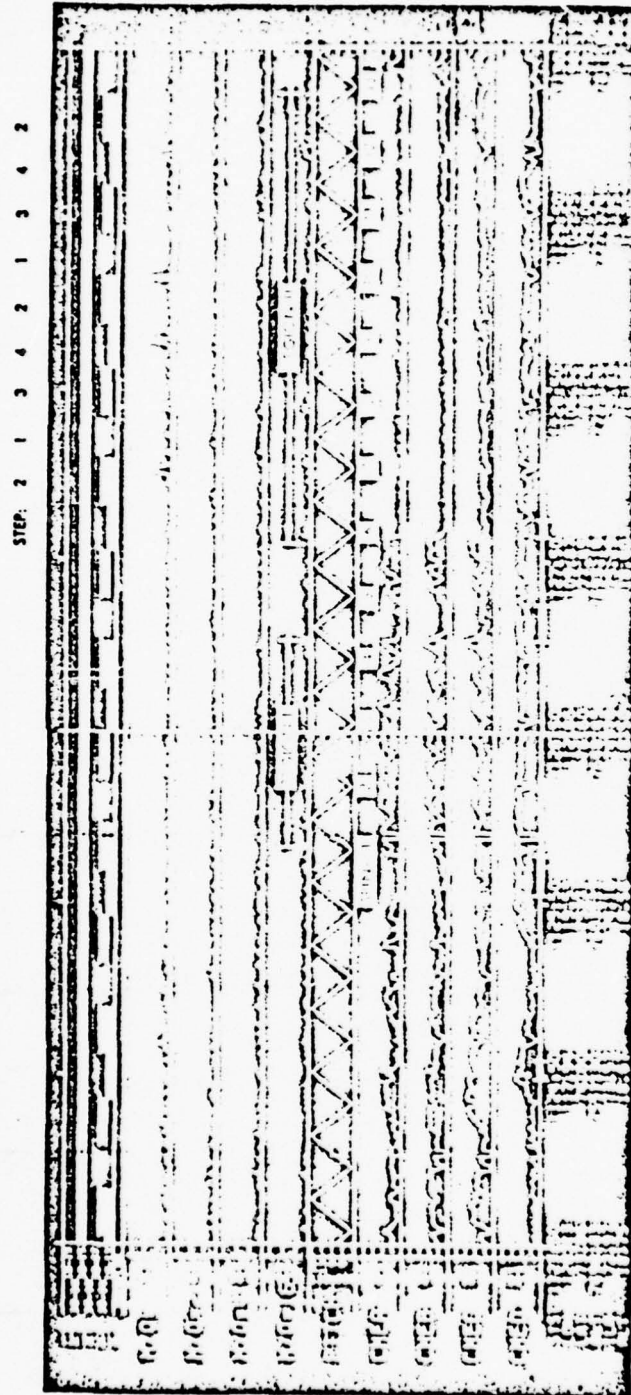
A-22

LMSC/D673078

TABLE I. DETECTOR CHARACTERISTICS

<u>DETECTOR</u>	<u>PARTICLE</u>	<u>ENERGY, keV</u>	<u>GDE, cm² sr keV</u>			
CMEA	Electrons	0.07 - 0.24	1.2 x 10 ⁻⁶			
CMEB	Electrons	0.35 - 1.1	6.5 x 10 ⁻⁶			
CMEC	Electrons	1.6 - 5.0	1.9 x 10 ⁻⁵			
CMED	Electrons	7.3 - 24	6.5 x 10 ⁻⁵			
Energy per unit charge						
		Step 1	2	3	4	
CXA 1	Ions	0.50	0.68	0.94	1.28	
CXA 2	Ions	1.76	2.4	3.3	4.5	
CXA 3	Ions	6.2	8.5	11.6	16.0	

LMSC/D673078



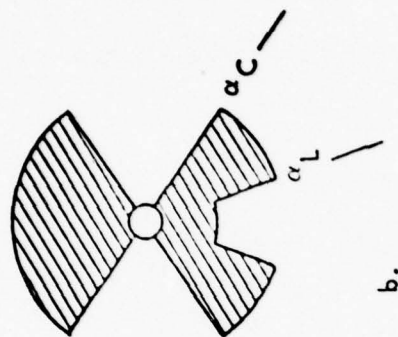
sion of the low energy secondary and degraded primary electrons in this region relative to Region I. A potential drop above the spacecraft is also

A-11

LMSC/D673078

ELECTRON PITCH ANGLE DISTRIBUTIONS

PRIMARIES, $E > \phi_A$



SECONDARIES AND DEGRADED
PRIMARIES, $E < \phi_A$

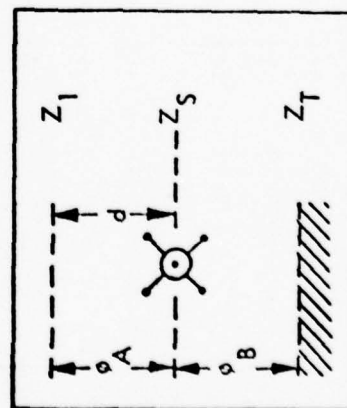
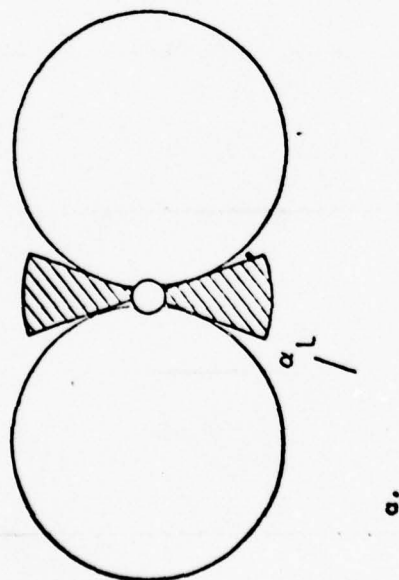


Figure 2

A-25

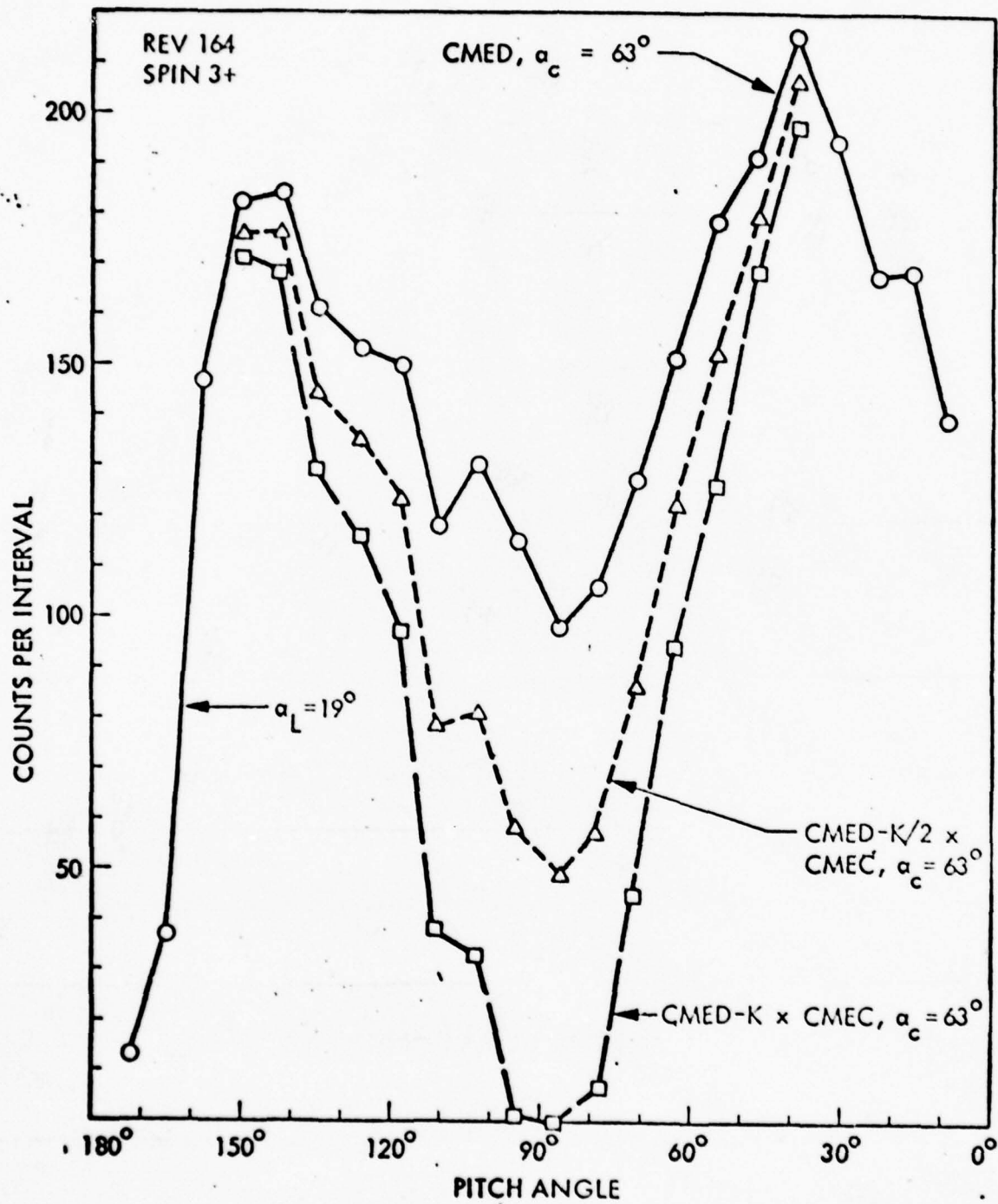


Figure 3

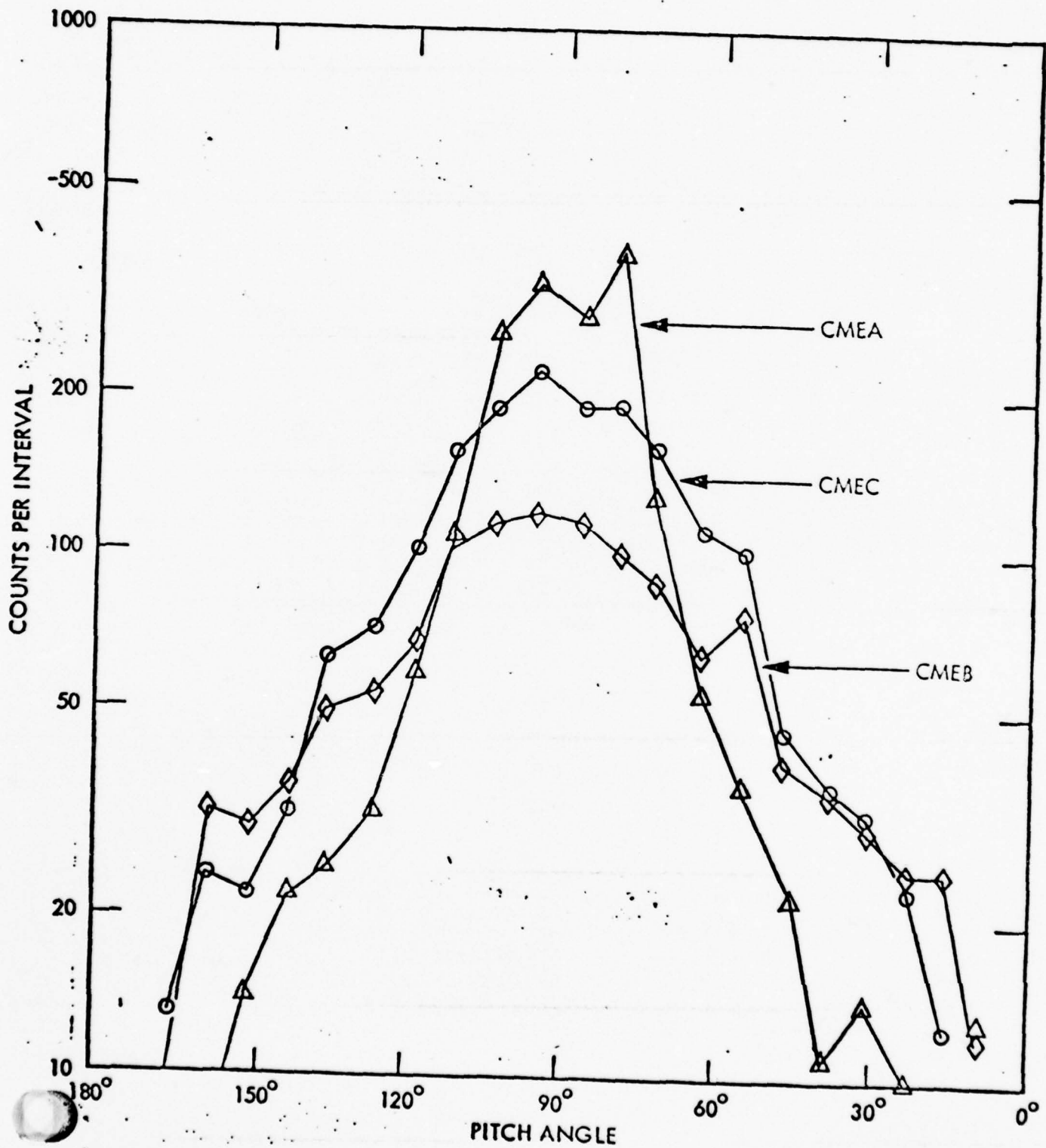


Figure 4

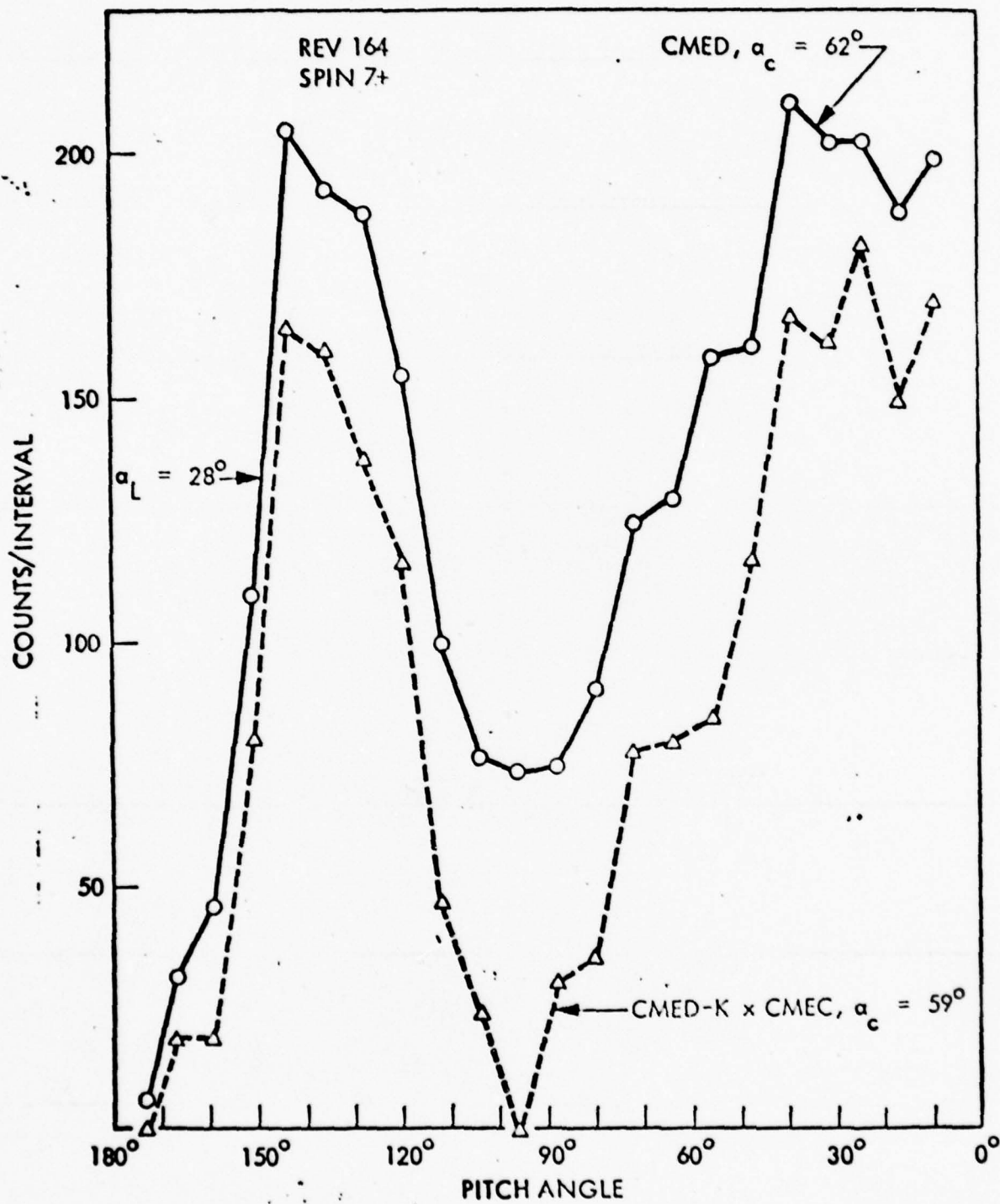


Figure 5

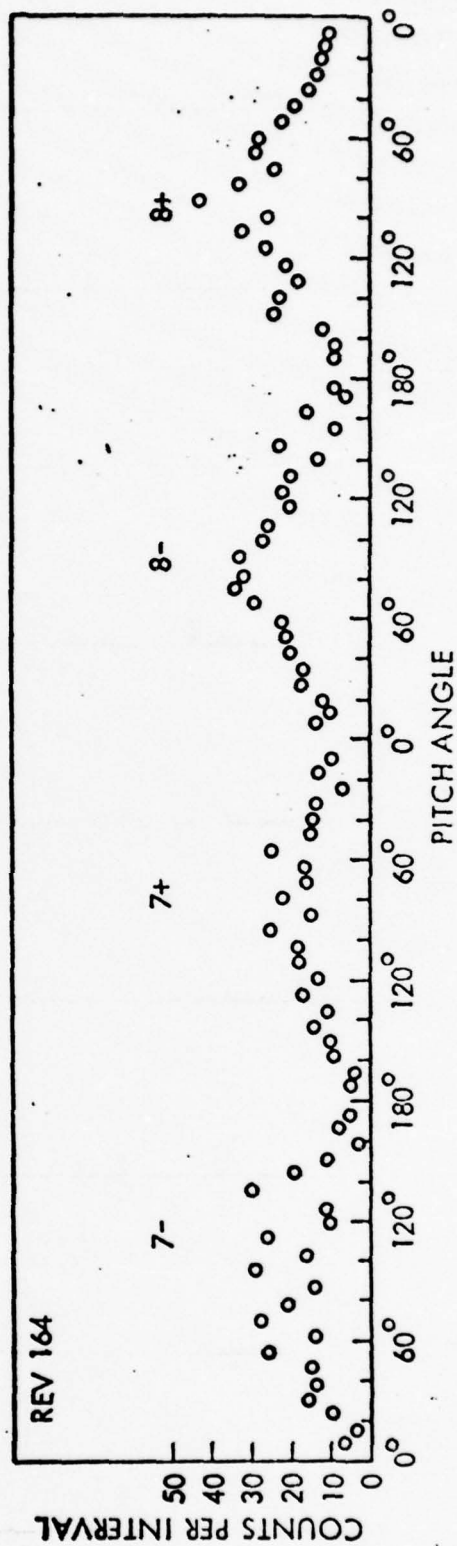


figure 6

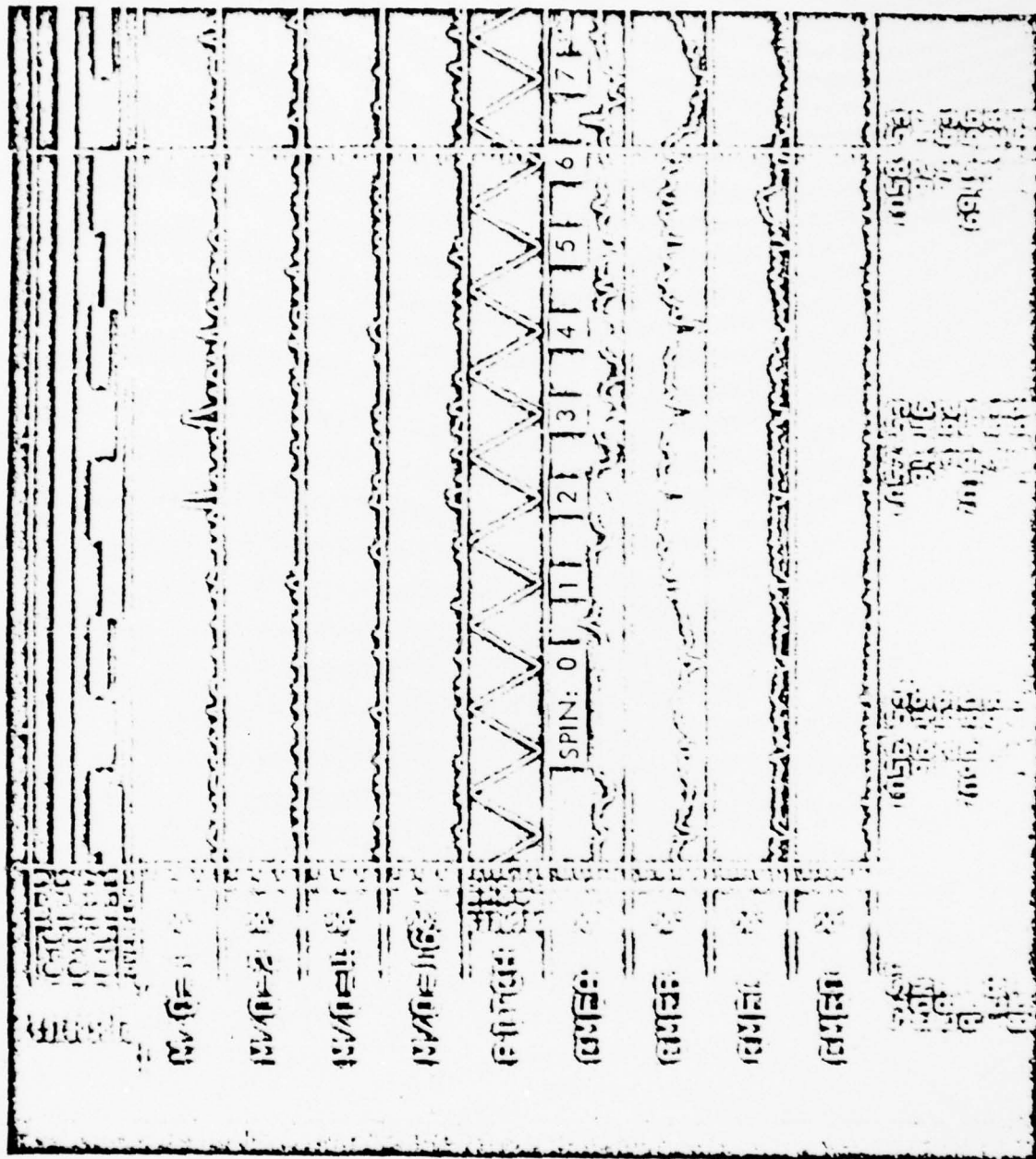
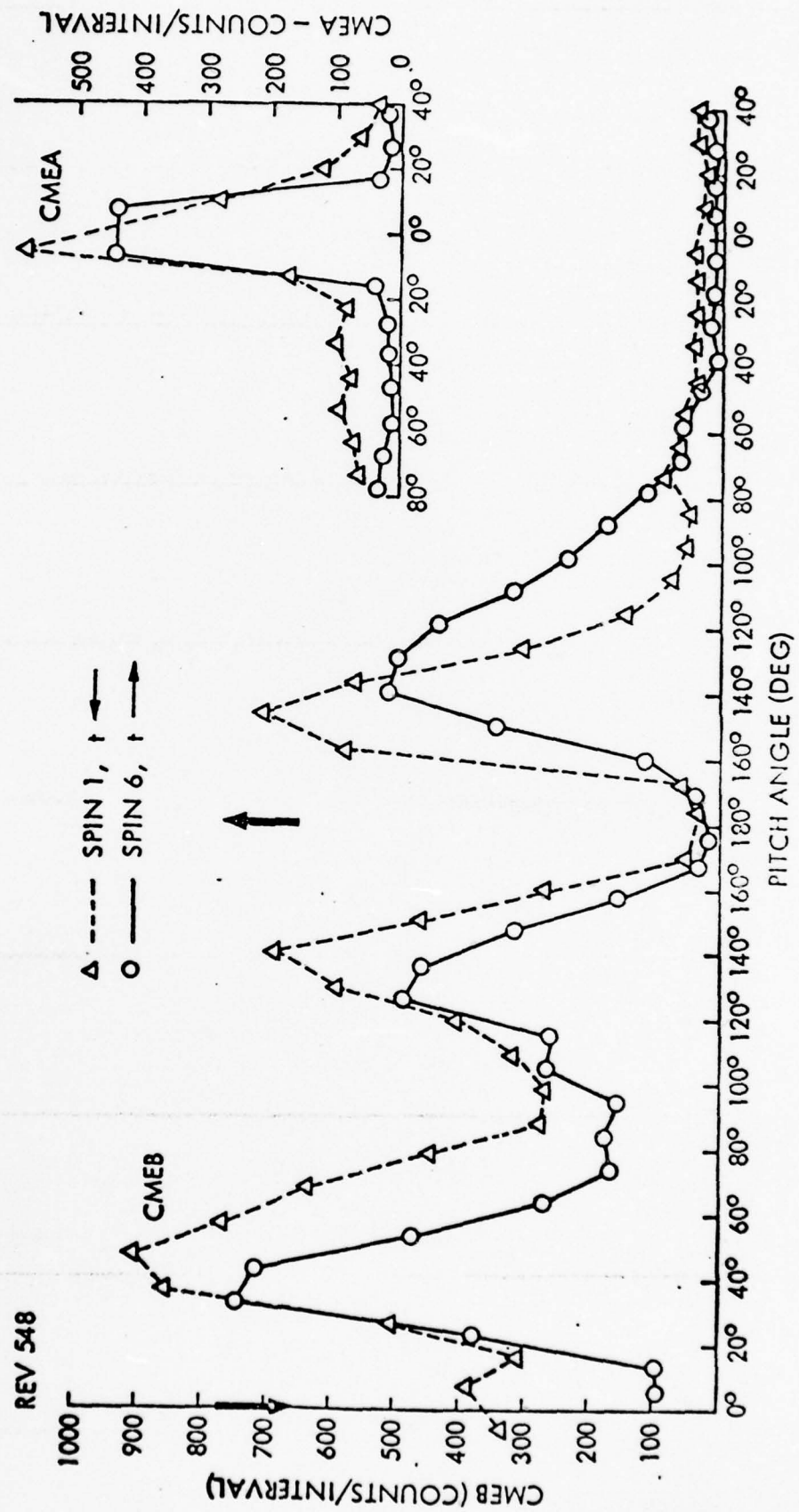
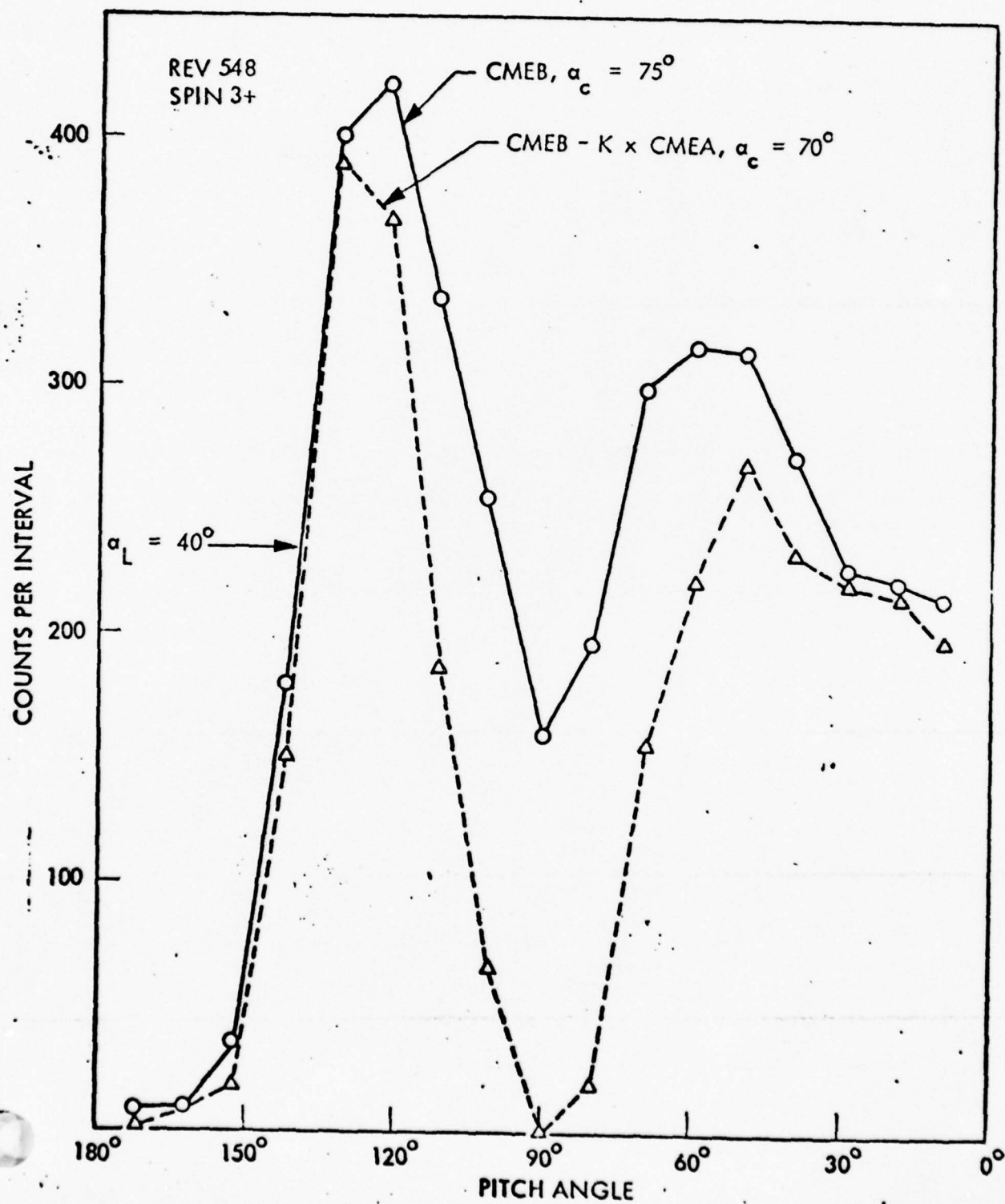


Figure 7





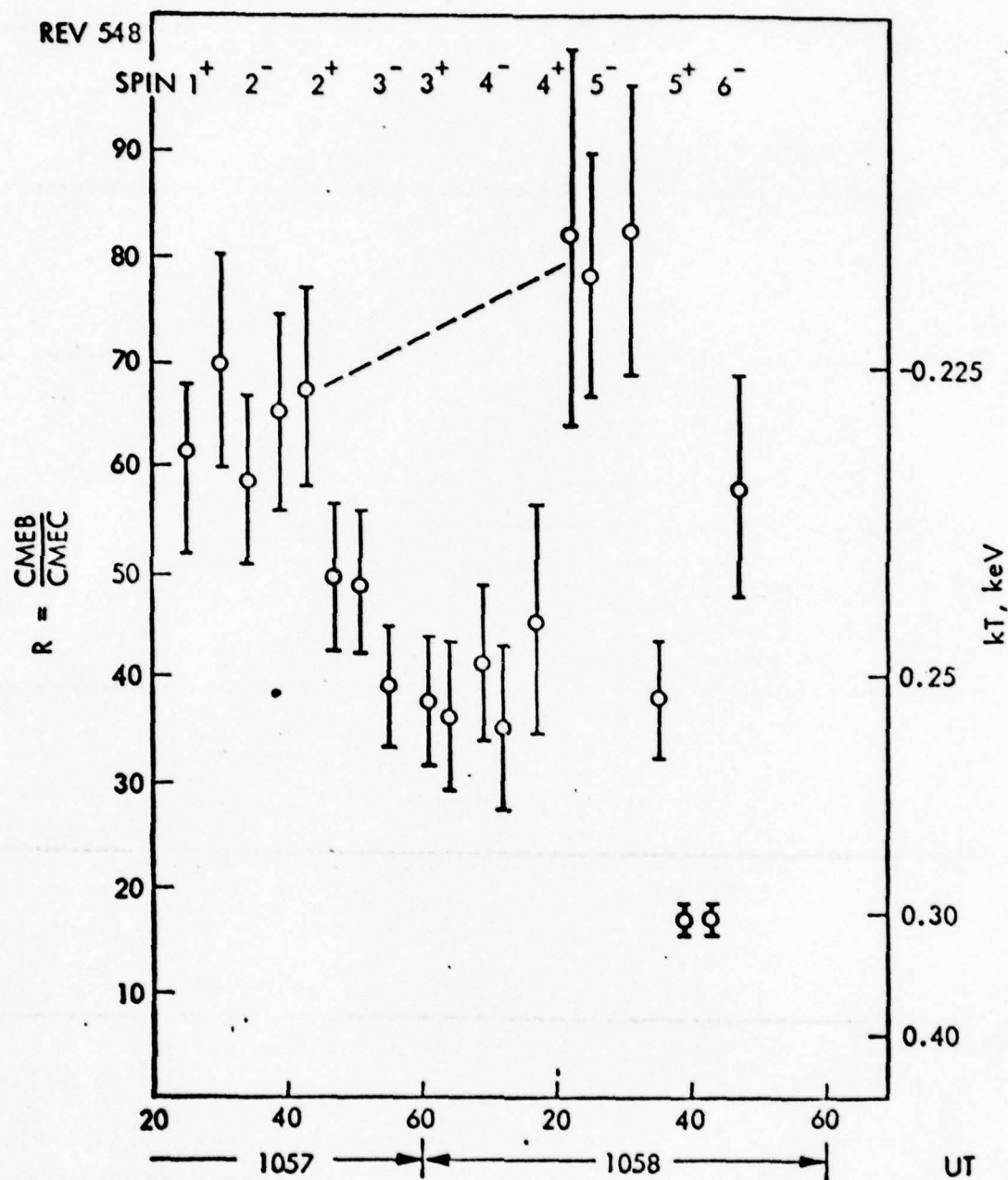


Figure 10

LMSC/D673078

APPENDIX B

Scale of Electric Field Along Magnetic
Field in an Inverted-V Event

J. B. Cladis and R. D. Sharp

Lockheed Palo Alto Research Laboratory

Palo Alto, California 94304

ABSTRACT

The characteristics of magnetic-field-aligned-electrostatic-potential differences in the structure of an inverted-V event were examined using data on the pitch-angle and energy distributions of electrons and ions obtained with the polar-orbiting S3-3 satellite. Potential differences were found to occur simultaneously above and below the altitude of the satellite (≈ 7260 km). Both of these potential differences were determined from an analysis of the electron distributions. The analysis also yielded the magnetic field intensity, B_1 , above the satellite where the potential was zero. This value of B_1 indicates that the potential extends above the satellite a distance ≈ 1200 km, implying an apparent electric field of ≤ 1 mV/m. The total potential difference was found to have an inverted-V distribution in latitude, with a peak value of ≈ 4.3 kV and a latitudinal width of $\approx 1^\circ$. Upward-flowing H^+ and O^+ ions, with pitch angles $\leq 10^\circ$ were observed in the structure. Their energy spectra were peaked at energies near the potential differences below the satellite, but were very broad indicating perpendicular heating and an ion source within the potential region. Implications to theory are discussed.

Moreover, analysis of the magnetometer data obtained on the S3-3 satellite during several traversals of the potential region revealed field-aligned current densities in those regions of $1-10 \mu\text{A}/\text{m}^2$ (Torbert and Mozer, 1977).

The observations indicate that a current-driven instability, generating electrostatic waves, may provide the mechanism necessary to support the field-aligned potential differences in the absence of collisions (see review by Fälthammar, 1977). Three such instabilities have been proposed, which may be identified experimentally by the scale of the electric field: (i) the electric double layer (Block, 1975; Block and Fälthammar, 1976) has a thickness measured in Debye lengths ($\leq 10\text{m}$ at an altitude of $1 R_E$ in the auroral zones); (ii) the oblique electrostatic shock (Swift, 1975) has a thickness measured in the gyro-radii of the energetic ion component; and (iii) anomalous resistivity (Kindel and Kennel, 1971) predicts a scale $> \Delta\phi/E_w$, where $\Delta\phi$ is the potential difference along the magnetic field and E_w is the electric field of the wave turbulence (Fälthammar, 1977).

In this report we will present an example of the ion and electron data obtained by the Lockheed instruments (see e.g. Shelley et al., 1976) on a satellite pass through one of the potential regions. The characteristics of the potentials inferred from these measurements will be described, and the implications of the results to theory will be discussed.

MEASUREMENTS

The Lockheed experiment (see Shelley et al., 1976; Sharp et al., 1977) on the S3-3 satellite measures the energy and pitch-angle distributions of ions in the energy-per-charge range 0.5 to 16 keV and electrons in the range 70 eV to 24 keV. The measurements are obtained with three ion mass spectrometers and four magnetic electron spectrometers mounted such that their view directions are perpendicular to the spin axis of the satellite. The spin rate of the satellite is ~ 3 RPM about an axis perpendicular to the orbital plane; hence a nearly complete pitch-angle scan is obtained in about 10 sec. The ion spectrometers sample the mass-per-charge (M/Q) distribution in the range 1-30 once per second. Each ion spectrometer has 4 energy-per-charge settings which are stepped every 16 sec. The energy settings of each ion spectrometer together with the energy response of the electron spectrometers are listed in Table I.

A survey plot of the data obtained over the northern hemisphere auroral zone on September 15, 1976 is shown in Figure 1. At the bottom of the chart are shown the universal time (SYST), longitude, latitude, altitude, invariant latitude (ILA), and magnetic local time. The four lowest panels show the logarithm of the counts per half-second of the electron spectrometers. The panel labeled PITCH shows the pitch angle of the measured particles. Here, the pitch angle of 0° denotes particles moving directly down the field lines. The next four panels show the logarithm of the sum of the counts per second of the 3 mass spectrometers for ions of $M/Q = 1, 2, 4$, and 16, respectively. A code designating the energy steps of the mass spectrometers is in the top panel.

Although upward moving ions, closely aligned with the magnetic field, are good indicators of a potential difference below the satellite, they do not provide accurate information on the magnitude of the potential difference; their energy spectra, as discussed by Ghielmetti et al (1978), are not simply related to the potential drop.

The satellite entered the potential region following the spin period denoted by the number 1 under the pitch-angle panel (1052:47 UT) and left the region on spin 5 (1054:37 UT). The spin numbers are labeled at the centers ($\alpha = 180^\circ$) of the spin periods. Note that for many spin periods prior to 1, the counting rates of the electron detectors were fairly uniform except for the loss cones due to the atmosphere below the satellite. In this region, the counting rates imply a Maxwellian electron distribution with a number density of $0.66/\text{cm}^3$ and a temperature of 0.8 keV. On spins 2 and 3 note that all the loss cones become wider and deeper, those of the lower energy electrons being more strongly affected; the CME B counting rate outside the loss cone increases somewhat; and the CME A counting rate becomes lower and has maxima at pitch angles near 90° . These characteristics, as discussed below, are due to a potential difference along the magnetic field, principally below the satellite, accelerating electrons, downward. On spin 4 the counting rates of the CME B and CME C detectors develop "butterfly" pitch-angle distributions (minima at 90°). These distributions imply a much higher potential difference above the satellite. Note from the $M/Q = 1$ and 16 panels that H^+ and O^+ ions were moving upward along the field during spins 2, 3, and 4.

ANALYSIS OF ELECTRON MEASUREMENTS

The potential differences along the magnetic field can be determined from the widths and depths of the loss cones. At two points, (B_s, ϕ_s) and (B, ϕ) , along the dynamical trajectory of an electron, the energy, w , and pitch angle, α , of the electron are related by the equations expressing the conservation of the magnetic moment of the electron and the total energy, viz.,

$$\frac{w_s}{B_s} \sin^2 \alpha_s = \frac{w}{B} \sin^2 \alpha \quad (1a)$$

and $w = w_s + e(\phi - \phi_s) \quad (1b)$

Here, B is the magnetic field intensity, ϕ is the electrostatic potential, and e is the absolute value of the electron charge. The subscript, s , denotes the values of the parameters at the location of the satellite. Hence, if B_t designates the limiting field intensity at the "top" of the atmosphere where the electron mirrors before suffering collisional effects, and where $\phi = \phi_m$, the edge of the loss cone, $\alpha_s = \alpha_c$, is given by the equation

$$\alpha_c = \sin^{-1} \left[\frac{B_s}{B_t} \left(1 + \frac{e(\phi_m - \phi_s)}{w_s} \right) \right]^{1/2} \quad (2)$$

The potential ϕ , toward lower altitudes, is assumed to increase monotonically from 0 to its maximum value, ϕ_m , and then to remain constant. The effect of the shape of ϕ along the magnetic field is mentioned below in the discussion of Figure 6. ✓

Expanded plots of the counting rates of the CME B and CME C detectors are shown in Figure 2 and 3. Here, the spin numbers, with the superscripts - and + denoting respectively the pitch angle scans obtained during the first and second halves of the spin period, are shown on the curves. These figures show clearly the increase in the widths and depths of the loss cones from spin 1 to spin 3. However, the value of $\phi_m = \phi_s$ obtained through the applications of Eq. (2) is somewhat uncertain, principally because the detectors respond to a fairly wide range of energies, rendering an uncertainty in the effective value of w_s and smearing α_c .

An improved determination of $\phi_m - \phi_s$ was obtained by computing the energy and pitch-angle distributions of electrons that were backscattered by the atmosphere using the AURORA code (Walt et al., 1968). The backscattered flux, computed as discussed below, was integrated over the energy response functions of the detectors to determine the expected counting rates of the detectors in the region of the loss-cone "knee" for various potential differences below the satellite. The value of $\phi_m - \phi_s$ was then determined by comparing the locations of the computed knees with the experimental values at the points of highest curvature. The AURORA code was also used as described below to determine the potential difference from the deepening of the loss cones. (The loss cones deepen because only those backscattered electrons with sufficient energy to penetrate the potential $\phi_m - \phi_s$ can reach the satellite.)

Many of the backscattered electrons are reflected by the potential ϕ_m and returned to the atmosphere where they combine with the primary electrons to enhance the backscatter (Evans, 1975). This effect was taken into account by using an iteration procedure to compute the equilibrium flux. The primary flux at B_1 , the magnetic field intensity where $\phi = 0$, was assumed to be the Maxwellian distribution that was measured on spin 1. This flux was transformed through ϕ_m to B_t , using Liouville's theorem, where it was used as input to the AURORA code to compute the first approximation to the backscattered flux. Those electrons which were reflected by the potential ϕ_m were then added to the previously-determined incident flux, and this flux was again used as input to the AURORA code to compute the next approximation to the backscattered flux. The computation was continued in this manner until the backscattered flux converged to a steady value. The flux was then transformed from B_t to B_s , through the

potential difference $\phi_m - \phi_s$, to compute the associated counting rates of the detectors in the loss cone. The computations were performed for values of $\phi_m - \phi_s$ of 0, 1.5, 3, and 4.5 kV. Figure 4 shows the computed widths of the loss-cones for the CME B and CME C detectors, measured to the largest-curvature point of the knee, plotted against $\phi_m - \phi_s$. These results are not very sensitive to the distribution of the electrons at $\phi=0$ for $\phi_m - \phi_s \geq 1.5$ kV.

In the center of the loss cones, the computed counting rates were less than the actual counting rates of the detectors, even for spin 1 where the potential was essentially zero. This discrepancy may exist because the version of the AURORA code used for this analysis does not compute the production of secondary electrons, which may contribute significantly to the backscattered flux. Because of this difficulty, the loss-cone depth computed for each value of $\phi_m - \phi_s$ was divided by the depth computed for $\phi_m - \phi_s = 0$, and these ratios were compared with the corresponding experimental ratios, i.e., the loss-cone depth observed in the potential region divided by the depth observed on spin 1. Here, the loss-cone depth is defined as the ratio of the counting rate at α_c to the counting rate at $\alpha = 180^\circ$. This procedure tends to cancel errors in the backscattered flux which are proportional to the flux. The computed ratios of the loss-cone depths for the CME C detector are shown in Figure 5 plotted against $\phi_m - \phi_s$.

The resulting potential differences below the satellite, inferred from both the widths and depths of the loss cones on the pass through the potential region, are shown in Figure 6. The values determined from the widths of the loss cones are regarded to be the more accurate, and the uncertainties of these values due to the uncertainties in α_c are estimated to be within the error bars shown in the figure. Another source of error may be due to an effect of the shape of the potential distribution in the calculation of the

backscattered flux at the satellite. The satisfaction of the conservation laws (1) at the two points (B_t, ϕ_m) and (B_s, ϕ_s) does not assure that the electron trajectory will go through those points. The electron moving upward from the atmosphere could still be reflected backward before reaching B_s because of an appropriately shaped potential distribution between the points (see Chiu and Schulz, 1978; Whipple, 1977; and Cladis, et al., 1977). Chiu and Schulz (1978) point out that such reflection does not occur if the potential, $\phi(B)$, when plotted against B , is concave downward between the two points. In general, the effect is less likely to occur if the scale of the electric field is large; according to Cladis, et al. (1977), a necessary condition for the reflection is that the downward electric force $e\nabla_{11}\phi$ acting on the electron be greater than the oppositely-directed magnetic force $-\mu\nabla_{11}B$, at least at one point within the interval (μ is the magnetic moment of the electron, and ∇_{11} is the component of the gradient parallel to the magnetic field). This is not a sufficient condition, however: Even if $\phi(B)$ is a step function, it can still be penetrated by an electron that satisfies (1) if the potential step is located at a sufficiently low value of B within the interval. Nevertheless, two aspects of the data indicate that an appreciable error was not introduced by the potential-shape effect: (i) for each spin period, the potential differences, $\phi_m - \phi_s$, inferred from the edges of the pitch-angle distributions given by the counting rates of the detectors with different pass-band energies (CME B and CME C), were in good agreement; and (ii) the shapes of the counting-rate curves for the different detectors in the regions of the pitch-angle knees were quite similar to the corresponding counting-rate curves based on the computed backscattered flux.

The potential differences ϕ_s above the satellite are also shown in Figure 6. The value of ϕ_s on spins 2 and 3 was estimated from the increase in the counting rates of the CME B and C detectors outside the loss cones, and the reduction of the CME A counting rate. The potential ϕ_s shifts the spectrum and, according to Liouville's theorem, increases the directional flux observed by the detectors ($w_s > e \phi_s$) by the factor $(w_s + e \phi_s)/w_s$. The value $\phi_s \sim 0.25$ kV was estimated from the increase in the electron flux implied by the counting rates of the detectors relative to those on spin 1 and using for w_s the central band pass energies. By falling through this potential, the primary electrons acquired energies beyond the pass band of the CME A detector. The magnitude of its counting rate and the approximate symmetry of the counting rate about $\alpha_s = 90^\circ$ indicate that it was detecting principally backscattered electrons that were reflected downward by the electric field above the satellite.

On the pitch-angle scans 2^+ and 4^- , the CME A detector was probably also counting electrons that were trapped, at least temporarily, between the magnetic field below the satellite and the electric field above. Electrons may become locally trapped in this manner by time and/or space variations of the electric field along the electron trajectories. Our analysis of the CME A counting rate, as well as the CME B counting rate on spin 4 which is discussed below, reveals that the local trapping consists mainly of degraded primaries and scattered electrons which had pitch angles near 90° at the "top" of the atmosphere, where $B = B_t$. The trapping may occur for energies in the range,

$$\frac{e (\phi_m - \phi_s)}{\frac{B_t}{B_s} \sin^2 \alpha_s - 1} \leq w_s \leq \frac{e \phi_s}{1 - \frac{B_1}{B_s} \sin^2 \alpha_s} \quad (3)$$

This range increases from zero at

$$\alpha_s = \alpha_s^* = \sin^{-1} \left[\frac{B_s \phi_m}{B_1 (\phi_m - \phi_s) + B_t \phi_s} \right]^{1/2} \quad (4)$$

where the limiting energy $w_s = w_s^*$ is obtained by putting $\alpha_s = \alpha_s^*$ in the equation on either side of (3), to a maximum at $\alpha_s = 90^\circ$.

The right-hand side of (3) follows from the conservation of the magnetic moment for electrons mirroring above the satellite, at B_1 where $\varphi = 0$. The left-hand side of (3) follows from the conservation of the magnetic moment for electrons mirroring at B_t . The minimum energy for trapping is given by the left-hand side of (3) for $\alpha_s = 90^\circ$. This energy is within the upper portion of the pass band of the CME A detector. The trapping of these electrons may therefore account for the sharp peaks of the CME A counting rate centered at $\alpha_s = 90^\circ$ on scans 2^+ and 4^- . Unfortunately, the maximum energy of the trapped electrons, given by the right-hand side of (3), is much beyond the pass band of the detector for all values of $\alpha_s > \alpha_s^*$, hence this detector cannot provide information on B_1 .

The CME B and CME C counting rates on spin 4 provided information on both ϕ_s and B_1 . Since the potential above the satellite increases the energy component of the primary electrons along the magnetic field, the electrons become more aligned with the magnetic field, and the alignment is closer for the lower-energy primaries. Such downgoing primaries, together with those which are reflected by the magnetic field below the satellite, form a butterfly pitch-angle distribution. The butterfly shape of the CME C counting rate (see Figure 3) on spin 4 is due mainly to the acceleration of the primaries. A potential ϕ_s that accounts for the pitch-angle distribution of the primaries detected by the CME C detector causes the lower-energy primaries observed by the CME B detector to appear only at very small angles to the field. Hence, the energy $e\phi_s$ must have been within the upper portion of the CME B pass band to account for both the higher counting rate near $\alpha_s = 0^\circ$ (due to downgoing primaries),

relative to that near $\alpha_s = 180^\circ$ (backscattered electrons), and the symmetry of the counting rate about 90° at pitch angles that are more inclined with the magnetic field. The latter is due to backscattered electrons that were also reflected downward by ϕ_s , and locally-trapped electrons.

The values of ϕ_s and B_s were estimated from the CME C counting rate by assuming the primary electrons at B_1 to be isotropic in the downward hemisphere and to have the Maxwellian distribution that was measured on spin 1. The directional flux of these electrons at the satellite, B_s , from Liouville's theorem, is

$$j(w_s, \alpha_s, B_s) = \frac{n_o w_s}{(2 \pi^3 m w_e^3)^{1/2}} \exp \left[-(w_s - e \phi_s)/w_e \right] \quad (5)$$

where, from the conservation of the magnetic moment,

$$\alpha_s = \sin^{-1} \left[\left(1 - \frac{e \phi_s}{w_s} \right) \frac{B_s}{B_1} \sin^2 \alpha_1 \right]^{1/2} \quad (6)$$

for $w_s \geq e \phi_s$. As mentioned previously, $n_o \approx 0.7/\text{cm}^3$ and $w_e \approx 0.8 \text{ keV}$; α_1 is the pitch angle of the electrons at B_1 . The counting rate of the CME C detector due to this flux is given by the integral,

$$\text{CR}(\alpha_s) = G \int_{w_1}^{5 \text{ keV}} j(w_s, \alpha_s, B_s) dw_s \quad (7)$$

$G = 5.4 \times 10^{-6} \text{ cm}^2 \text{ sr}$ is the geometric factor of the detector, and w_1 is the larger of $w_L = 1.6 \text{ keV}$ (the low-energy limit of the detector band pass) or

$$w_1 = \frac{e \phi_s}{1 - \frac{B_1}{B_s} \sin^2 \alpha_s} \quad (8)$$

which follows from (6) for $\alpha_1 = 90^\circ$. Note that the flux given by (5) is constant over the pass band of the detector in the pitch-angle range $0 \leq \alpha_s \leq \alpha_L$, where α_L follows from (8) for $w_1 = w_L$. Hence, the counting rate of the detector should be constant in that pitch angle interval. The situation is illustrated in Figure 7, which depicts the response of the detector, as a function of pitch angle, on the contours of constant flux obtained by transforming the isotropic flux from $B_1, \phi = 0$ to B_s, ϕ_s . The relationship between ϕ_s and B_1 at the limit of the constant counting-rate interval, given by the equation,

$$e \phi_s = w_L \left(1 - \frac{B_1}{B_s} \sin^2 \alpha_L\right) \quad (9)$$

is valid for an isotropic flux at B_1 , regardless of the energy distribution. From Figure 3, on spin 4⁻, it appears that $\alpha_L \approx 60^\circ$. At the higher pitch angles, the counting rate decreases because w_1 increases and the integration (7) is over the higher-energy portion of the energy spectrum. The distribution shown on spin 4⁻ can be closely matched with $\phi_s = 0.8$ kV and $B_1/B_s = .77$.

In order to test the sensitivity of these results to the assumed conditions, these calculations were also done for Maxwellians of different temperatures and for lower counting rate minima at 90° . (The counting rate due to the primaries would be lower there if the detector were also counting backscattered and trapped electrons). A distribution similar to that on spin 4⁻, but with zero counting rate at 90° , was computed for $\phi_s = 0.66$ kV and $B_1/B_s = .86$. Using $\phi_s = .8$ keV and $B_1/B_s = .77$, but changing the temperature of the Maxwellian from .8 to .6 keV principally decreased the counting rate at 90° by about 50%; increasing the temperature from .8 to 1 keV, increased the 90° counting rate by about 43%. A variation of the 90° counting rate of $\pm 50\%$ was found to correspond to a variation in ϕ_s of $\pm 5\%$, and in B_1/B_s of $\pm 5\%$.

Note that the value $\phi_s \approx .8$ kV, which is near the upper limit of the pass band of the CME B detector, is also consistent with the discussion above regarding the counting rate of that detector on spin 4. Moreover, by substituting the values $\phi_s = .8$ kV, $\phi_m = 2.6$ kV, $B_1/B_s = 0.77$, and $B_s/B_t \approx 1/8$ in Equation (3), the energy range of the temporarily-trapped electrons near the edge of the loss cone, where the CME B counting rate is a maximum, is found to be 0.6 to 1.3 keV. The minimum energy of the downgoing primaries at B_s is .8 keV, for $\phi_s = .8$ kV; hence, a high flux of degraded primaries would return to the satellite with energies in the trapping range. The flux at the maximum, therefore, appears to consist of degraded primaries that are backscattered and temporarily trapped, as discussed before, making at least one bounce from the electric field above the satellite. The decrease of the counting rate toward $\alpha_s = 90^\circ$ appears to be due to the decreasing fluxes of successively lower energy electrons of the atmospheric backscatter that are temporarily trapped.

As the boundary of the potential region was approached, near the end of the 4^+ scan, ϕ_s decreased to zero, as evidenced by the sharp increase in the counting rate of the CME A detector (note counting rate "spike" in Figure 1). Simultaneously, as shown in Figure 1, the flux of the high-energy primaries seen by the CME C detector increased sharply to a maximum (see also Figure 3). Subsequently, the CME C and CME B counting rates decreased steadily, reaching the minimum values at the end of the 5^- scan. There, the potential difference below the satellite also must have been near zero because the upward-moving ions were not observed.

ION MEASUREMENTS

The upward-moving ions observed on spins 2, 3, and 4 had pitch angles less than about 10° . They consisted of H^+ and O^+ , but the O^+ flux was lower than the H^+ flux by about an order of magnitude. The energy spectra of the H^+ ions on the 3 spins, which include the data from the Aerospace electrostatic analyzer (Mizera and Fennel, 1978) as well as the Lockheed mass spectrometer, are shown in the 3 panels of Figure 8. The Aerospace data have not been corrected for the small contribution from O^+ . The times of the measurements are shown in the panels. Because of the angular displacement of the spectrometer apertures about the spin axis, the Lockheed observations of the source cones followed by Aerospace observations by ≈ 5 seconds. The differences between the two data sets seen in Figure 8 could result from spatial and/or temporal fluctuations during this interval. The calibrations of the two spectrometers were reconciled by inter-comparisons in the slowly varying, nearly isotropic fluxes of the radiation belts, but no attempt has been made to unfold the angular distributions of the upflowing ions from the instrument response functions. The values given, therefore, represent averages over the fields of view of the respective spectrometers ($6^\circ \times 5^\circ$ full width for the Lockheed instrument and $10^\circ \times 25^\circ$ full width for the Aerospace instrument). Since the field of view of the Aerospace instrument was larger than the angular width of the ion beams, the Aerospace points should be considered strictly as lower limits. The spectral shapes shown should be valid, however, if the cone widths are not a strong function of energy.

Since the Lockheed mass spectrometer is designed to scan rapidly with respect to mass, it acquires only a three-point energy distribution on each spin. The more complete spectrums determined by the Aerospace spectrometers indicate that the peak fluxes are at energies that are roughly comparable to the values of $e(\phi_m - \phi_s)$ shown in Figure 6 at the appropriate times; i.e., at points on the

abscissa about one-fourth of a spin period prior to the numbered spins. The fewer Lockheed data points indicate that the peaks may have been at higher energies on spins 2 and 3, and at a lower energy on spin 4, in agreement with Figure 6.

Note also that the spectra are very broad, much more so than expected for a pure acceleration by the potential difference, notwithstanding plausible time variations of the potential and the long transit time of the ions. Moreover, according to Ghielmetti et al. (1978), ions with conical pitch-angle distributions, with maxima ranging from very small angles to 90° , are also occasionally observed in the potential regions. It appears, therefore, that the ions are being accelerated perpendicular to the magnetic field, as well as in the parallel direction, in the potential region. Since the maxima of the spectra shown in Figure 8 are correlated fairly well with the potential differences below the satellite, a high fraction of the ions must have fallen through the entire potential drop.

DISCUSSION

The inverted-V distribution of the potential difference as a function of spin number, shown in Figure 6, is in agreement with the similarly-shaped energy versus time displays of the precipitating electrons (the inverted-V electron events observed at lower altitudes (Frank and Ackerson, 1972) and of the upward-moving ions observed on the S3-3 satellite (Ghielmetti et al., 1978; Mizera and Fennell, 1977). As discussed by Ghielmetti et al., (1978), the potential structure, as inferred from the ion measurement, is evidently a commonly-occurring feature of the auroral zone. Analyses of different sets of the S3-3 data, have yielded results similar to those shown in Figure 6 (see e.g., Sharp et al., 1978; Mizera and Fennell, 1977), including simultaneous potential differences above and below the satellite.

The apparent electric field, E_{11} , along the magnetic field above the satellite can be estimated from the values of B_1 and ϕ_s obtained from the

spin 4 data. The ratio $B_1/B_s = .77$ corresponds to a distance of about 1200 km above the satellite. Hence $E_{11} \sim 0.8/1200$ or .7 mV/m. The value of E_{11} below the satellite can be estimated from the values of $\phi_m - \phi_s$ by assuming that ϕ_m is located at some low altitude, say 3000 km. Such an altitude is reasonable since many observations of highly field-aligned ($\leq 20^\circ$), low-energy electrons (sometimes fairly monoenergetic) have been made in the auroral zones which indicate that ϕ_m may be located at altitudes ≤ 2000 km (see, e.g. Arnoldy et al., 1974); and Ghielmetti et al., (1978) found that the probability of seeing upward flowing ions above 4000 km on satellite passes over the auroral zones is high, about 60%. That altitude for ϕ_m implies an extent of the potential below the satellite of ~ 4000 km. The corresponding electric fields, from the spin 2, 3 and 4 results, are .4, .9, and .4 mV/m, respectively.

The apparent scale of the potentials is therefore much larger than the Debye length or the energetic ion gyroradius. Moreover, since electrostatic ion cyclotron (EIC) turbulence is occasionally observed by the S3-3 satellite (Mozier et al. 1977; Kintner et al., 1978), it appears that the electric field is most likely supported by anomalous resistivity, as discussed by Kindel and Kennel (1971), Papadopoulos (1977), and Lysak et al. (1978).

Such large-scale potential distributions can, in principle, be computed from the quasi-neutrality principle (see, e.g., Persson, 1963). That is, the potential distribution must be such that the electron and ion number densities are essentially identical at each point along the magnetic field. If it is assumed that the electrostatic-wave turbulence prevents the "thermal" ions and electrons from moving along the magnetic field, as is necessary to achieve the anomalous resistance, the charge neutrality must be established by the more energetic

particles. An analysis by Cladis et al. (1978) has been conducted to determine whether the number densities of the upgoing ions and electrons observed on spin 4, and the downgoing electrons, assumed to be Maxwellian at B_1 as discussed previously, might yield such a self-consistent potential distribution in the region above the satellite between B_1 and B_s . The fluxes above the satellite were computed from an application of Liouville's theorem, and the potentials at the boundaries B_1 and B_s were kept at the values, 0 and .8 kV respectively, determined from the electron pitch-angle distributions. The Aerospace data on the proton spectrum on spin 4 were not available at that time, hence the analysis was performed for various mathematical forms for the proton flux that seemed to bound the Lockheed data shown in Figure 8. The proton flux was normalized such that the number density of the protons was equal to that of the electrons at B_s . With the proton flux proportional to $w e^{-w/w_p}$, where $w_p = .2$ keV, for example, excellent agreement of the number densities throughout the interval was achieved for a potential that increased almost linearly with B from $B = .785 B_s$ to B_s .

The results of that analysis reveal that a self-consistent solution for the potential distribution cannot be obtained with the Aerospace flux shown in the third panel of Figure 8. In the first place the flux is too low by a factor of about 8 to match the number density of the electrons at B_s . Even if this flux were raised to match the number densities at B_s , the proton densities would exceed the electron densities, regardless of the potential shape, at the lower B values. A self-consistent solution can be obtained only if, toward higher altitudes, the ion spectrum becomes progressively softer and/or the ion pitch-angle distribution becomes progressively wider. Both such effects would be

expected from a streaming instability of the ions.

If the fluxes above the satellite are correctly given by Liouville's theorem, it would then appear that lower-energy electrons and/or ions, not included in the observations, are contributing to the necessary transport of charge. From the standpoint of anomalous resistivity theory, these particles might be due to run-away electrons from the locally-heated electron distribution and/or ions that are accelerated locally by resonating with the electrostatic ion cyclotron waves. In fact, such ions, which escape from the local turbulence, and are subsequently accelerated by a portion of the potential difference below the satellite, may also account for the ion fluxes shown in Figure 8 at energies below the peaks. Of course, a streaming instability of the ion beam might also explain the presence of the low energy ions.

Quite often, within the potential region, one or more narrow regions ($< .1^\circ$ in latitude) appear which are characterized by high electric fields ($\sim 10^2$ mV/m), principally perpendicular to the magnetic field, with associated potentials in the kV range (Mozer et al., 1977). These structures may be the oblique electrostatic shocks discussed by Swift (1975). An observation of several such "shocks" within the potential region is discussed by Sharp et al. (1978). They might represent different dynamical states of the same current driven instability.

CONCLUSIONS

The simultaneous electrostatic potential differences above and below the satellite inferred from the ion and electron measurements, indicate that the scale of the potential along the magnetic field is large. This characteristic, together with observations of electrostatic turbulence and high field-aligned currents by the S3-3 satellite, indicate that the electric field along the magnetic field may be supported by anomalous resistivity.

A self-consistent solution for the potential distribution above the satellite cannot be found for the observed distributions of the upgoing ions and electrons and the assumed Maxwellian electron distribution above the satellite where the potential is zero. The quasi-neutrality condition can be satisfied only if (i) the ion distribution is altered above the satellite by interactions that continually soften the spectrum and/or widen the pitch-angle distribution or (ii) particles with energies lower than those seen by the detectors are also transported along the field. A streaming instability of the ion beam might account for (i). Likely candidates for (ii) are particles which may escape from the local turbulence: run-away electrons from the heated electron distribution and ions which are perpendicularly heated by EIC waves. Such a source of the ions within the potential structure below the satellite is consistent with the observed energy spectra of the ions, which reveal the presence of ions with energies less than the potential differences below the satellite. Nevertheless, since the peaks of the ion spectra are at energies corresponding roughly to the full potential differences below the satellite, it appears that most of the ions originated near the altitude of the maximum value of the potential. The low-energy ions might also result from an ion-streaming instability.

ACKNOWLEDGMENTS

We wish to thank Drs. P. F. Mizera and J. F. Fennell of the Aerospace Corporation for providing the energy spectra of the protons, and Drs. G. T. Davidson and M. Walt of the Lockheed Research Laboratory for helpful discussions on the analysis of the data. This research was supported by the Atmospheric Research Section of the National Science Foundation, the Defense Nuclear Agency, and the Office of Naval Research.

- Ackerson, K. L., and L. A. Frank, "Correlated satellite measurements of low-energy electron precipitation and ground-based observations of a visible auroral arc," J. Geophys. Res. 77, 1128, 1972.
- Arnoldy, R. L., P. B. Lewis, and P. O. Isaacson, "Field-aligned auroral electron fluxes," J. Geophys. Res. 79, 4208, 1974.
- Block, L. P., "Double layers," in Physics of the Hot Plasma in the Magnetosphere, B. Hultqvist and L. Stenflow, ed., p. 229, Plenum Press, New York 1975.
- Block, L. P., and C-G. Fälthammar, "Mechanisms that may support magnetic-field-aligned electric fields in the magnetosphere," Ann. Geophys., 32, 161, 1976.
- Chiu, Y. T. and M. Schulz, "Self-consistent particle and parallel electrostatic field distributions in the magnetosphere-ionospheric auroral region," J. Geophys. Res., 83, 629, 1978.
- Cladis, J. B., and R. D. Sharp, "Electrostatic potential differences along magnetic field lines inferred from satellite measurements of electron and ion distributions," EOS, 58, 473, 1977a.
- Cladis, J. B., R. D. Sharp, "Distribution of electrostatic potential along magnetic field inferred from observations of ion and electron fluxes," EOS, 58, 716, 1977b.
- Cladis J. B., G. T. Davidson, W. E. Francis, L. L. Newkirk, and M. Walt, "Assessment of processes related to plasma irregularities," Final Report, DNA 4473F, Defense Nuclear Agency, Washington, D. C. 20305, 1978.

- Evans, D. S., "Evidence for the low-altitude acceleration of auroral particles," in Physics of the Hot Plasma in the Magnetosphere," B. Hultqvist and L. Stenflo, ed., p. 319, Plenum Press, New York, 1975.
- Falthammar, C-G., "Problems related to macroscopic electric fields in the magnetosphere," (Paper 7R0704), Rev. Geophys. Space Phys., 15, 457, 1977.
- Frank, L. A., and K. L. Ackerson, "Local-time survey of plasma at low altitudes over the auroral zones," J. Geophys. Res., 77, 4116, 1972.
- Ghielmetti, A. G., R. G. Johnson, R. D. Sharp, and E. G. Shelley, "The latitudinal, diurnal, and altitudinal distributions of upward flowing energetic ions of ionospheric origin," Geophys. Res. Lett., 5, 59, 1978.
- Iijima, T., and T. A. Potemra, "The amplitude distribution of field-aligned currents at northern high latitudes observed by triad, J. Geophys. Res., 81, 2165, 1976.
- Kindel, J. M., and C. F. Kennel, "Topside current instabilities," J. Geophys. Res., 76, 3055, 1971.
- Kintner, P. M., M. C. Kelley, and F. S. Mozer, "Electrostatic hydrogen cyclotron waves near one earth radius altitude in the polar magnetosphere," Geophys. Res. Lett., 5, 139, 1978.

Lysak, R. L., M. K. Hudson, and J. M. Kindel, "Turbulent heating by the current-driven electrostatic ion cyclotron mode in the auroral magnetosphere," Preprint, University of California, Berkeley, California 1978.

Mizera, P. F., and J. F. Fennell, (private communication), 1978.

Mizera, P. F., and J. F. Fennell, "Signatures of electric fields from high and low altitude particles distributions," Geophys. Res. Lett. 4, 311, 1977.

Mozzer, F. S., C. W. Carlson, M. K. Hudson, R. B. Torbert, B. Parady, J. Yatteau, and M. C. Kelley, "Observations of paired electrostatic shocks in the polar magnetosphere," Phys. Rev. Lett., 38, 292, 1977.

Papadopoulos, K., "A review of anomalous resistivity for the ionosphere," Rev. Geophys. Space Phys., 15, 113, 1977.

Persson, H., "Electric field along a magnetic line of force in a low-density plasma," Phys. Fluids, 6, 1756, 1963.

Sharp, R. D., R. G. Johnson, and E. G. Shelley, "Observation of an ionospheric acceleration mechanism producing (keV) ions primarily normal to the geomagnetic field direction," J. Geophys. Res., 82, 3324, 1977.

Sharp, R. D., R. G. Johnson, and E. G. Shelley, "Energetic particle measurements from within ionospheric structures responsible for auroral acceleration processes," submitted to J. Geophys. Res., 1978.

Shelley, E. G., R. D. Sharp, and R. G. Johnson, "Satellite observations of an ionospheric acceleration mechanism," Geophys. Res. Lett., 3, 654, 1976.

Swift, D. W., "On the formation of auroral arcs and acceleration of auroral electrons," J. Geophys. Res., 80, 2096, 1975.

Torbert, R. B., and F. S. Mozer, "Electrostatic shocks as the source of discrete auroral arcs," Geophys. Res. Lett. 5, 135, 1978.

Walt, M., W. M. McDonald, and W. E. Francis, "Penetration of auroral electrons into the atmosphere," in Physics of the Magnetosphere, ed., R. Carovillano and J. F. McClay, p. 534, Reinhold, New York, 1968.

Whipple, E. C., Jr., "The signature of parallel electric fields in a collisionless plasma," J. Geophys. Res., 82, 1525, 1977.

TABLE I. DETECTOR CHARACTERISTICS

<u>DETECTOR</u>	<u>PARTICLE</u>	<u>ENERGY, keV</u>	<u>GDE, cm² sr keV</u>
CMEA	Electrons	0.07 - 0.24	1.2×10^{-6}
CMEB	Electrons	0.35 - 1.1	6.5×10^{-6}
CMEC	Electrons	1.6 - 5.0	1.9×10^{-5}
CMED	Electrons	7.3 - 24	6.5×10^{-5}

Energy per unit charge

		Step 1	2	3	4
CXA 1	Ions	0.50	0.68	0.94	1.28
CXA 2	Ions	1.76	2.4	3.3	4.5
CXA 3	Ions	6.2	8.5	11.6	16.0

FIGURE CAPTIONS

1. Survey plots for September 15, 1976. (see text).
2. Counting rate of CME B detector as function of pitch angle. The satellite spin number, with the subscripts - and + denoting the first and second pitch-angle scans made during the satellite spin, are shown at the curves.
3. Counting rate of CME C detector as function of pitch angle. (see caption of Figure 2).
4. Loss-cone width measured to point of largest curvature of "knee", as computed with the AURORA code, as function of potential difference below satellite.
5. Loss-cone depths computed with AURORA code for various potential differences below satellite divided by the computed loss-cone depth for the potential difference equal to zero. (see text).
6. Electrostatic potential differences inferred from measurements of electron distributions on satellite pass through potential region. The circles and the triangles denote the potential differences below the satellite determined from the loss-cone widths and depths, respectively, with the error bars indicating the uncertainties based on the loss-cone width determinations. The squares denote the total potential differences, which include the potential differences above the satellite.
7. Illustration of detector response to primary electrons in downward hemisphere. In diagram (a), contours of constant flux at $B_1, \phi = 0$ - where the flux is assumed

isotropic - are shown in velocity space; the corresponding contours at B_s, ϕ_s are shown in (b). The contour segments between the dots labeled 1, 1; 2, 2; etc., in (a) map into the similarly labeled segments in (b). At the contours are given the fluxes in units of $(\text{cm}^2 \cdot \text{sec} \cdot \text{sr} \cdot \text{keV})^{-1}$ with the power of 10 in parenthesis, for $n_0 = .7/\text{cm}^3$ and $w_e = .8 \text{ keV}$ (see Eq. (5)), and the electron energies in keV. The detector response (in the range 1.6 to 5 keV) at α_s is depicted by the cross-hatched area. Note that the detector counting rate is constant from $\alpha_s = 0$ to $\alpha_s = \alpha_L$.

8. Energy spectra of ions measured by the Lockheed and Aerospace (Mizera and Fennell, 1978) groups on spins 2, 3, and 4. The times of the measurements are shown in the panels.

SEPT 15, 1976

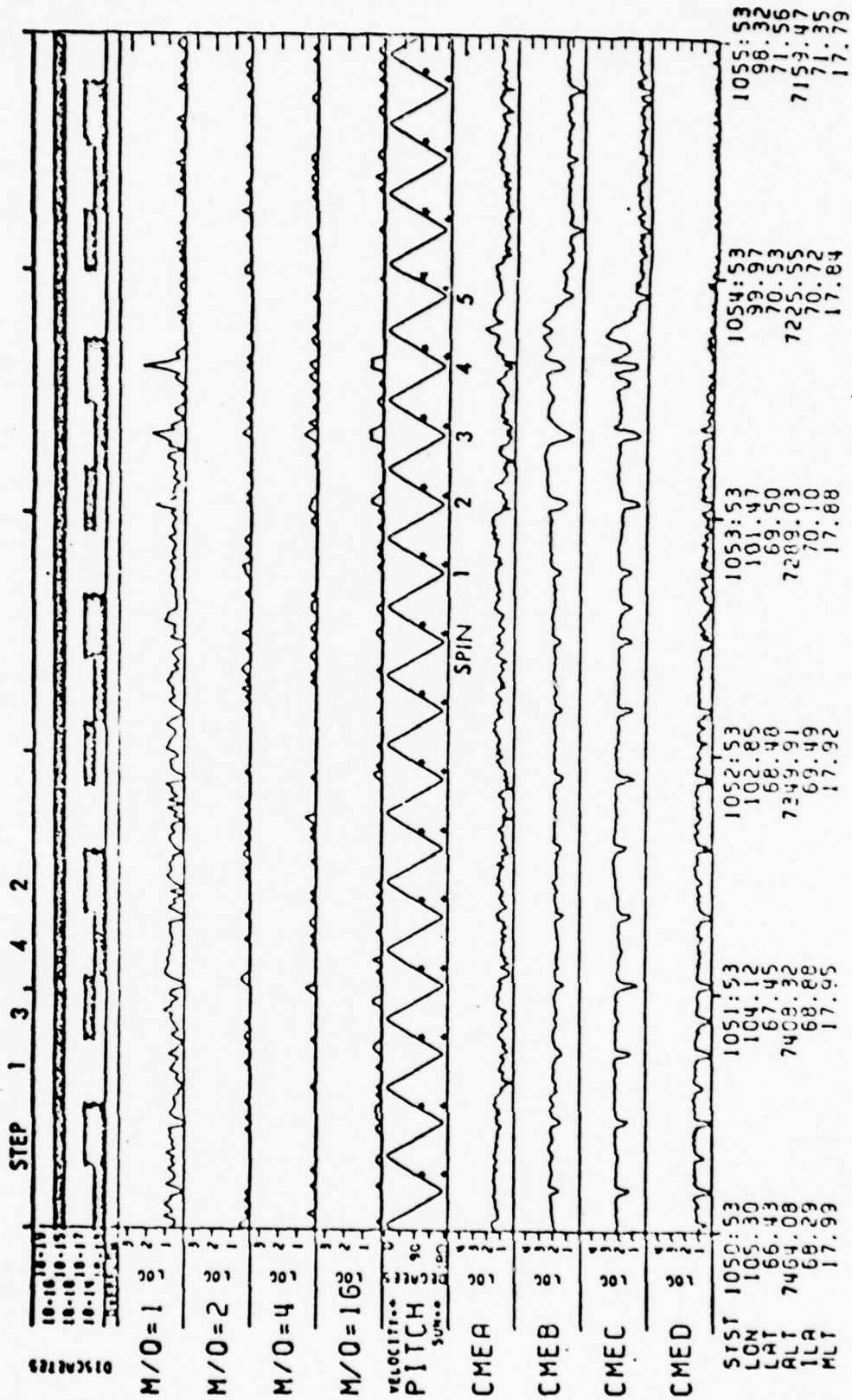


Figure 1.

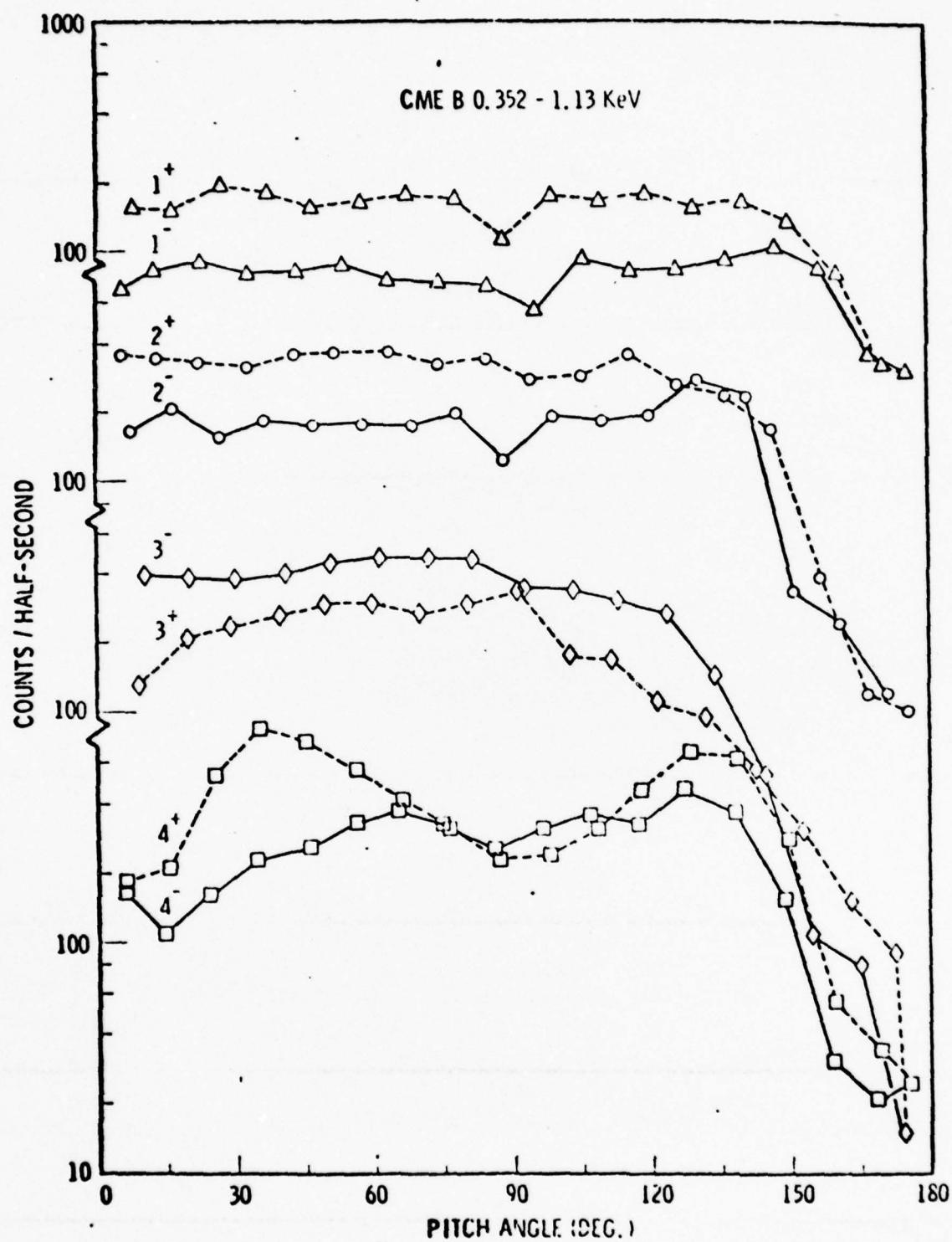


Figure 2.

B-31

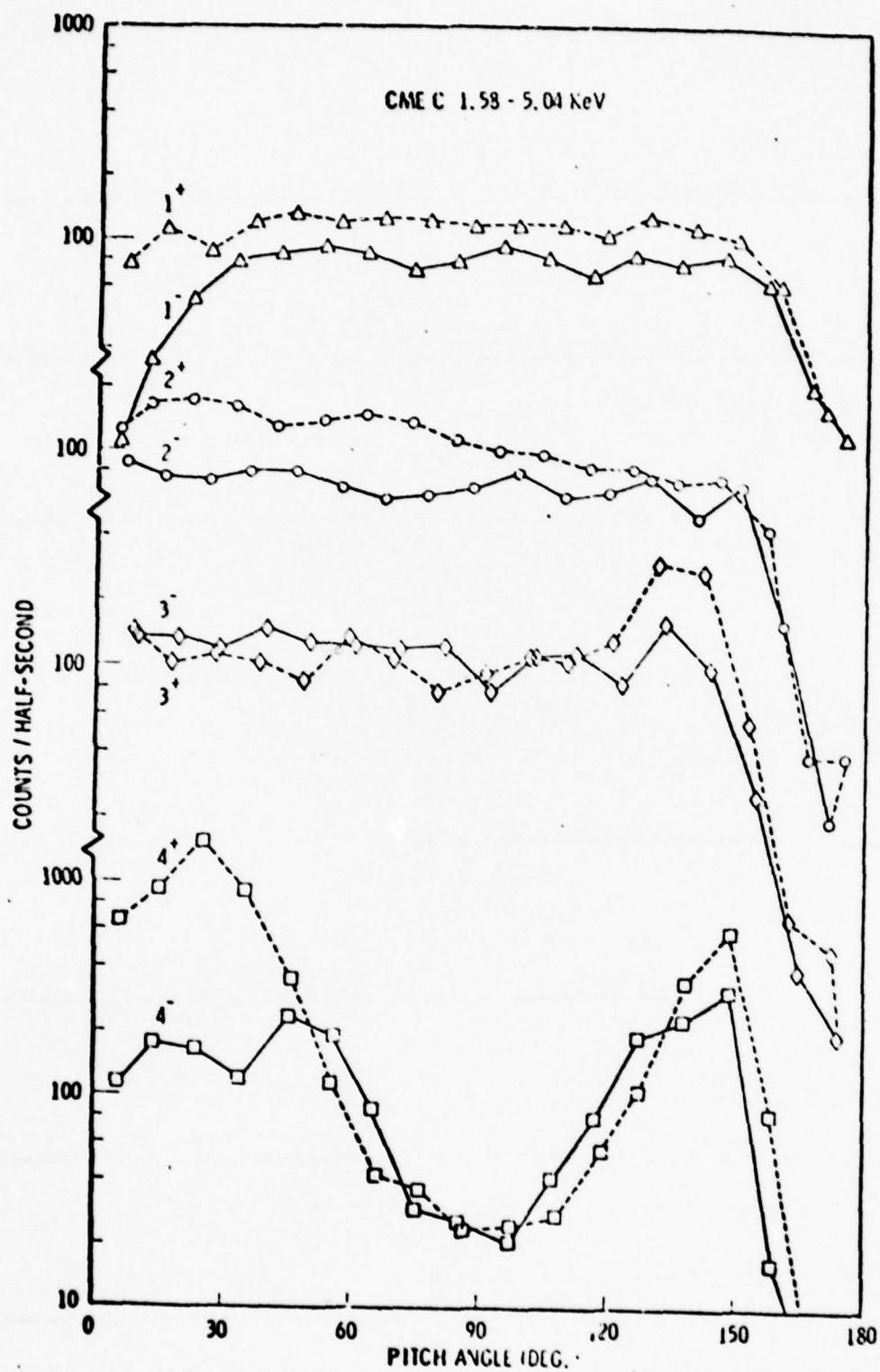


Figure 3.

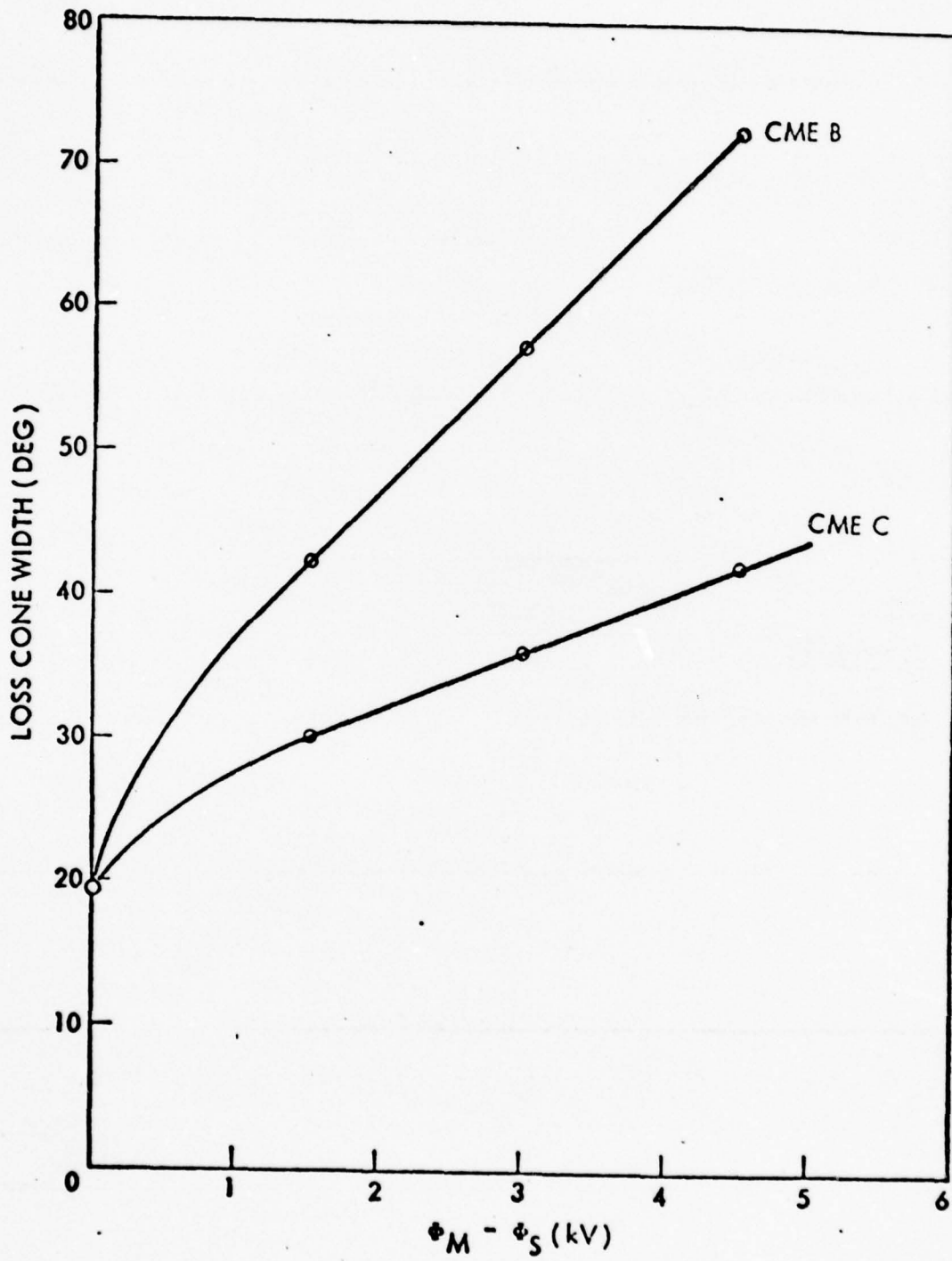


Figure 4.

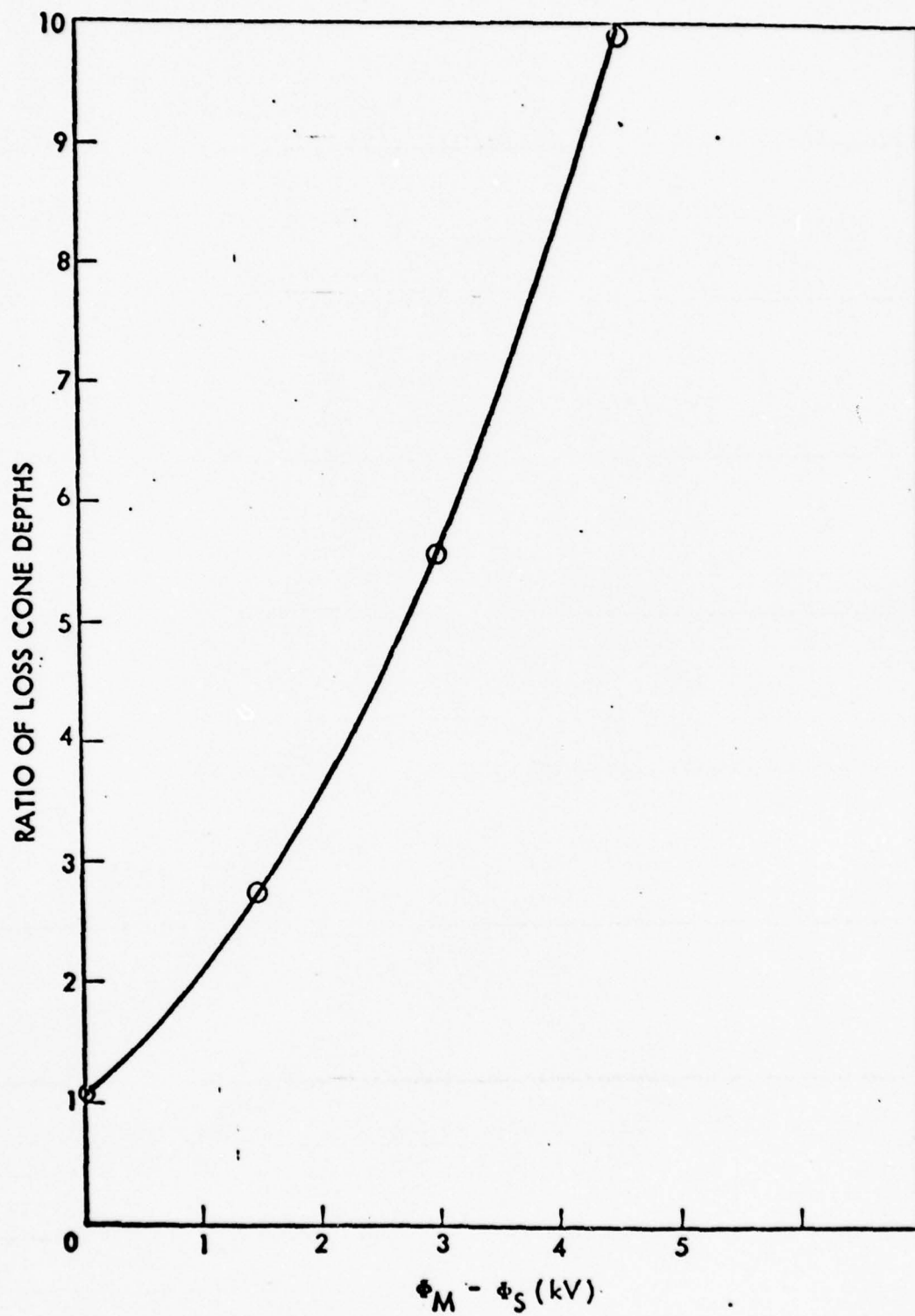
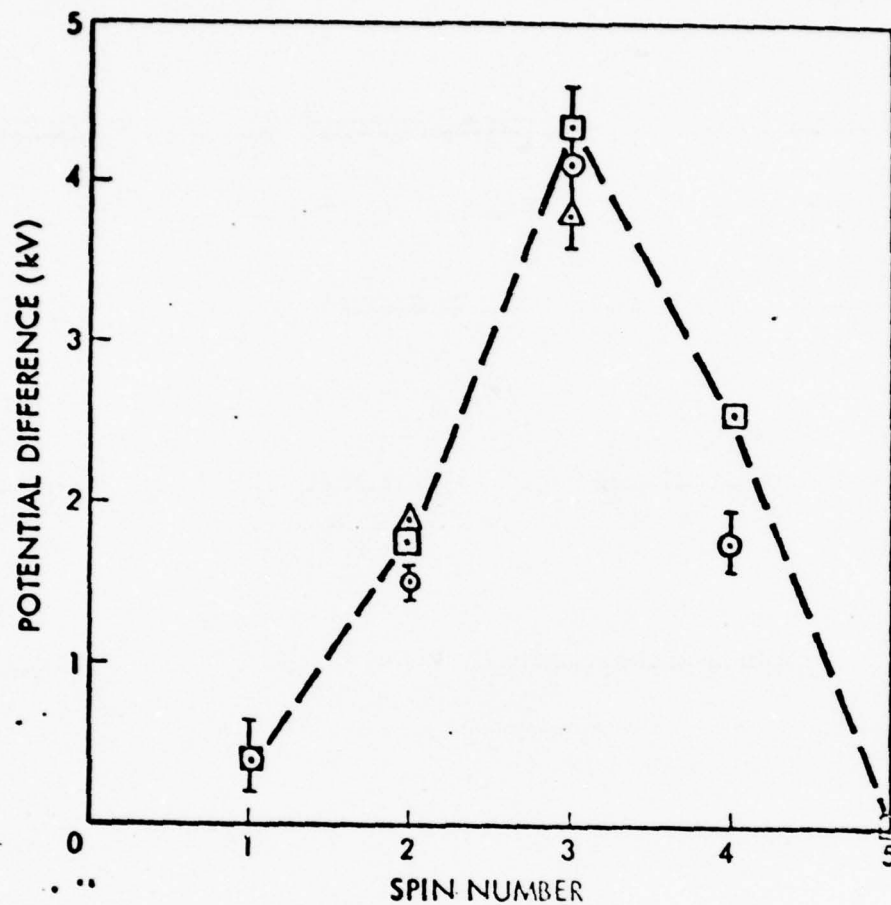


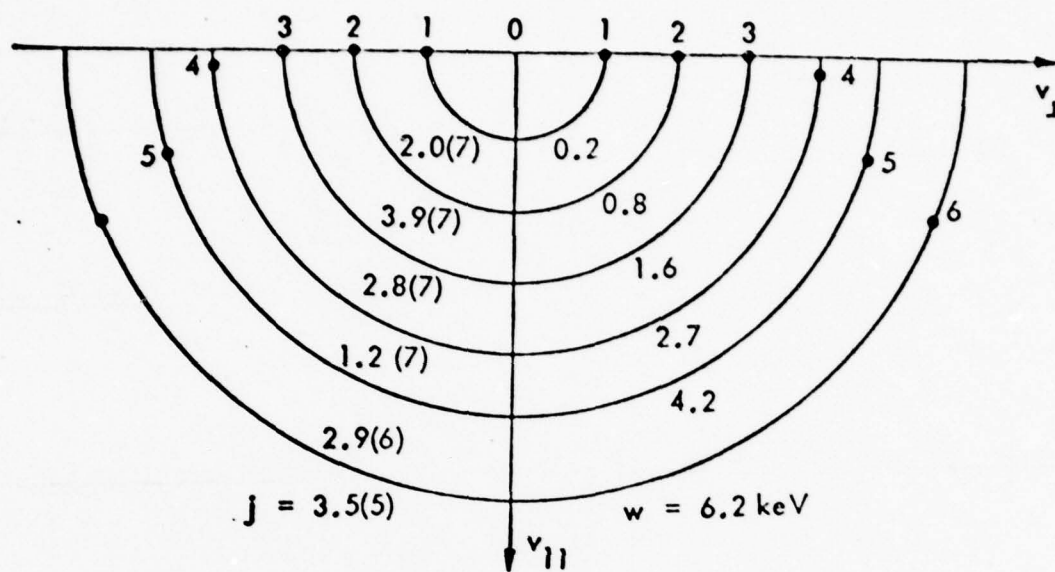
Figure 5.

POTENTIAL DIFFERENCE ALONG MAGNETIC FIELD
THROUGH STRUCTURE OF INVERTED-V EVENT

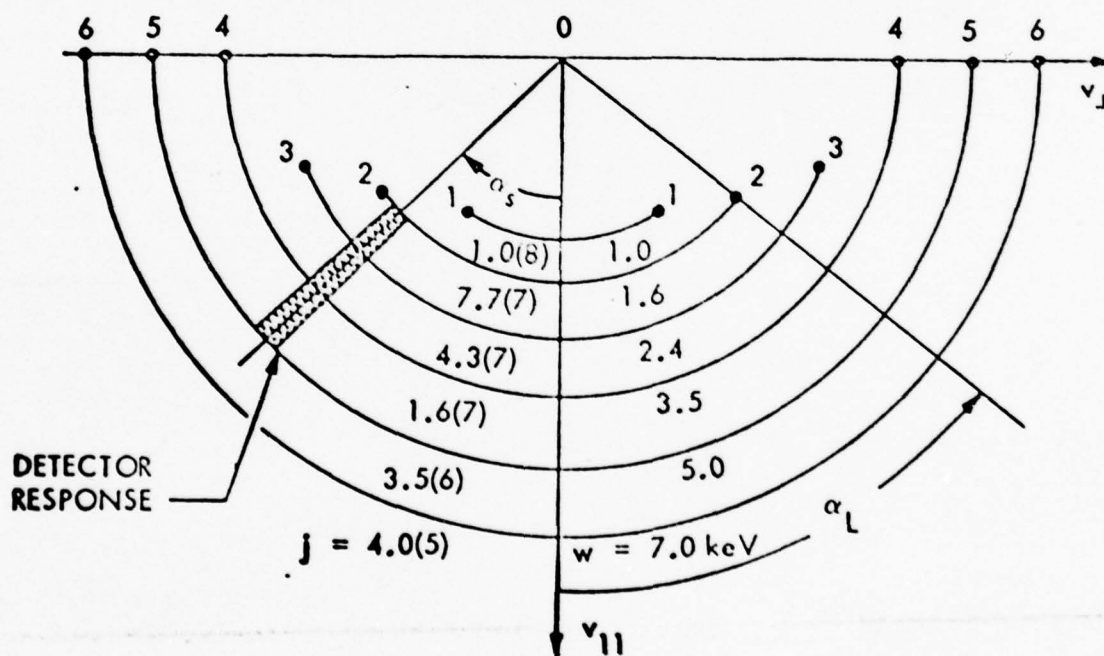


- LEGEND:
- POTENTIAL BELOW SATELLITE FROM DATA ON LOSS CONE WIDTHS WITH ESTIMATED UNCERTAINTIES
 - △ POTENTIAL BELOW SATELLITE FROM DATA ON LOSS CONE DEPTHS
 - TOTAL POTENTIAL (INCLUDES ESTIMATES OF POTENTIAL ABOVE SATELLITE)

Figure 6.



(a) $B_1, \varphi = 0$



(b) B_3, φ_s

Figure 7.

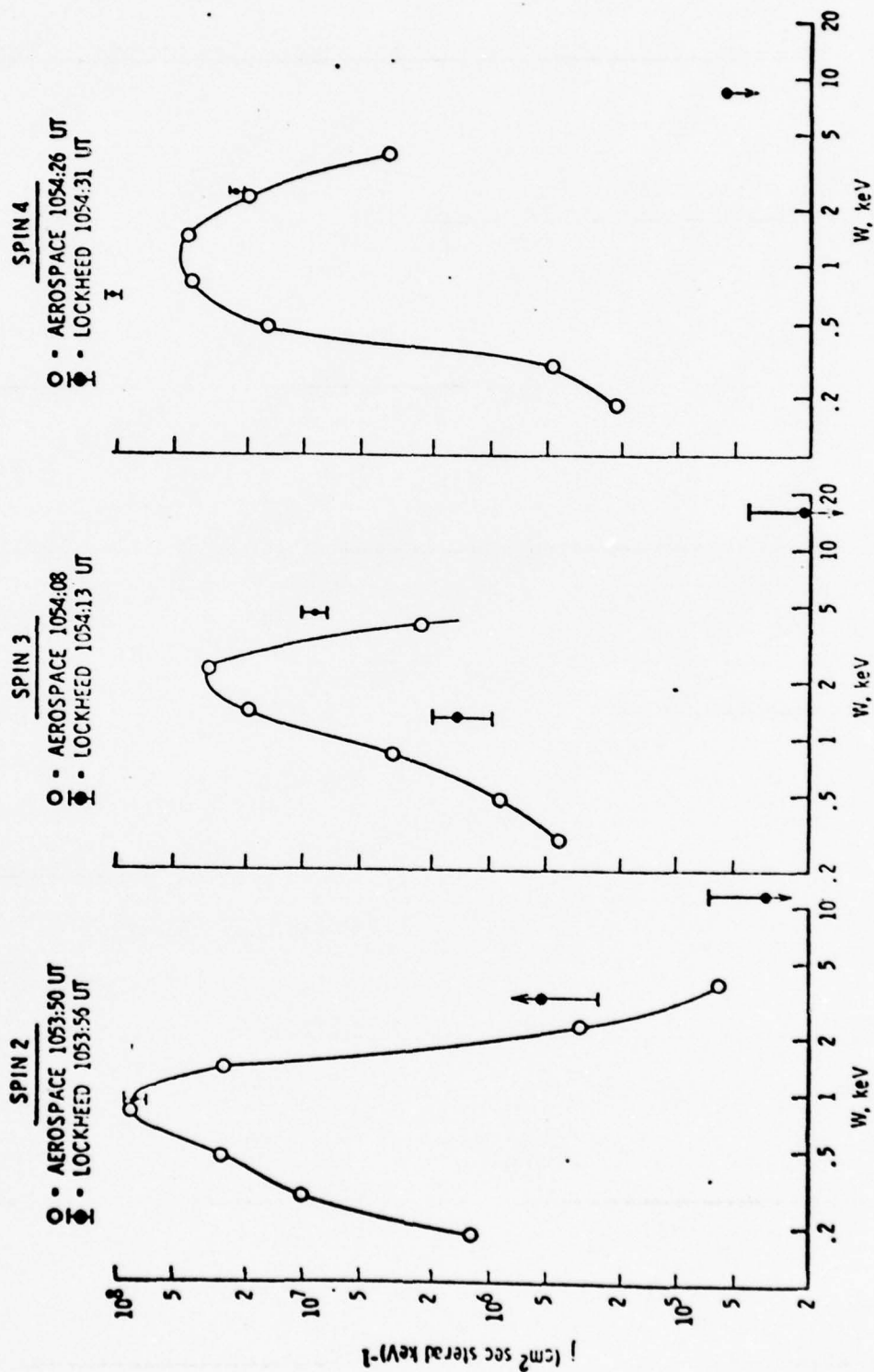


Figure 8.

LMSC/D673078

APPENDIX C

DOWNWARD FLOWING IONS AND EVIDENCE FOR INJECTION
OF IONOSPHERIC IONS INTO THE PLASMA SHEET

A. Ghielmetti^{*}, R. D. Sharp,
E. G. Shelley and R. G. Johnson

Lockheed Palo Alto Research Laboratory
3251 Hanover Street
Palo Alto, California 94304

Submitted to
Journal of Geophysical Research

January 4, 1979

*Visiting scientist, University of Bern, Switzerland

ABSTRACT

Energetic (keV) ions with field aligned pitch angle distributions have been observed streaming downward in the high altitude ($\sim 1 R_E$) auroral ionosphere by the ion-mass spectrometer on the S3-3 satellite. These downward streaming ion events were observed much less frequently than the previously reported upward flowing ion events. They exhibited peak fluxes of up to $\sim 7 \times 10^7 \text{ (cm}^2\text{-sec-ster-keV)}^{-1}$ and typically consisted only of protons with energies less than $\sim 3 \text{ keV}$. In two examples investigated in detail, the similarities between the downward flowing and coincident trapped ion distributions, suggest a common origin. Spatially localized regions of enhanced hot ($\sim \text{keV}$) plasma density were frequently observed in the low L portion of the plasma sheet. The statistical location of these "plasma clouds" correlates well with the substorm injection boundary near dusk inferred by McIlwain (1974) and the downward flowing ion events occur preferentially within such "plasma clouds". It is suggested that upward flowing ions from the auroral acceleration regions are responsible for both the downward flowing ions and for at least some of the "plasma clouds". It is concluded that injection of energetic ions from this ionospheric source into the trapped population of the plasma sheet is common and may contribute significantly to the equatorial plasma density. The significant difference in the frequency of upstreaming and downstream ion events further suggests that parallel electric fields involving potential drops of $\geq 500 \text{ volts}$ are directed preferentially upward in the altitude range from 2000 km to $\sim 3 R_E$.

INTRODUCTION

A general discussion of the energetic ion composition in the magnetosphere is provided in the reviews by Johnson et al. (1975) and Shelley (1978). Specifically, the presence of large fluxes of energetic trapped O^+ ions in the inner ring current (Johnson et al., 1977) and of precipitating O^+ ions in the auroral zone (Shelley et al., 1972, 1974; Sharp et al., 1974, 1976a,b; Johnson et al., 1975) during geomagnetic storms implies that a sizeable fraction of the energetic magnetospheric particle population is of ionospheric origin. On the basis of morphological studies on these precipitating ions Sharp et al. (1976b) have inferred a local injection process that may be operating over a wide region of local times. More recently Shelley et al. (1976) and Sharp et al. (1977) have directly observed energetic ions being accelerated out of the ionosphere and injected into the magnetosphere. Synoptic studies have identified the statistical auroral oval and the altitude range from 2000 to ≥ 8000 km as a source region where this upward acceleration of ionospheric ions is commonly occurring (Ghielmetti et al., 1978a). How and to what extent this ionospheric source contributes to the various magnetospheric particle populations and its relation to other dynamical processes in the magnetosphere remain open questions at present however.

Strong perpendicular electric fields are frequently encountered in the regions of upward flowing ions (Mozzer et al., 1977; Torbert and Mozzer, 1978). These field measurements and the signatures observed in the particle distributions have been interpreted as evidence for upward directed parallel electric fields (Mozzer et al., 1977; Mizera and Fennell, 1977; Torbert and Mozzer, 1978; Cladis and Sharp, 1978; Sharp et al., 1978a). If oppositely directed parallel electric fields existed in these regions they would be expected to give rise

to similar field aligned ion distributions flowing in the downward direction. Thus, the relative frequency of occurrence of downward flowing ion (DFI) and of upward flowing ion (UFI) distributions has direct implications on the nature of auroral acceleration processes.

If upward flowing ions occur on closed field lines they may become trapped through pitch angle scattering and contribute to the equatorial particle populations. In the absence of significant pitch angle scattering these ions would appear in the conjugate hemisphere as DFI distributions. Thus the occurrence frequency and the characteristics of DFI distributions provide information not only on the interactions taking place during transport through the equatorial region but also on the injection of this ionospheric plasma into the equatorial population.

Downward flowing ion distributions in the altitude range of $\sim 1 R_E$ have only recently been observed (Fennell et al., 1978; Ghielmetti et al., 1978b). At low altitudes (≤ 2000 km) anisotropically precipitating ions have previously been reported (Rème and Bosqued, 1971; Hultqvist, 1971, 1978). Similar field aligned "source cone" structures of energetic ions (Mauk and McIlwain, 1975; Borg et al., 1978; Geiss et al., 1978), and bouncing clusters of ions inferred to be O^+ (McIlwain, 1976) have been reported at geosynchronous altitude.

In this paper we present the results of a study of downward flowing field aligned ion distributions observed by the S3-3 satellite in the critical altitude range of $\sim 1 R_E$ where ions are generally accelerated upward. The characteristics of these events, their relationship to magnetospheric boundaries and to the trapped particles are investigated and the implications are discussed. Two examples of broad regions of downward flowing ions and enhanced plasma regions are described in detail, followed by a statistical study of the occurrence of these events.

EXPERIMENT DESCRIPTION

The measurements to be described were made by a set of 3 energetic ion mass spectrometers and 4 broadband electron spectrometers aboard the S3-3 (1976-65B) satellite. The spacecraft is in an elliptical polar orbit with apogee at ~8000 km, perigee at 250 km, an inclination of 97.5 degrees and a period of ~3 hours. Since the spin axis is oriented perpendicular to the orbital plane and the sensors are mounted with their view directions perpendicular to the spin axis, nearly complete pitch angle scans are obtained once every half spin (~9 seconds). The three ion spectrometers, each at a different energy setting, simultaneously acquire complete mass scans over the mass/charge range from 1 through ~32 AMU/charge once every second. Every 16 seconds the energy setting of each spectrometer is stepped through one of 4 exponentially spaced values, thus providing a 12 point energy spectrum between 0.5 - 16 keV/charge in 64 sec. The mass resolution is sufficient to separate H^+ , $^4He^{++}$, $^4He^+$ and O^+ ions at relative intensities of less than 10^{-2} . The electron spectrometers cover the energy range from $0.07 \leq E \leq 23.5$ keV in four almost contiguous energy bands with a nearly constant response function. The acceptance angles of the ion and electron spectrometers are approximately $\pm 3^\circ$ at full width. More detailed descriptions of the instrument have been presented in previous publications (Johnson et al., 1977; Sharp et al., 1978a).

OBSERVATIONS

Approximately 370 orbits of data were examined for downward flowing ion (DFI) events. From this data set we have selected the two most conspicuous DFI events for detailed discussion. Both involve large fluxes of highly anisotropic H^+ ions precipitating over a wide latitudinal region.

Downward flowing ion event of REV 619

Overview. This event was observed near local evening 7600 km above the northern auroral zone. It occurred on September 24, 1976 at -0020 UT during the late recovery phase of a minor magnetic storm that had developed on September 18. This storm is characterized by a peak Kp of 6 on September 18 and 20, only moderate ring current injection with a peak Dst of -72γ , and a slow recovery. The sum of Kp was 13+ for the day of the observation (a Q-day) and 20 for the preceeding day. A few hours before this event Dst showed a small negative excursion to -35γ which is suggestive of a substorm injection.

A survey plot showing the raw detector counting rates from this event as a function of universal time (UT), altitude (ALT), invariant latitude (ILA), magnetic local time (MLT) and L value is given in Figure 1. The top panel indicates the energy step of the 3 ion spectrometers and the period (16 sec) spent on each step. The next two panels show the logarithms of the sums of the counts from all three spectrometers from the mass channels sensitive to ions with mass per charge $M/Q = 1$ and 16 respectively. These values are displayed once per second corresponding to 20° rotation in pitch angle. The latter is indicated in the panel labeled PITCH, where zero is the direction

of precipitation into the ionosphere. During this section of the orbit pitch angles down to -5° were sampled. The four bottom panels give the logarithm of the count rates from the four electron detectors sampled twice per second. For a better characterization of the various plasma regimes encountered during this section of the satellite trajectory we present the derived plasma properties in Figure 2. These include the electron and proton number densities, energy densities, average energies, and precipitated energy fluxes projected to ionospheric altitude. They were calculated on the assumption that the fluxes are concentrated at the logarithmic centers of the detector energy bands and take into account the measured pitch angle distributions. The periods of averaging, generally approximately one minute, and the statistical uncertainties, unless smaller than the symbol size, are indicated by the horizontal and vertical bars respectively. We note first in Figure 2 a rapid increase by about an order of magnitude in the electron energy density accompanied by a decrease and a minimum in the average energy at -71° ILA. These features are interpreted as the inner edge of the plasma sheet (Vasyliunas, 1968, 1970; Frank, 1971; Schield and Frank, 1970). The unusually low number densities and high average energies just equatorward of this boundary may result from the limited energy range of the electron detectors ($E \geq 75$ eV). The region of relatively high proton and electron fluxes extending poleward of this boundary up to -80° ILA is identified in Figure 2, as the plasma sheet. Further poleward the fluxes drop to near the detector backgrounds. The more energetic electrons (1.6 - 5 keV and 7.3 - 23.5 keV) exhibit up and downcoming loss cones out to -78° ILA where they drop below the sensitivity threshold of the detectors (see Figure 1). This boundary is indicated in Figure 2 as the energetic electron "trapping boundary". Although it is not possible to unambiguously identify the boundary

of closed field lines from particle signatures the presence of downcoming loss cones in the pitch angle distributions is generally interpreted as indicative of a closed field line geometry. The actual boundary of closed field lines may be further poleward however.

For the purpose of the following discussion we subdivide the data period into three principal regions based on the proton plasma characteristics. These are designated as regions I, II and III in the upper margins of Figures 1 and 2. The region designated I, extending inward of the inner edge of the plasma sheet, exhibits low proton number densities and high average energies. Region II was chosen to cover the lower latitude section (-71° to -74° ILA) of the plasma sheet, containing large fluxes of low energy protons. Region III covers the remaining high latitude section.

A subregion between 0019:40 and 0021:00 UT within Region II and designated as IIa in Figures 1 and 2, is of key interest. Referring to Figure 1, we note that the H^+ ($M/Q = 1$) fluxes peak in the downward direction ($PITCH \approx 0^\circ$) within this subregion. To quantify this peaking in the distributions we define the anisotropy as the ratio of average source cone ($0^\circ \leq \alpha \leq 30^\circ$) flux to the average trapped ($60^\circ \leq \alpha \leq 120^\circ$) flux. For the 4 consecutive satellite spins in Region IIa the anisotropies ranged between 2 and 26 with statistical significance typically $\geq 3\sigma$. The repetitive character of the anisotropy is convincing evidence that it resulted from a genuine pitch angle dependence and not from temporal or spatial variations in the fluxes. In addition to this extended region of DFI distributions, three other isolated DFI distributions occurred in the higher latitude portion of Region II with anisotropies ranging between 2.2 and 2.9 and statistical significance above 2σ . Between the extended DFI event indicated by the shaded area in Figure 2 and the isolated DFI events, a subregion of enhanced electron energy fluxes and field

aligned precipitation of low energy (~ 1 keV) electrons was encountered. This subregion, extending from approximately 72° to 72.5° ILA, is indicated by the shaded area labeled UFI in Figure 2. It also included an upward flowing field aligned beam of 0.5 keV O^+ ions with peak flux of $\sim 9 \times 10^6$ ($\text{cm}^2\text{-sec-ster-keV}$) $^{-1}$ (Figure 1). The significant decrease in the proton number density and increase in the average energy within this subregion resulted from a reduction of the trapped low energy component of the proton distribution. These features are suggestive of downward electron and upward ion acceleration. Two additional multiple spin UFI events occurred in region III. The event equatorward of the electron "trapping boundary" was the most intense with peak fluxes of $\sim 1 \times 10^8$ protons ($\text{cm}^2\text{-sec-ster-keV}$) $^{-1}$ at 0.5 keV. The more poleward event involved both H^+ and O^+ ions at energies of 0.5 - 1.76 keV.

Angular and energy distributions. The average energy and pitch angle distributions for regions I, II and III are shown in Figures 3 and 4. The differential energy spectra were obtained by averaging the fluxes over pitch angles from 30° to 150° for the trapped component and from 0° to 30° for the precipitating component. The angular distributions were obtained by integrating the fluxes over the specific energy ranges indicated in the figures. We see that the proton fluxes peaked at energies of ~ 10 keV or above in region I (Figure 3a), and exhibited the typical upward and downward loss cones of trapped fluxes with weak or no pitch angle diffusion (Figure 4c). In region II, both the trapped and precipitating components of the proton fluxes increased dramatically at low energies (Figures 3b and 4d) resulting in an energy spectrum peaked at ~ 1 keV. The angular distribution of these low energy protons was peaked well within the downward loss cone. This peak is primarily caused by the multiple spin DFI event in subregion IIa since the fluxes were approximately isotropic in the downward hemisphere for the remaining section of

region II (Figure 5). The precipitated energy flux resulting from the DFI's in this subregion is strongly enhanced (Figure 2) and sufficiently intense to excite visible proton auroras. The more energetic, ring current-like, component of the proton flux remained comparable to that of region I except that the downward coming loss cone (0°) was filled in. At higher latitudes, in region III, the fluxes decreased over the entire spectrum, but most dramatically at low energies (Figure 3c), and became isotropic in the downward hemisphere (Figure 4g,h,i). The peak near 180° in Figure 4g results from the UFI's discussed previously.

Ion composition. The abundances of ion species other than H^+ were determined for the low ($0.5 \leq E \leq 2.1$ keV) and high ($5.4 \leq E \leq 16$ keV) energy parts of both the trapped and precipitating components. No statistically significant amounts of He^{2+} , He^+ or O^+ ions were detected in any of the three regions however. Note that the upstreaming O^+ event in region II is not included in these averages since only trapped and precipitating fluxes are considered. The limits to the flux ratios in the low energy downward streaming component of region II were $(3 \pm 5) \times 10^{-3}$ for He^{2+}/H^+ and $(1 \pm 6) \times 10^{-3}$ for O^+/H^+ .

Downward flowing ion event of REV 1398

Overview. The second example of downward flowing ions to be discussed occurred during the main phase of the December 29, 1976 magnetic storm at -1051 UT. The observations of ionospheric ions in the ring current during this time period are discussed by Johnson et al. (1977). This event was observed in the premidnight local time sector near -0300 hours MLT at an altitude of ~5000 km above the southern auroral zone. The inner edge of the

plasma sheet, although not as clearly defined as in the previous example, was estimated to be at $\sim 56^\circ$ ILA on the basis of the decrease in the electron energy density. The plasma sheet extended to $\sim 69^\circ$ ILA where the more energetic electron and proton fluxes dropped below the sensitivity threshold of the instrument. Both upward and downward loss cones were observed in the energetic electrons up to $\sim 67^\circ$ ILA, which is indicative of closed field lines in the region equatorward of this "trapping boundary". Downward flowing ions were encountered on 8 consecutive spins during a 2.5 minute interval between 59.5° to 62.8° ILA. They involved peak fluxes of up to $6.7 \times 10^7 \text{ (cm}^2\text{-sec-ster-keV)}^{-1}$ and pitch angle anisotropies ranging from 1.7 to 11.1 with a statistical significance of typically $\geq 3\sigma$. Although significant fluxes of trapped O^+ ions were present in this event only the H^+ ions were field aligned (i.e. maximum along the magnetic field direction). As in the previous case this region of downward flowing ion distributions was designated as region II. Regions I and III were taken to extend from 57.0° to 59.5° and 62.8° to 65.7° ILA respectively. Thus, the DFI event was located in the more central section of the plasma sheet. A region of downward auroral electron acceleration approximately 1.5° wide occurred at the electron "trapping boundary", but the data showed no evidence of UFI distributions. Although the plasma number and energy densities exceeded those of the first example (see Table I), they were not unusual for these regions of the plasma sheet (Vasyliunas, 1970).

Energy and angular distributions. The differential energy spectra for the three regions are shown in Figure 6. We note the presence of a low energy trapped proton component in regions I and II with a relatively flat distribution below ~ 1 keV. These fluxes decreased significantly (by nearly a factor of 10) in region III. At higher energies (≥ 5 keV) the ring

current proton fluxes gradually decreased with latitude, but remained significant in all 3 regions. A comparison of the number densities and integral flux ratios (see Table 1) indicates that the low energy trapped protons were enhanced in region II with respect to the neighboring regions. As a result the average energy minimized here. The angular distribution of these low energy protons in region II was strongly peaked in the downward direction (180° pitch angle for this case since it was in the southern hemisphere) with a peak flux that was about an order of magnitude higher than the 90° flux (Figure 7d). At intermediate and high energies the angular distributions indicated onset of strong pitch angle scattering near the poleward edge of region II. Thus the differential energy spectrum for the precipitating component showed decreased fluxes at higher energies and a broad peak at about 1 keV (Figure 6). Although the electron fluxes were generally isotropic outside the loss cones in this region, strongly field aligned precipitating electrons with energies ≤ 1 keV were observed on 4 spins. Examples of these are displayed in Figure 8. The precipitated energy flux from these electrons projected to the ionosphere was ~ 3.5 (erg/cm²-sec) (on spin 7) while the low energy protons precipitated at an average rate of ~ 0.2 (erg/cm²-sec).

Ion composition. Although H^+ was again the major constituent of the ion fluxes, significant fluxes of O^+ and He^+ ions were also observed. The O^+ ions were more abundant at higher energies as indicated by the differential energy spectrum for region I, shown in Figure 6. The O^+/H^+ flux ratio in this higher energy component ($5.4 \leq E \leq 16$ keV) decreased progressively with increasing latitude going from $(1.3 \pm .1) \times 10^{-1}$ in region I, to $(7.8 \pm 1) \times 10^{-2}$ in region II, to $(4.1 \pm .8) \times 10^{-2}$ in region III. At low energies ($0.5 \leq E \leq 2.1$ keV) this ratio was $(3.6 \pm 1.9) \times 10^{-2}$ in region I. A statistically significant He^+/H^+ ratio $(2.4 \pm .6) \times 10^{-2}$ was obtained only for the

high energy component in region I. For all other regions and plasma components the fluxes of the minor ion species were consistently near background, (e.g. within the low energy downward flowing component of region II these ratios were $(-.9 \pm 1.3) \times 10^{-2}$ for $\text{He}^{2+}/\text{H}^+$, $(.8 \pm 1) \times 10^{-2}$ for He^+/H^+ and $(.6 \pm .7) \times 10^{-2}$ for O^+/H^+).

Statistical features of downward flowing ion events

To determine the morphology of the DFI events, data in form of survey plots of the type shown in Figure 1 were scanned visually for signatures of field aligned anisotropies. The study was limited to the high latitude regions poleward of the radiation belts (usually $\geq 60^\circ$ ILA) and to altitudes above ~ 2000 km. It was based on the same data set that was used in the statistical study of UFI distributions (Ghielmetti et al., 1978a), covering the time period from July 1976 to February 1977 and including ~ 370 satellite orbits.

For the purpose of this survey we defined the pitch angle anisotropy as the ratio of flux in the downward direction to the flux at $\sim 90^\circ$. In general, a downward field aligned component must be distinguished from statistical fluctuations of the isotropic population. The estimated sensitivity thresholds for this survey are as follows: the pitch angle anisotropy must exceed ~ 7.5 , 4 and 2.5 if the isotropic fluxes are ~ 1 , 7 and 20×10^6 ($\text{keV}/\text{cm}^2\text{-sec-ster-keV}$), respectively. To be accepted as a DFI event we required that either anisotropies meeting the above criteria recur for at least two consecutive spins (multiple) or that the anisotropy exceed ~ 10 on single spins (single). With these constraints only 2 multiple and 6 single spin DFI events were observed; corresponding to a frequency of occurrence of less than .05 per orbit.

These DFI events were observed at altitudes above ~4000 km on the night side (1500 - 0700 MLT). They typically consisted of field aligned H^+ ions only, with energies less than ~3 keV. Occasionally more energetic protons with energies up to 16 keV and O^+ ions were observed. DFI events were frequently located equatorward of and at times immediately adjacent to UFI or auroral electron acceleration regions. At least one event (REV 2210) was discovered where DFI distributions occurred on several spins within a wide region of UFI distributions. In this case the UFI's consisted largely of O^+ ions with energy less than ~4 keV while the DFI's were exclusively H^+ with energies up to 16 keV.

The local time region around dawn was inadequately sampled during the time period of the initial study. Therefore, to investigate whether or not a dawn-dusk asymmetry of the type observed in the UFI events existed, a separate study of data acquired when the orbit of the S3-3 satellite was in the dawn-dusk plane was made. For this purpose data from May to September 1977 were added. A total of ~200 orbits satisfied the condition of passing within ~2 hours MLT of dusk and dawn. In this separate study we identified 9 single spin events and 1 multiple spin event in the dusk sector and 7 single spin events and no multiple spin event in the dawn sector. Thus, in contrast to the UFI events (Ghielmetti et al., 1978), no statistically significant difference is indicated in the occurrence frequency of DFI events between dawn and dusk.

DFI events were often observed in association with subregions of enhanced fluxes of trapped ions of similar energies. To determine the frequency of occurrence of these subregions, data from the dusk portion of the previously described separate study were examined. For this analysis we defined an "enhanced plasma event" as a large (~10x) energy flux increase in

AD-A066 150

LOCKHEED MISSILES AND SPACE CO INC PALO ALTO CALIF PA--ETC F/G 4/1
LOW-ENERGY PARTICLE EXPERIMENT.(U)

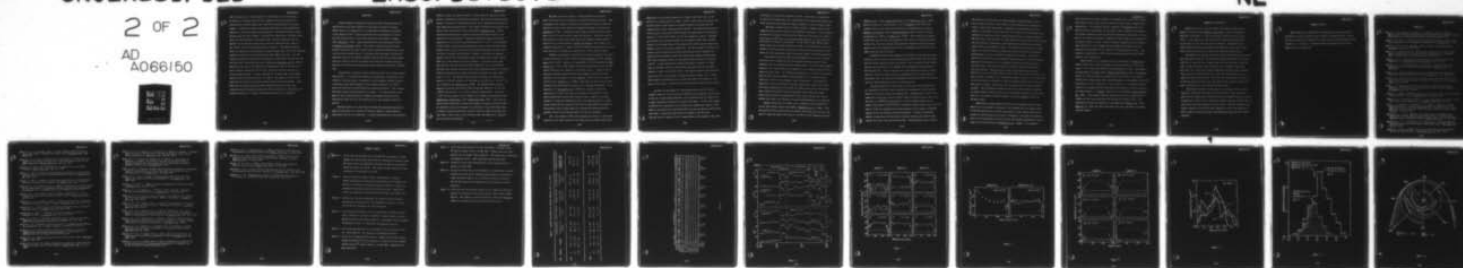
FEB 79 R D SHARP
LMSC/D673078

N00014-72-C-0234
NL

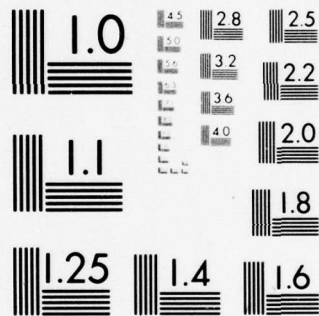
UNCLASSIFIED

2 OF 2

AD
A066150



END
DATE
FILMED
5-79
DDC



MICROCOPY RESOLUTION TEST CHART
NATIONAL BUREAU OF STANDARDS-1963-A

the soft protons ($E \leq 5$ keV) relative to the harder ($E \geq 5$ keV) protons. In addition we required that the more energetic protons be present over latitudinally extended regions both equatorward and poleward of these subregions. Using this criterion any plasma enhancements located immediately adjacent to the low or high latitude boundary of observable energetic proton fluxes would have been excluded. The study was restricted to the dusk sector where the inner boundary of the plasma sheet could be identified from the decrease in the electron energy fluxes (see for example REV 619, Figure 1). The results of this study are presented in Figure 9. The shaded histogram shows the probability of observing an enhanced plasma event within the indicated latitude interval in the 16-20 MLT sector above 6000 km altitude. For comparative purposes the latitudinal distribution of UFI events averaged over the two dusk local time sectors has been included from Chielmetti et al. (1978a). Enhanced plasma events were observed on approximately 25% of the orbits and most frequently between 66° and 74° ILA. Their low latitude boundary was on the average located ~ 1 L-unit poleward of the inner edge of the plasma sheet and their average width was ~ 1.7 L-units. The majority of DFI events observed were found to occur within these enhanced plasma subregions. Since both types of events occur relatively infrequently and both types have relatively narrow latitudinal extension, this correlation is significant and further indicative of a causal relationship between the two phenomena.

DISCUSSION

In both examples of downward flowing ions (DFI) presented above the distributions were field aligned in pitch angle and peaked in energy. These features are suggestive of an acceleration preferentially parallel to the magnetic field. Several mechanisms have been proposed to account for such distributions in the auroral electrons (see reviews by Evans, 1975; Fälthammar, 1977). Fermi acceleration has been discussed in detail by Sharber and Heikkila (1972). This process requires multiple bounces between hemispheres and thus results in both upward and downward loss cones in the ion and electron fluxes. In contrast the pitch angle distributions described above for the protons (Figures 5 and 7) and for the field aligned electrons (Figures 1 and 8) are peaked well within the downward loss cone, and thus are inconsistent with having resulted primarily from Fermi acceleration.

Alternatively, parallel electric fields may give rise to field aligned distributions. If the DFI are produced by electrostatic acceleration of an initially isotropic plasma, the degree of field alignment observed requires a relatively cold source population with energies typically $\leq 1 \times 10^2$ eV (near the satellite) and decreasing with increasing altitude. This excludes the hotter plasma sheet population as a source. It is not possible on the basis of the ion distributions to uniquely distinguish between parallel acceleration above but near the satellite and at the conjugate hemisphere however.

The detectability of a DFI event resulting from downward acceleration above the spacecraft is a function of both the degree of field alignment (anisotropy) and the flux amplitude. A precise determination of the effective

probing distance for downward directed fields above the spacecraft would require a knowledge of many plasma parameters that are not presently known; however, estimates of the probing distance can be obtained on the basis of some simplifying considerations. For a model of parallel electrostatic and scatter-free acceleration such as discussed by Kaufmann et al., (1976), the minimum plasma density required to provide detectable fluxes at the satellite may be calculated. Assuming a Maxwellian plasma with typical temperatures of ≤ 10 eV the required densities are $\sim 1 \text{ cm}^{-3}$. In the absence of pitch angle scattering and perpendicular heating these resultant field aligned fluxes will be contained in the downward hemisphere if the source is within $\sim 8 R_E$ above the satellite. However, in view of the observed angular width of UFI distributions within the acceleration region (10 - 20° FWHM) this simple model may not be realistic. If one uses pitch angle distributions with these greater widths immediately after acceleration, and takes into account the sensitivity levels discussed earlier, the maximum effective probing distance above the satellite reduces to a more typical value of $\sim 3 R_E$. The typical ambient plasma densities and temperatures measured on the S3-3 satellite at altitudes up to 8000 km are 5 - 50 cm^{-3} and 1 - 5 eV respectively (Mozier et al., 1978). The ambient plasma densities measured during the DFI events on REV 619 and REV 1398 were $\sim 10 \text{ cm}^{-3}$ and $\sim 10^2 \text{ cm}^{-3}$ respectively (F. S. Mozer, private communication). Values of $\sim 1 \text{ cm}^{-3}$ are not unusual for the regions at or beyond the synchronous orbit (Lennartsson and Reasoner, 1978; Gurnett and Frank, 1974). Since the ambient plasmas conditions are generally adequate to produce detectable DFI's we conclude from the low frequency of occurrence of these DFI events that if downward directed quasistatic parallel electric fields involving potential drops ≥ 500 V occur in the altitude range from 2000 km to $\sim 3 R_E$ they are an infrequent phenomenon.

The above conclusion implies a strong asymmetry in the mechanism for parallel ion acceleration, favoring the upward direction. Such an asymmetry may indeed be expected if the parallel electric fields are primarily related to the effects of magnetic mirroring as discussed by Lennartsson (1976). According to other models parallel electric fields may result from current driven plasma instabilities. Since the peak current densities of the large scale upward and downward flowing currents observed by the TRIAD satellite (Iijima and Potemra, 1976, 1978) are of comparable magnitude, it appears that the downward flowing currents may be less effective in driving such instabilities in this altitude range.

Evidence that downward acceleration of positive particles may occur at lower altitudes has been reported by Rème and Bosqued (1971) and Hultqvist (1971, 1978). However, the anisotropic ion fluxes observed by Hultqvist et al. (1971, 1978) exhibit different characteristics from the DFI events presented here suggesting a different process. Intense beams of narrowly collimated upward flowing field aligned electrons have been observed near the magnetic equator (McIlwain, 1975) and more recently at the S3-3 orbit (Sharp et al., 1978b). They have not been observed simultaneously with DFI events and appear to be a separate phenomenon. At an altitude of $\sim 1 R_E$ Fennell et al. (1978) have recently reported the observation of a DFI event that was interpreted as consistent with a local downward directed parallel electric field. However, the observations of a region of downward electron acceleration within the region of DFI in REV 619 and concurrent with DFI's in REV 1938 do not appear to be consistent with a simple model of a quasistatic downward directed parallel electric field located above but near the satellite.

The two examples of DFI events presented in detail in this paper occurred in the inner regions of the plasma sheet on closed field lines.

Examination of the plasma parameters in Figure 2 and Table I and of the differential energy spectra in Figure 3 and 6 reveals that both events were located within a wider region of strongly enhanced low energy (≤ 2 keV) trapped proton fluxes (enhanced plasma events). The enhancement was particularly large in the case of REV 619 where the number density increased by factors of ~ 8 and $> 10^2$ relative to the two neighboring regions. Although the increase was relatively smaller in the example of REV 1398, possibly because of the larger fluxes of hot ring current plasma present during the magnetic storm, it was still significant. The more energetic (≥ 5 keV) ring current protons exhibited relatively unstructured fluxes throughout the plasma sheet and remained unaffected during these enhanced plasma events. Thus these subregions appear as high density plasma clouds of relatively cold ($kT \sim .5$ keV) protons with limited latitudinal extension ($\sim 3^\circ$ ILA). They are embedded within the plasma sheet and within the more extended regions of hotter ring current fluxes. The enhanced plasma cloud ions and concurrent DFI's were observed at similar energies (Figure 3, 6). Since their angular distributions were in both cases wider (see Figure 5b, 7d) than the loss cones, a fraction of the downstreaming population was trapped.

In order to investigate the relationship between the DFI and the trapped components in more detail we subjected the anisotropy and the ratio of the low to high energy components of the trapped fluxes in region II to a linear regression analysis on a spin-by-spin basis. In the first example of REV 619 the correlation was not found to be significant; however, this data set contained only 4 spins with DFI's and the statistical uncertainties were large. Using the 8 spin periods in region II and the first and last spin of regions III and I respectively in the example of REV 1398

we obtained a correlation coefficient of 0.8. This value is significant at the 1% level suggesting that a correlation did in fact exist between the field aligned precipitating and trapped component of the low energy fluxes.

The ionic composition of the fluxes provides a further means of distinguishing between the origins of the different components. In the example of REV 619 only protons were positively identified; the absence of significant fluxes of He^{2+} ions in the precipitating component is consistent with an ionospheric origin for the plasma. In the event of REV 1398 the high energy component contained substantial amounts of O^+ and He^+ ions while the enhanced low energy plasma was devoid of these species and exhibited essentially the same composition within statistical limits as the DFI population.

The results discussed above are thus suggestive of a causal relationship between the trapped and the field aligned precipitating low energy components and are consistent with a common origin. Since the field aligned component has a higher phase space density it is a potential source for the enhanced plasma cloud. It is therefore suggested that in these two examples both the DFI's and the enhanced trapped plasma clouds resulted from the injection of UFI's in the conjugate auroral ionosphere. The absence of significant fluxes of O^+ ions in the DFI component may have resulted from the initial composition of the source UFI and/or from velocity dispersion. Since upward streaming O^+ ions have generally lower fluxes and longer bounce periods than the accompanying H^+ ions, their filling times become considerably longer and transport processes correspondingly more effective.

Upward flowing ions are known to be a commonly occurring phenomenon in the high altitude auroral ionospheres (Ghielmetti et al., 1978a). They are generally highly anisotropic and involve peak fluxes that are up to one order of magnitude higher than those of the DFI's in the examples presented

(Shelley et al., 1977; Mizera and Fennell, 1977; Ghielmetti et al., 1978a). Bouncing clusters of ions inferred to be O^+ (McIlwain, 1976) and field aligned energetic ions have been observed at the geosynchronous orbit by DeForest and McIlwain (1971), Mauk and McIlwain (1975), and more recently by Geiss et al. (1978), and Borg et al. (1978). These observations suggest indeed that some UFI cross the equatorial plane prior to becoming isotropic and may thus reach the conjugate high altitude ionosphere where they would appear as DFI's or enhanced plasma events, depending on the degree of pitch angle scattering during transit.

A comparison between the frequency of occurrence of DFI and UFI events indicates that the latter occurred approximately 10x to 100x more frequently than the former during the same time period. Only a fraction of this difference may be attributed to the somewhat lower sensitivity for detection of DFI distributions. Thus we conclude that pitch angle scattering is usually effective within 1/2 bounce period in isotropizing the UFI distributions, and further that the injection of energetic ions from the auroral UFI source into the trapped population must be a common process.

The time required for a UFI source to fill a flux tube isotropically to a specified flux level can be estimated by comparing the total particle contents of the flux tube to the upgoing flux. Assuming that the UFI's are completely isotropized within 1/2 bounce period and using typical values for the flux ($\sim 1 \times 10^8/\text{cm}^2\text{-sec-ster-keV}$) at 1 keV and typical widths of the angular distributions ($10\text{-}20^\circ$ FWHM) we calculate filling times of the order of 1 hour to reach the isotropic flux levels observed in the regions of enhanced plasmas in the two examples discussed previously. However, considerably shorter filling times (of the order of minutes) would result from the most intense UFI events that have been observed. These estimates do not include

the effects of losses from e.g. charge exchange and longitudinal and radial transport; however, these effects are not expected to be important in cases of rapid flux tube filling. Although the actual durations of UFI events are not known, times of the order of 1 hour are not unreasonable considering the duration of other related phenomena such as auroral substorms. Thus UFI fluxes are sufficient to inject clouds of trapped ions on time scales and with densities comparable to the substorm associated equatorial plasma clouds (DeForest and McIlwain, 1971). The proposed injection process could result in a cloud of ions of latitudinally limited extension with energies corresponding to those of the UFI's (typically a few keV). The process would not directly affect an equatorial population such as the more energetic ring current component that was transported inward from regions deeper in the plasma sheet and could thus result in multiple component plasmas of the type observed. Enhanced plasma events as described above are often observed in the same general regions as UFI events in the dusk local time sector, but peak at somewhat lower latitudes as shown in Figure 9. The difference in the latitudinal distributions of UFI and enhanced plasma events may result from radial transport combined with the much longer filling times at higher L-values. The latitudinal location of the peak in the occurrence frequency of enhanced plasma events is also seen to be in good agreement with the quiet time ($K_p = 2$) substorm injection boundary inferred by McIlwain (1974) for the dusk region.

These facts strongly suggest that some of the enhanced plasma events observed at low altitudes correspond to the substorm injected plasma clouds in the equatorial plane, and that they result at least in part from the injection of upward flowing ions from the ionosphere. UFI events are known to occur in a latitudinally well defined zone with maximum probability of occurrence in the dusk hemisphere (Ghielmetti et al., 1978a). For a qualita-

tive illustration we show in Figure 10 a mapping of the local time-latitude distribution of UFI events into the equatorial plane using a simple dipole approximation. The substorm injection boundary from McIlwain (1974) has been included for comparison. We note that in this projection the location of the most frequently occurring UFI events generally corresponds to the region of the injection boundary, although the peak frequency of occurrence is at somewhat higher L values. Thus the auroral ionosphere may be a significant contributor to the trapped ions that dominate the dynamics of the equatorial magnetosphere in the vicinity of the geostationary orbit. The statistical association of DFI events with enhanced plasma events further supports these suggestions.

These results are in agreement with the conclusions of Sharp et al., (1976a, 1976b) that a local ionospheric injection process acts over wide range of local times and latitudes during geomagnetic storms. Near equatorial measurements by Frank (1970), DeForest and McIlwain (1971) and McIlwain (1974) have indicated plasma injection events well inside of the geostationary orbit during magnetically disturbed periods. The example of REV 1398 corresponds to such an injection at low L-values of ~ 4 . Structured intense fluxes of low energy ions have been previously observed in the near equatorial region beyond $L \approx 8$ (Frank, 1967) and at low altitudes (Frank and Ackerson, 1972). These exhibit similar characteristics to the enhanced plasma regions and DFI events presented here and may be related to them. The antisunward flowing ions observed in the magnetotail (Frank et al., 1977; Hardy et al., 1977) may result from UFI's that were injected in the higher latitude regions.

SUMMARY AND CONCLUSIONS

Enhanced clouds of ions with fluxes and energies similar to the equatorial plasma clouds (DeForest and McIlwain, 1971) are frequently observed at altitudes of $\sim 1 R_E$ in the auroral zones by the S3-3 satellite. In the dusk local time sectors these regions map equatorially to the region of the substorm injection boundary. Downward flowing field aligned ions have occasionally been detected in the auroral zones. They occurred preferentially within these enhanced plasma regions.

Two examples of downward flowing ion (DFI) and enhanced plasma events were described in detail. The correlations observed between the two populations are suggestive of a common origin for both phenomena in the upward flowing ion (UFI) events occurring in the conjugate hemisphere. DFI events are a much less frequent phenomenon than UFI events, implying that injection of upward flowing ions into the trapped population is a common and significant process. The local time and latitude distributions of UFI and enhanced plasma events and their similar energies further suggest a relationship to the equatorial plasma clouds.

The results described in this paper are consistent with the direct injection of spatially localized clouds of hot (0.5-5 keV) ionospheric ions into the plasma sheet, from the auroral zone upward flowing ion source. A significant fraction of the equatorial substorm injected plasma clouds may thus result from this ionospheric source region. The more energetic ring current component (≥ 5 keV) may have originated in part from injection of UFI on higher latitude field lines and subsequent energization by inward transport.

ACKNOWLEDGEMENTS

This research was supported by the Atmospheric Sciences section of the National Science Foundation and the Office of Naval Research. One of us (A.C.) was partially supported by a grant from the Swiss National Science Foundation. We thank Dr. W. Lennartsson for providing Figure 10 from a paper of his in preparation.

REFERENCES

- Borg, H., L. A. Holmgren, B. Hultqvist, F. Cambou, H. Rème, A. Bahnsen and G. Kremser, "The keV plasma experiment on GEOS-1 and some early results," KGI Preprint No. 78:303, Kiruna Geophys. Institute, Kiruna, 1978.
- Cladis, J. B. and R. D. Sharp, "Scale of electric field along magnetic field in an inverted-V event," accepted for publication, J. Geophys. Res., 1978.
- DeForest, S. E. and C. E. McIlwain, "Plasma clouds in the magnetosphere," J. Geophys. Res., 76, 3587, 1971.
- Evans, D. S., "Evidence for the low-altitude acceleration of auroral particles," in Physics of the Hot Plasma in the Magnetosphere, B. Hultqvist and L. Stenflo, ed., p. 319, Plenum Press, New York, 1975.
- Fälthammar, C. G., "Problems related to macroscopic electric fields in the magnetosphere," Rev. Geophys. and Space Phys., 15, 457, 1977.
- Fennell, J. F., P. F. Mizera and D. R. Croley, Jr., "Observation of ions accelerated toward the earth at high latitudes," EOS Trans. AGU, 59, 348, 1978.
- Frank, L. A., "Several observations of low energy protons and electrons in the earth's magnetosphere withOGO3," J. Geophys. Res., 72, 1905, 1967.
- Frank, L. A., "Direct detection of asymmetric increases of extraterrestrial 'ring current' proton intensities in the outer radiation zone," J. Geophys. Res., 75, 1263, 1970.
- Frank, L. A., "Relationship of the plasma sheet, ring current, trapping boundary, and plasmopause near the magnetic equator and local midnight," J. Geophys. Res., 76, 2265, 1971.
- Frank, L. A., and K. L. Ackerson, "Local-time survey of plasma at low altitudes over the auroral zones," J. Geophys. Res., 77, 4116, 1972.
- Frank, L. A., K. L. Ackerson, and D. M. Yeager, "Observations of atomic oxygen (O^+) in the earth's magnetotail," J. Geophys. Res., 82, 129, 1977.
- Geiss, J., H. Balsiger, P. Eberhardt, H. P. Walker, L. Weber, D. T. Young and H. Rosenbauer, "Dynamics of Magnetospheric ion composition by the GEOS mass spectrometer," 13th ESLAB Symposium, Innsbruck, Austria, Space Sci. Rev., in press, 1978.
- Ghielmetti, A. G., R. G. Johnson, R. D. Sharp, and E. G. Shelley, "The latitudinal, diurnal, and altitudinal distributions of upward flowing energetic ions of ionospheric origin," Geophys. Res. Lett., 5, 59, 1978a.
- Ghielmetti, A. G., E. G. Shelley, R. D. Sharp and R. G. Johnson, "Downward streaming field aligned ion fluxes in the auroral zone," EOS Trans. AGU, 59, 348, 1978b.
- Gurnett, D. A. and L. A. Frank, "Thermal and suprathermal plasma densities in the outer magnetosphere," J. Geophys. Res., 79, 2355, 1974.

- Hardy, D. A., J. W. Freeman, and H. K. Hills, "Double-peaked ion spectra in the lobe plasma: evidence for massive ions?" J. Geophys. Res., 82, 5529, 1977.
- Hultqvist, B., H. Borg, W. Riedler and P. Christophersen, "Observations of magnetic field aligned anisotropy for 1 and 6 keV positive ions in the upper ionosphere," Planet. Space Sci., 19, 279, 1971.
- Hultqvist, B. and H. Borg, "Observations of energetic ions in inverted V-events," Planet. Space Sci., 26, 673, 1978.
- Iijima, T., and T. A. Potemra, "The amplitude distribution of field-aligned currents at northern high latitudes observed by triad," J. Geophys. Res., 81, 2165, 1976.
- Iijima, T., and T. A. Potemra, "Large scale characteristics of field-aligned currents associated with substorms," J. Geophys. Res., 83, 599, 1978.
- Johnson, R. G., R. D. Sharp, and E. G. Shelley, "Composition of the hot plasma in the magnetosphere," in Physics of the Hot Plasma in the Magnetosphere, B. Hultqvist and L. Stenflo, eds., p. 45, Plenum, New York, 1975.
- Johnson, R. G., R. D. Sharp, and E. G. Shelley, "Observation of ions of ionospheric origin in the storm-time ring current," Geophys. Res. Lett., 4, 403, 1977.
- Kaufmann, R. L., D. N. Walker, and R. L. Arnoldy, "Acceleration of auroral electrons in parallel electric fields," J. Geophys. Res., 81, 1673, 1976.
- Lennartsson, W., "On the magnetic mirroring as the basic cause of parallel electric fields," J. Geophys. Res., 81, 5583, 1976.
- Lennartsson, W. and D. L. Reasoner, "Low-energy plasma observations at synchronous orbit," J. Geophys. Res., 83, 2145, 1978.
- Mauk, B. H., and C. E. McIlwain, "ATS-6 UCSD auroral particles experiment," IEEE Trans. on Aerospace and Electronic Systems, 11, 1125, 1975.
- McIlwain, C. E., "Substorm injection boundaries," in Magnetospheric Physics, B. M. McCormac, ed., D. Reidel, Dordrecht, Holland, p. 143, 1974.
- McIlwain, C. E., "Auroral electron beams near the magnetic equator," in Physics of the Hot Plasma in the Magnetosphere, B. Hultqvist and L. Stenflo, eds., p. 91, Plenum Press, New York, 1975.
- McIlwain, C. E., "Bouncing clusters of ions at seven earth radii," EOS Trans. AGU, 57, 307, 1976.
- Mizera, P. F., and J. F. Fennell, "Signatures of electric fields from high and low altitude particle distributions," Geophys. Res. Lett., 4, 311, 1977.

- Mozer, F. S., C. W. Carlson, M. K. Hudson, R. B. Torbert, B. Parady, J. Yatteau, and M. C. Kelley, "Observations of paired electrostatic shocks in the polar magnetosphere," Phys. Rev. Lett., 38, 292, 1977.
- Mozer, F. S., C. Cattell, M. Temerin, R. B. Torbert, S. Von Glinski, M. Woldorff, J. Wygant, "The DC and AC electric field, plasma density, plasma temperature and field aligned current experiments on the S3-3 satellite. Submitted to J. Geophys. Res., 1978.
- Rème, H. and J. M. Bosqued, "Evidence near the auroral ionosphere of a parallel electric field deduced from energy and angular distributions of low-energy particles," J. Geophys. Res., 76, 7683, 1971.
- Schield, M. A. and L. A. Frank, "Electron observations between the inner edge of the plasma sheet and the plasmasphere," J. Geophys. Res., 75, 5401, 1970.
- Sharber, J. R. and W. J. Heikkila, "Fermi acceleration of auroral particles," J. Geophys. Res., 77, 3397, 1972.
- Sharp, R. D., R. G. Johnson, E. G. Shelley, and K. K. Harris, "Energetic O^+ ions in the magnetosphere," J. Geophys. Res., 79, 1844, 1974.
- Sharp, R. D., R. G. Johnson, and E. G. Shelley, "The morphology of energetic O^+ ions during two magnetic storms: temporal variations," J. Geophys. Res., 81, 3283, 1976a.
- Sharp, R. D., R. G. Johnson, and E. G. Shelley, "The morphology of energetic O^+ ions during two magnetic storms: latitudinal variations," J. Geophys. Res., 81, 3292, 1976b.
- Sharp, R. D., R. G. Johnson, and E. G. Shelley, "Observation of an ionospheric acceleration mechanism producing energetic (keV) ions primarily normal to the geomagnetic field direction," J. Geophys. Res., 82, 3324, 1977.
- Sharp, R. D., R. G. Johnson and E. G. Shelley, "Energetic particle measurements from within ionospheric structures responsible for auroral acceleration process," accepted for publication, J. Geophys. Res., 1978a.
- Sharp, R. D., E. G. Shelley, R. G. Johnson and A. G. Ghielmetti, "Counterstreaming electron beams at altitudes of $\sim 1 R_E$ over the auroral zone," EOS Trans. AGU, 59, 1978b.
- Shelley, E. G., R. G. Johnson and R. D. Sharp, "Satellite observations of energetic heavy ions during a geomagnetic storm," J. Geophys. Res., 77, 6104, 1972.
- Shelley, E. G., R. G. Johnson and R. D. Sharp, "Morphology of energetic O^+ in the magnetosphere," in Magnetospheric Physics, B. M. McCormac, ed., p. 135, D. Reidel, Dordrecht, Holland, 1974.

Shelley, E. G., R. D. Sharp, and R. C. Johnson, "Satellite observations of an ionospheric acceleration mechanism, Geophys. Res. Lett., 3, 654, 1976.

Shelley, E. G., "Heavy ions in the magnetosphere," invited review, International Symposium on Solar-Terrestrial Physics, Innsbruck, Austria, Space Sci. Rev., in press, 1978.

Torbert, R. B., and F. S. Mozer, "Electrostatic shocks as the source of discrete auroral arcs," Geophys. Res. Lett., 5, 135, 1978.

Vasyliunas, V. M., "A survey of low-energy electrons in the evening sector of the magnetosphere with OGO 1 and OGO 3," J. Geophys. Res., 73, 2839, 1968.

Vasyliunas, V. M., "Magnetospheric plasma," in Solar-Terrestrial Physics, E. R. Dyer, ed., D. Reidel, Dordrecht, Holland, p. 192, 1970.

FIGURE CAPTIONS


 Figure 1: Survey plot for the dusk section of REV 619 on September 24, 1976 showing ion and electron count rates as a function of universal time. The count scales are logarithmic and each tic mark on the vertical scales represents one decade. The various regions indicated in the top margin are described in the text.

Figure 2: Electron and proton number density, energy density, average energy and precipitated energy flux projected to the ionosphere are given as a function of invariant latitude for REV 619. Values are averaged over periods indicated by horizontal bars. Statistical errors are indicated by vertical bars when larger than symbol size.

Figure 3: Differential energy distributions for trapped (circles) and for precipitating (triangles) H^+ ions averaged over regions I, II and III of REV 619. Background has been subtracted.

Figure 4: Pitch angle distributions for low, intermediate and high energy H^+ ions in regions I, II and III of REV 619. Number fluxes were integrated over the energy ranges indicated. The dashed lines correspond to background levels. 0° represents the downward direction.

Figure 5: Pitch angle distributions for low energy H^+ ions in region IIa and II - IIa of REV 619. 0° represents the downward direction.

Figure 6: Differential energy distributions for trapped (circles) and precipitating (triangles) H^+ ions in regions I, II and III and for trapped (solid circles) O^+ ions in region I of REV 1398. Background has been subtracted.

Figure 7: Pitch angle distributions for low, intermediate and high energy H^+ ions in regions I and II of REV 1398. Number fluxes were integrated over the energy ranges indicated. The dashed lines correspond to background levels. 180° represents downward direction.

Figure 8: Examples of pitch angle distributions of low energy electron in region II of REV 1398.

Figure 9: Histogram distribution of the probability of observation of upward flowing ion events and of enhanced plasma events in the altitude range from 6000 - 8000 km, as a function of invariant latitude. The UFI distribution was averaged over the 2 local time sectors indicated.

Figure 10: Projection into the equatorial plane of the regions of high probability of occurrence of UFI events using a simple dipole approximation. The substorm injection boundaries inferred by McIlwain, (1974) are indicated by the heavy lines for Kp-2 and 5.

TABLE I. PLASMA PARAMETERS FOR TRAPPED PROTONS ($30^\circ \leq \alpha \leq 150^\circ$)

REV	Region	L-Range	Number density $0.5 \leq E \leq 2.1$ keV (cm^{-3})	Number density $0.5 \leq E \leq 16$ keV (cm^{-3})	Energy density $0.5 \leq E \leq 16$ keV ($\text{keV}/\text{cm}^{-3}$)	Average energy $0.5 \leq E \leq 16$ keV (keV)	Integral flux ratio $\frac{0.5 \leq E \leq 2.1 \text{ keV}}{0.5 \leq E \leq 16 \text{ keV}}$
619	I	6.5 - 9.3	$.004 \pm .007$	$.070 \pm .008$	$.70 \pm .03$	10.0 ± 1.2	$.02 \pm .03$
	II	9.3 - 13.7	$.88 \pm .03$	$.93 \pm .03$	$1.58 \pm .04$	$1.61 \pm .07$	$5.0 \pm .3$
	III	13.7 - 28.	$.11 \pm .01$	$.17 \pm .01$	$.54 \pm .03$	$3.19 \pm .25$	$1.0 \pm .1$
1398	I	3.4 - 3.9	$1.57 \pm .08$	$2.94 \pm .09$	$12.2 \pm .26$	$4.16 \pm .15$	$.56 \pm .03$
	II	3.9 - 4.8	$1.90 \pm .09$	$2.77 \pm .09$	$8.44 \pm .19$	$3.05 \pm .12$	$1.07 \pm .06$
	III	4.8 - 5.9	$.25 \pm .04$	$.67 \pm .04$	$4.06 \pm .14$	$6.10 \pm .42$	$.22 \pm .03$

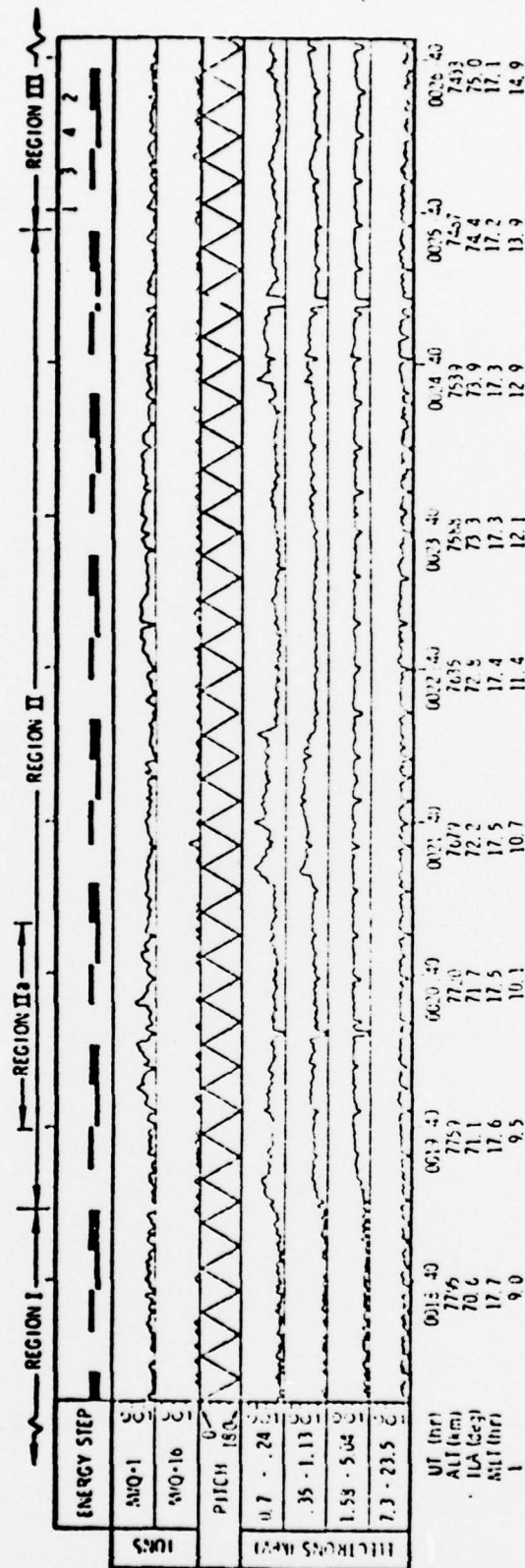


Figure 1

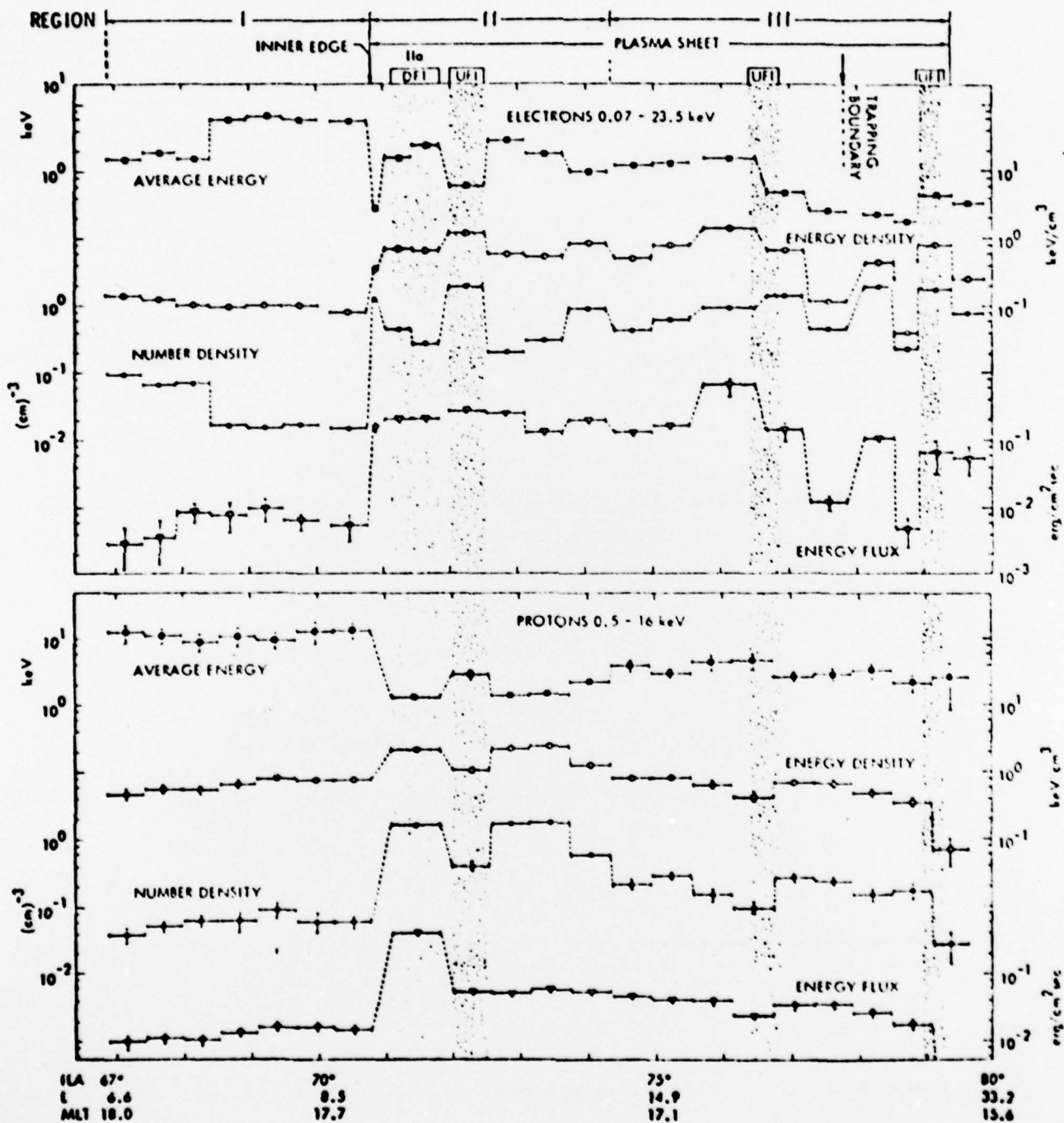


Figure 2

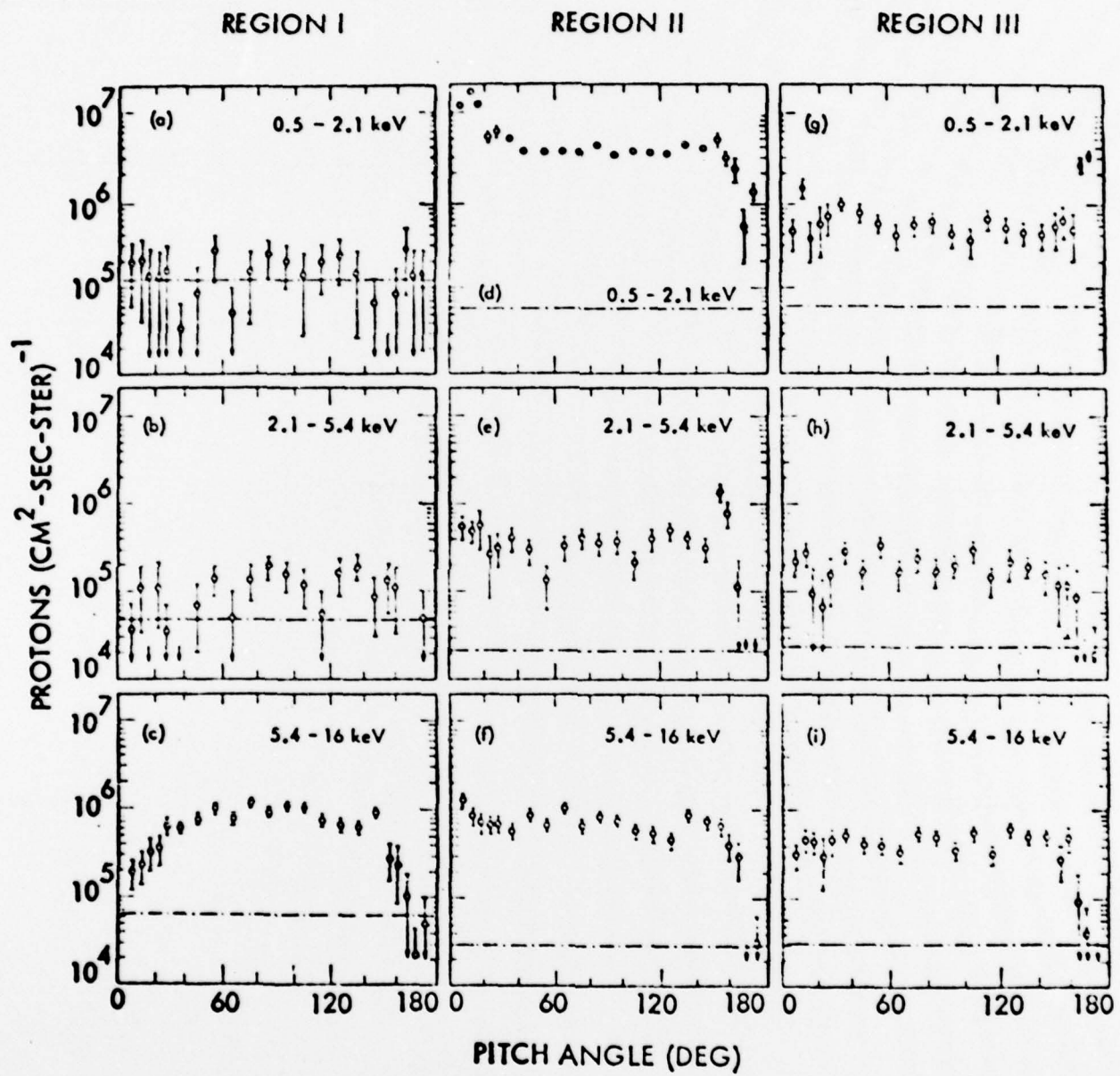


Figure 4

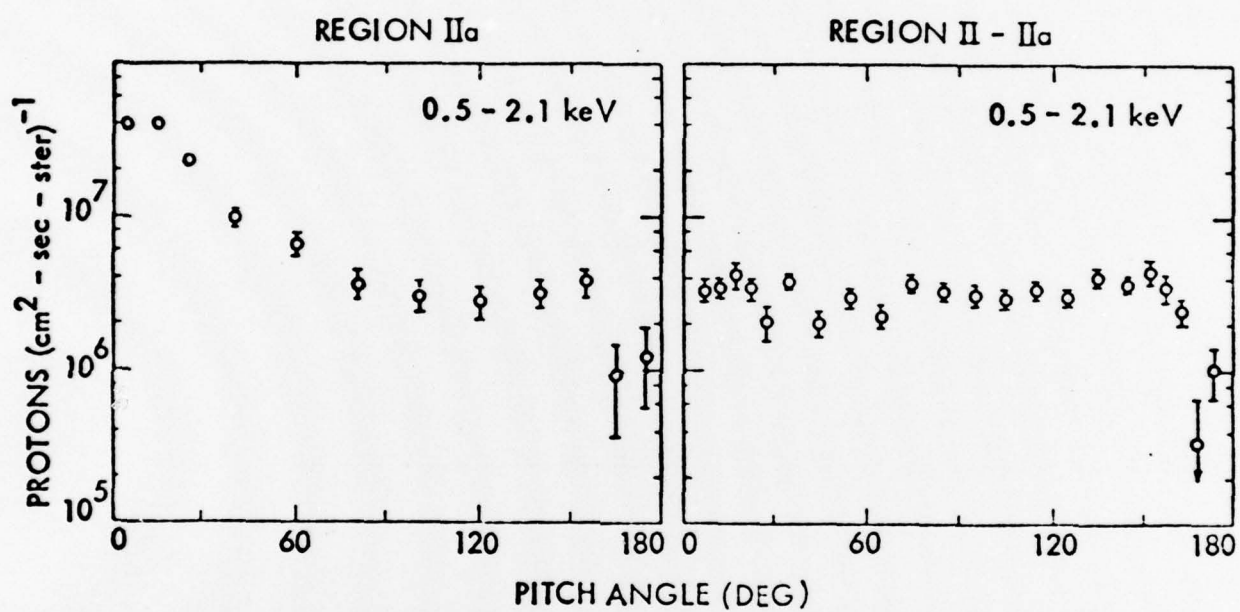


Figure 5

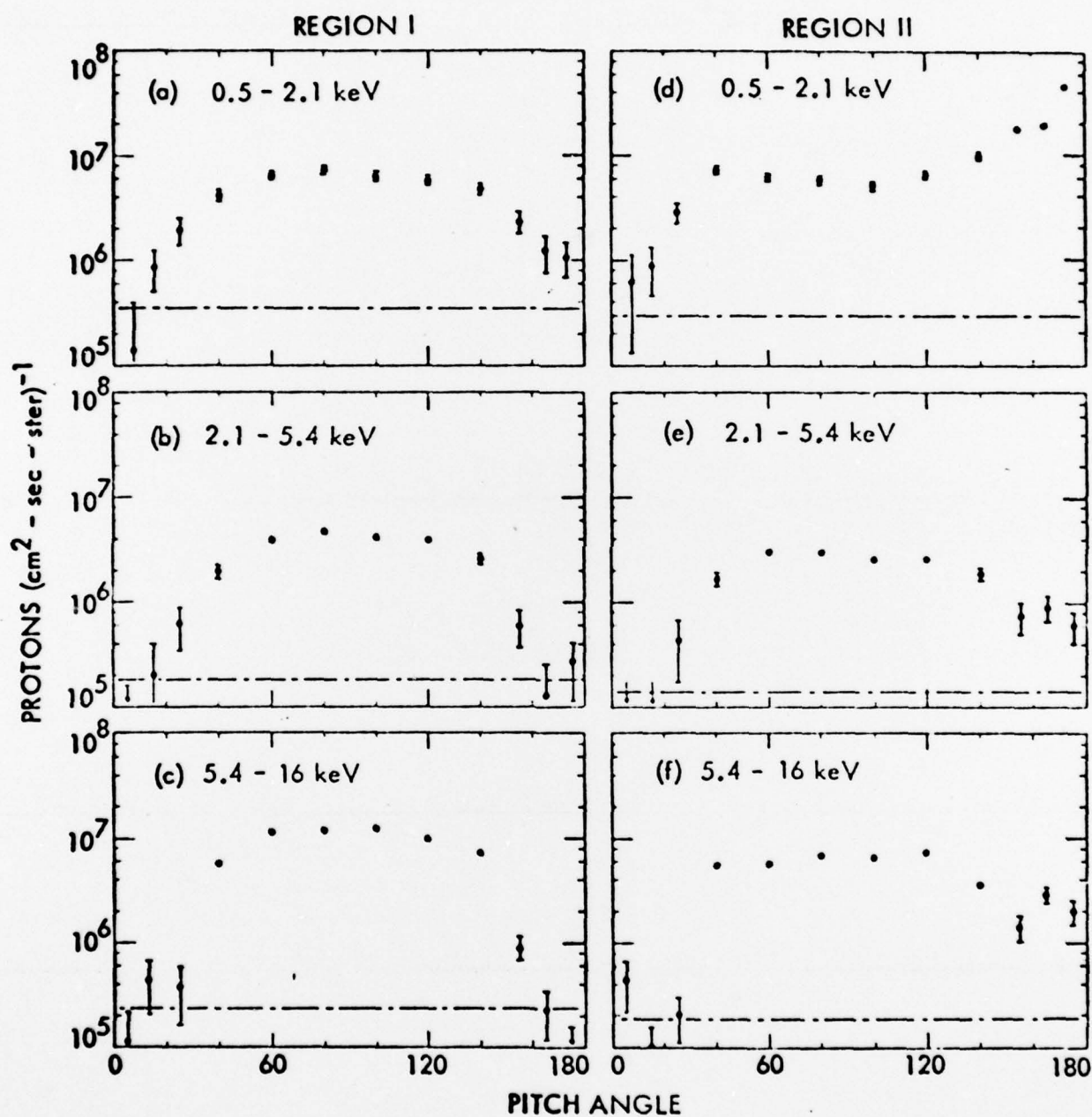


Figure 7

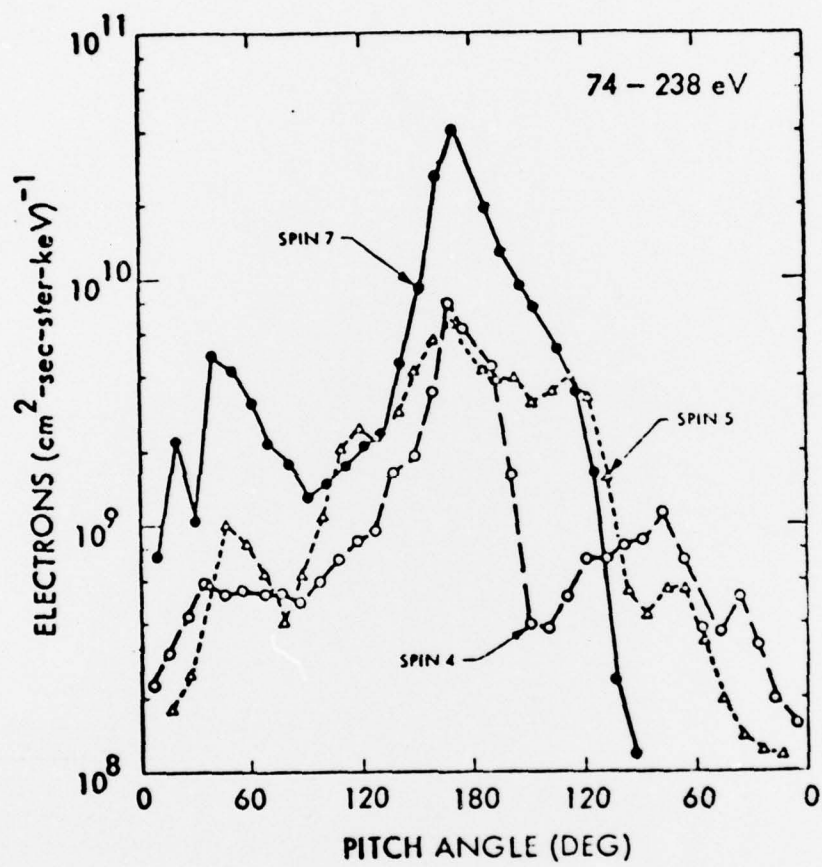


Figure 8

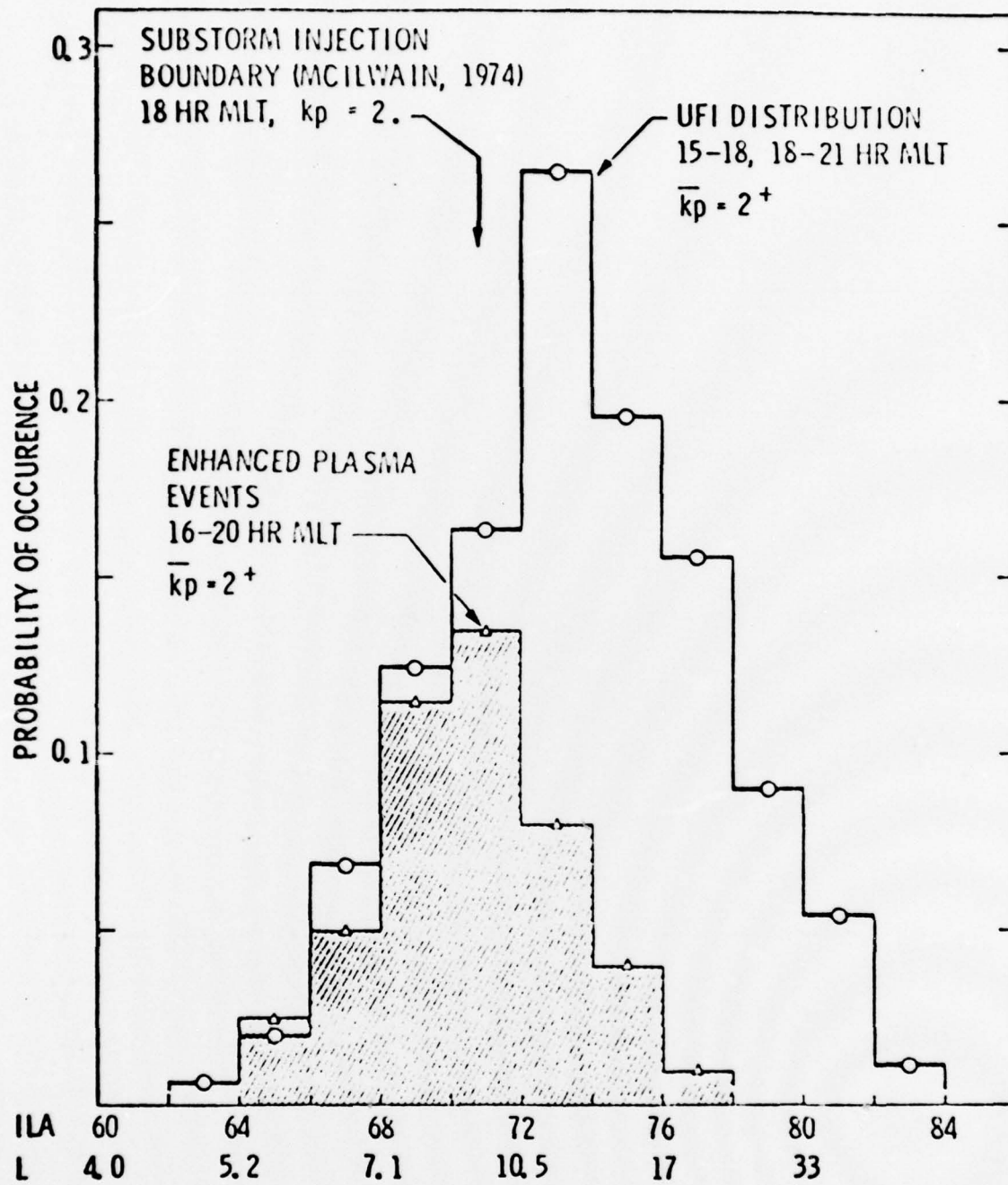


Figure 9

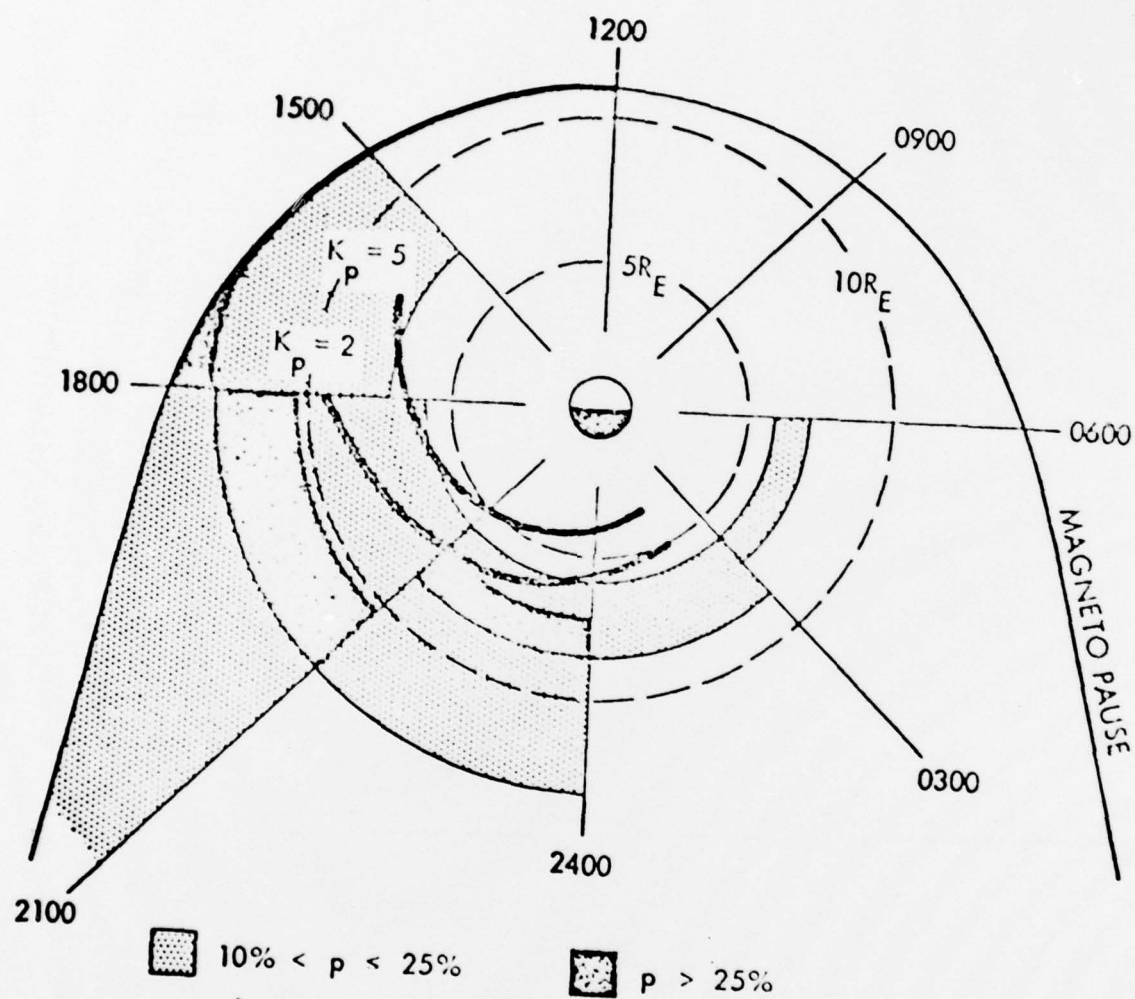


Figure 10